

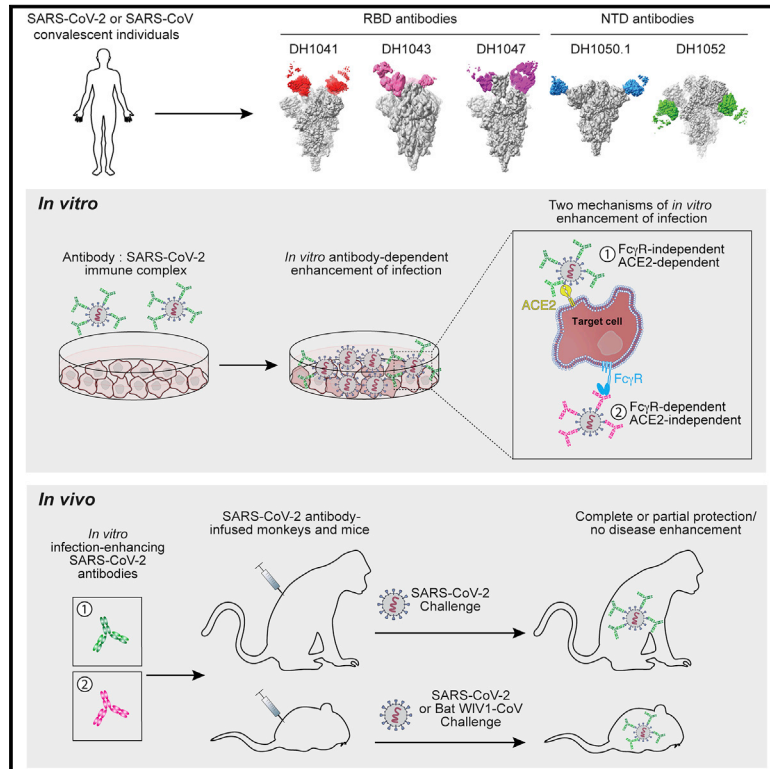


Since January 2020 Elsevier has created a COVID-19 resource centre with free information in English and Mandarin on the novel coronavirus COVID-19. The COVID-19 resource centre is hosted on Elsevier Connect, the company's public news and information website.

Elsevier hereby grants permission to make all its COVID-19-related research that is available on the COVID-19 resource centre - including this research content - immediately available in PubMed Central and other publicly funded repositories, such as the WHO COVID database with rights for unrestricted research re-use and analyses in any form or by any means with acknowledgement of the original source. These permissions are granted for free by Elsevier for as long as the COVID-19 resource centre remains active.

In vitro and *in vivo* functions of SARS-CoV-2 infection-enhancing and neutralizing antibodies

Graphical abstract



Authors

Dapeng Li, Robert J. Edwards, Kartik Manne, ..., Priyamvada Acharya, Barton F. Haynes, Kevin O. Saunders

Correspondence

barton.haynes@duke.edu (B.F.H.), kevin.saunders@duke.edu (K.O.S.)

In brief

Convalescent human-derived SARS-CoV-2 RBD and NTD antibodies mediated neutralization as well as infection enhancement *in vitro*, yet infusion of these antibodies in mice or cynomolgus macaques resulted in suppression of virus replication.

Highlights

- RBD or NTD antibodies exhibited infection enhancement *in vitro* but not *in vivo*
- Neutralizing or infection-enhancing NTD antibodies bound distinct epitopes
- *In vitro* infection-enhancing antibodies protected from SARS-CoV-2 *in vivo*
- Cross-reactive RBD-neutralizing antibodies were protective—most potent DH1047



Article

In vitro and *in vivo* functions of SARS-CoV-2 infection-enhancing and neutralizing antibodies

Dapeng Li,^{1,2,15} Robert J. Edwards,^{1,2,15} Kartik Manne,^{1,2,15} David R. Martinez,^{3,15} Alexandra Schäfer,^{3,15} S. Munir Alam,^{1,2} Kevin Wiehe,^{1,2} Xiaozhi Lu,^{1,2} Robert Parks,^{1,2} Laura L. Sutherland,^{1,2} Thomas H. Oguin III,^{1,2} Charlene McDanal,⁴ Lautaro G. Perez,⁴ Katayoun Mansouri,^{1,2} Sophie M.C. Gobeil,^{1,2} Katarzyna Janowska,^{1,2} Victoria Stalls,^{1,2} Megan Kopp,^{1,2} Fangping Cai,^{1,2} Esther Lee,^{1,2} Andrew Foulger,^{1,2} Giovanna E. Hernandez,^{1,2} Aja Sanzone,^{1,2} Kedamawit Tilahun,^{1,2} Chuancang Jiang,^{1,2} Longping V. Tse,³ Kevin W. Bock,⁵ Mahnaz Minai,⁵ Bianca M. Nagata,⁵ Kenneth Cronin,^{1,2} Victoria Gee-Lai,^{1,2} Margaret Deyton,^{1,2} Maggie Barr,^{1,2} Tarra Von Holle,^{1,2} Andrew N. Macintyre,^{1,2} Erica Stover,^{1,2} Jared Feldman,⁶ Blake M. Hauser,⁶ Timothy M. Caradonna,⁶ Trevor D. Scobey,³ Wes Rountree,^{1,2} Yunfei Wang,^{1,2} M. Anthony Moody,^{1,7} Derek W. Cain,^{1,2} C. Todd DeMarco,^{1,2} Thomas N. Denny,^{1,2} Christopher W. Woods,^{1,2,8} Elizabeth W. Petzold,⁸ Aaron G. Schmidt,^{6,9} I-Ting Teng,¹⁰ Tongqing Zhou,¹⁰ Peter D. Kwong,^{10,11} John R. Mascola,¹⁰ Barney S. Graham,¹⁰ Ian N. Moore,⁵ Robert Seder,¹⁰ Hanne Andersen,¹² Mark G. Lewis,¹² David C. Montefiori,⁴ Gregory D. Sempowski,^{1,2} Ralph S. Baric,³ Priyamvada Acharya,^{1,4} Barton F. Haynes,^{1,2,13,*} and Kevin O. Saunders^{1,4,13,14,16,*}

¹Duke Human Vaccine Institute, Duke University School of Medicine, Durham, NC 27710, USA

²Department of Medicine, Duke University School of Medicine, Durham, NC 27710, USA

³Department of Epidemiology, University of North Carolina at Chapel Hill, Chapel Hill, NC 27599, USA

⁴Department of Surgery, Duke University, Durham, NC 27710, USA

⁵Infectious Disease Pathogenesis Section, Comparative Medicine Branch, National Institute of Allergy and Infectious Diseases, National Institutes of Health, Bethesda, MD 20892, USA

⁶Ragon Institute of MGH, MIT and Harvard, Cambridge, MA 02139, USA

⁷Department of Pediatrics, Duke University School of Medicine, Durham, NC 27710, USA

⁸Center for Applied Genomics and Precision Medicine, Duke University Medical Center, Durham, NC 27710, USA

⁹Department of Microbiology, Harvard Medical School, Boston, MA 02115, USA

¹⁰Vaccine Research Center, National Institute of Allergy and Infectious Diseases (NIAID), NIH, Bethesda, MD 20892, USA

¹¹Department of Biochemistry and Molecular Biophysics, Columbia University, New York, NY 10032, USA

¹²BIOQUAL, Rockville, MD 20850, USA

¹³Department of Immunology, Duke University School of Medicine, Durham, NC 27710, USA

¹⁴Department of Molecular Genetics and Microbiology, Duke University School of Medicine, Durham, NC 27710, USA

¹⁵These authors contributed equally

¹⁶Lead contact

*Correspondence: barton.haynes@duke.edu (B.F.H.), kevin.saunders@duke.edu (K.O.S.)

<https://doi.org/10.1016/j.cell.2021.06.021>

SUMMARY

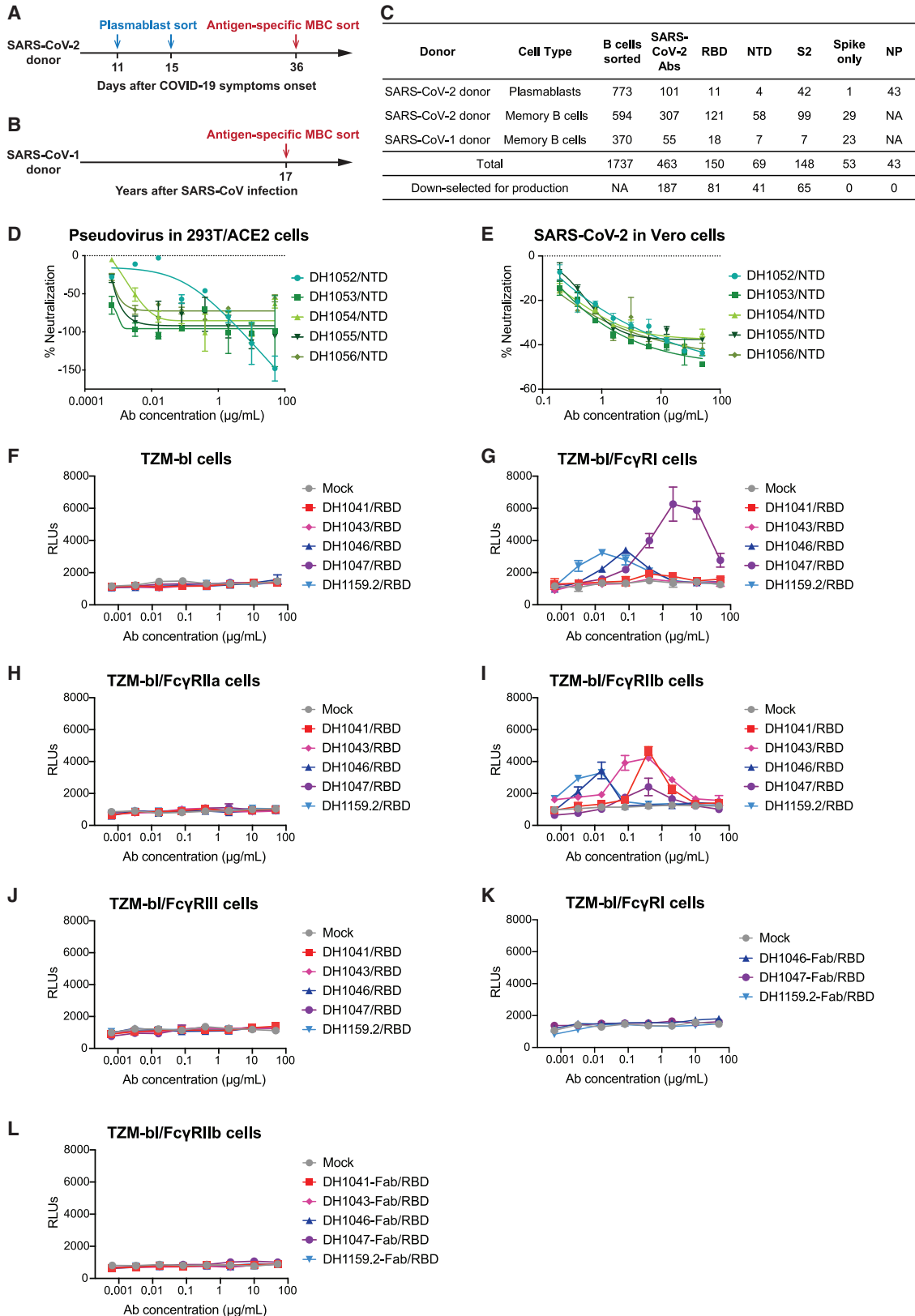
SARS-CoV-2-neutralizing antibodies (NABs) protect against COVID-19. A concern regarding SARS-CoV-2 antibodies is whether they mediate disease enhancement. Here, we isolated NABs against the receptor-binding domain (RBD) or the N-terminal domain (NTD) of SARS-CoV-2 spike from individuals with acute or convalescent SARS-CoV-2 or a history of SARS-CoV infection. Cryo-electron microscopy of RBD and NTD antibodies demonstrated function-specific modes of binding. Select RBD NABs also demonstrated Fc receptor- γ (Fc γ R)-mediated enhancement of virus infection *in vitro*, while five non-neutralizing NTD antibodies mediated Fc γ R-independent *in vitro* infection enhancement. However, both types of infection-enhancing antibodies protected from SARS-CoV-2 replication in monkeys and mice. Three of 46 monkeys infused with enhancing antibodies had higher lung inflammation scores compared to controls. One monkey had alveolar edema and elevated bronchoalveolar lavage inflammatory cytokines. Thus, while *in vitro* antibody-enhanced infection does not necessarily herald enhanced infection *in vivo*, increased lung inflammation can rarely occur in SARS-CoV-2 antibody-infused macaques.

INTRODUCTION

The severe acute respiratory syndrome coronavirus 2 (SARS-CoV-2) has caused a global pandemic with over 157 million

cases and 3 million deaths (<https://coronavirus.jhu.edu>). While the ultimate solution to control the COVID-19 pandemic is a safe and effective vaccine, neutralizing Ab (NAB) prophylaxis or treatment of infection may help to control the pandemic





(legend on next page)

(Graham, 2020; Sempowski et al., 2020). Prophylactic or therapeutic use of SARS-CoV-2 NAbs in non-human primates (Baum et al., 2020a; Jones et al., 2020; Zost et al., 2020a) or rodent models (Hassan et al., 2020; Rogers et al., 2020; Wu et al., 2020) have protected against SARS-CoV-2 infection. Potent SARS-CoV-2 NAbs reported to date predominantly target the RBD region (Baum et al., 2020b; Brouwer et al., 2020; Cao et al., 2020; Hansen et al., 2020; Ju et al., 2020; Liu et al., 2020a; Pinto et al., 2020; Robbiani et al., 2020; Rogers et al., 2020; Shi et al., 2020; Wrapp et al., 2020a; Wu et al., 2020). In contrast, neutralizing SARS-CoV-2 NTD antibodies (Abs) exhibit more modest neutralization potency (Brouwer et al., 2020; Chi et al., 2020; Wec et al., 2020; Zost et al., 2020a, 2020b).

A safety concern for clinical use of antibodies is antibody-dependent enhancement (ADE) of infection. ADE *in vitro* has been reported for respiratory syncytial virus vaccination, dengue virus vaccination, or dengue virus infection (Arvin et al., 2020). ADE is often mediated by Fc receptors for immunoglobulin G (IgG) (Fc γ Rs), complement receptors (CRs), or both and is most commonly observed in monocytes/macrophages and B cells (Iwasaki and Yang, 2020; Ubol and Halstead, 2010). *In vitro* studies have demonstrated Fc γ R-mediated ADE of SARS-CoV infection of ACE2-negative cells (Jaume et al., 2011; Kam et al., 2007; Wan et al., 2020; Wang et al., 2014; Yilla et al., 2005; Yip et al., 2014, 2016). Additional research has demonstrated Fc γ R-independent infection enhancement of SARS-CoV in Vero cells and isolated an Ab that may have enhanced lung viral load and pathology *in vivo* (Wang et al., 2016). The ability of SARS-CoV-2 S Abs to mediate infection enhancement *in vivo* is unknown but is a theoretical concern for COVID-19 vaccine development (Arvin et al., 2020; Bournazos et al., 2020; Haynes et al., 2020; Iwasaki and Yang, 2020).

Here, we identified potent *in vitro*-neutralizing RBD and NTD Abs as well as *in vitro* infection-enhancing RBD and NTD Abs from individuals infected with SARS-CoV or SARS-CoV-2. Negative stain electron microscopy (NSEM) and cryo-electron microscopy (cryo-EM) revealed distinct binding patterns and the precise epitopes of infection-enhancing and neutralizing Abs. *In vitro* studies demonstrated that select RBD Abs mediated Fc γ R-dependent infection enhancement, whereas the NTD Abs induced Fc γ R-independent infection enhancement. However, using monkey and mouse models of SARS-CoV-2 infection, none of the *in vitro* infection-enhancing Abs enhanced SARS-CoV-2 virus replication or infectious virus in the lung *in vivo*. Three of 46 monkeys had lung pathology or bronchoalveolar lavage (BAL) cytokine levels greater than controls. How-

ever, repeat studies with dose ranges of *in vitro* enhancing Abs did not increase lung pathology. Thus, *in vitro* infection-enhancing RBD and NTD Abs controlled virus *in vivo* and was rarely associated with enhanced lung pathology.

RESULTS

Isolation of neutralizing and infection-enhancing SARS-CoV-2 Abs

SARS-CoV-2-reactive monoclonal Abs from plasmablasts or SARS-CoV-2-reactive memory B cells were isolated (Liao et al., 2009, 2013) from a SARS-CoV-2-infected individual 11, 15, and 36 days post-onset of symptoms. To identify neutralizing Abs against both SARS-CoV and SARS-CoV-2, SARS-CoV-2 S-reactive B cells were isolated from an individual infected with SARS-CoV ~17 years prior to sample collection (Figures 1A, 1B, and S1A–S1D). From 1,737 total B cells, we isolated 463 Abs that bound to SARS-CoV-2 S or nucleocapsid proteins in high-throughput binding screens (Figure 1C; Table S1). We selected 187 Abs using high binding magnitude, cross-reactivity with human CoVs, high somatic mutation frequency, and a long HCDR3 as selection criteria. Downselected Abs were examined for neutralization of SARS-CoV-2 pseudovirus and replication-competent SARS-CoV-2. Forty-four of 81 RBD Abs exhibited neutralization of SARS-CoV-2 pseudovirus or replication-competent virus (Figures S1E–S1J; Table S2). Ten of 41 NTD Abs neutralized SARS-CoV-2 in the 293T/ACE2 pseudovirus and plaque reduction assays, at an IC₅₀ as low as 39 ng/mL (Figures S1K–S1M; Table S2). In addition, 5 non-neutralizing NTD Abs enhanced SARS-CoV-2 pseudovirus infection in 293T/ACE2 and replication-competent SARS-CoV-2 nano-luciferase virus infection of Vero cells (Figures 1D and 1E; Huo et al., 2020). NTD Ab infection enhancement was dependent on ACE2 expression. Both ACE2-expressing 293T cells used for pseudovirus assays and Vero cells lack Fc γ R expression (Takeda et al., 2007). Thus, NTD enhancement of SARS-CoV-2 infection was Fc γ R independent.

To assess Fc γ R-dependent infection enhancement, 100 S-reactive IgG1 Abs were tested for their ability to facilitate SARS-CoV-2 infection of TZM-bl cells expressing various Fc γ Rs but lacking ACE2 and TMPRSS2 (Table S2). Three or five Abs enabled SARS-CoV-2 infection of TZM-bl cells expressing either Fc γ RI or Fc γ RIIb, respectively (Figures 1F–1J). The antigen-binding fragments (Fabs) of these Abs did not mediate infection enhancement of TZM-bl cells expressing Fc γ RI or Fc γ RIIb, demonstrating Fc-dependence for enhancement (Figures 1K

Figure 1. SARS-CoV-2 receptor-binding domain (RBD) and N-terminal domain (NTD) Abs mediate enhancement of infection

(A and B) Timeline of blood sampling, plasmablasts and/or antigen-specific memory B cells (MBC) sorting, and Ab isolation from convalescent (A) SARS-CoV-2 and (B) SARS-CoV donors.

(C) Summary of number and specificity of Abs isolated from each donor.

(D and E) *In vitro* neutralization curves for NTD infection-enhancing Abs against (D) pseudotyped SARS-CoV-2 D614G in 293T-hACE2 cells, and (E) replication-competent nano-luciferase (nLuc) SARS-CoV-2 in Vero cells.

(F–J) Fc γ R-dependent pseudotyped SARS-CoV-2 infection enhancement when RBD Abs or mock medium control was added to (F) parental TZM-bl cells, and TZM-bl cells stably expressing human Fc γ R receptors (G) Fc γ RI, (H) Fc γ RIIa, (I) Fc γ RIIb or (J) Fc γ RIII.

(K and L) The effect of RBD Ab fragment antigen-binding regions (Fabs) on pseudotyped SARS-CoV-2 D614G infection was tested in (K) Fc γ RI-expressing TZM-bl cells and (L) Fc γ RIIb-expressing TZM-bl cells. Data are represented as mean \pm SEM. Three or four independent experiments were performed, and representative data are shown.

See also Figure S1.

and 1L). Thus, RBD Abs can be either neutralizing in ACE2-expressing 293T cells, infection-enhancing in the Fc γ R-expressing TZM-bl cells, or both (Figure 2A). NTD Abs can either be neutralizing or infection enhancing in the ACE2⁺ 293T cells or VeroE6 cells (Figure 2A).

Characterization of infection-enhancing Spike Abs

We compared the phenotypes and binding modes of RBD Abs that either did or did not enhance infection in order to elucidate differences between them. The selected RBD Abs neutralized SARS-CoV-2 pseudovirus and/or replication-competent virus in ACE2-expressing cells (Figures 2A and S2), despite five of these Abs mediating infection enhancement in ACE2-negative, Fc γ R-positive TZM-bl cells (Figures 1F–1L, 2A, and S2). Both types of selected RBD Abs blocked ACE2 binding to S protein and both types of RBD Abs bound to S with high affinities (range = 0.1 to 9 nM) (Table S3; Figure 2A). Thus, the infection-enhancing or non-enhancing RBD Abs showed similarities in ACE2 blocking, affinity, and neutralization of ACE2-dependent SARS-CoV-2 infection (Figure 2A).

For six representative RBD Abs, we obtained NSEM reconstructions of Fabs in complex with stabilized S ectodomain trimer. Infection-enhancing RBD Abs DH1041 and DH1043 bound with a vertical approach (Figure 2B), parallel to the central axis of the S trimer, similar to non-infection-enhancing Abs DH1042 and DH1044 (Figure 2C). The epitopes of Abs DH1041, DH1042, and DH1043 overlapped with that of the ACE-2 receptor (Wec et al., 2020), consistent with their ability to block ACE-2 binding to S protein (Figures 2A, S3A, and S3B). Their epitopes were similar to those of three previously described Abs, P2B-2F6 (Ju et al., 2020), H11-H4, and H11-D4 (Figure S3C; Huo et al., 2020; Zhou et al., 2020a). The epitope of another non-infection-enhancing RBD Ab DH1044 was only slightly shifted relative to DH1041, DH1042, and DH1043 (Figure 2C), but resulted in DH1044 not blocking ACE2 binding (Figures 2A, S3A, and S3B). The remaining two RBD Abs, DH1045 and DH1047, cross-reacted with both SARS-CoV and SARS-CoV-2 S (Figures 2A, S2A, and S2B). DH1047 also reacted with bat and pangolin CoV spike proteins (Figures 2A and S2A). Although DH1047 mediated Fc γ R-dependent infection of TZM-bl cells and DH1045 did not, both Abs bound to RBD-up S conformations with a more horizontal angle of approach (Figures 2B, 2C, and S3A; Pak et al., 2009). Thus, epitopes and binding angles of RBD Abs determined by NSEM did not discriminate between Abs that mediated Fc γ R-dependent infection enhancement and those that did not.

Next, we characterized NTD Abs. The Fabs of neutralizing NTD Abs DH1050.1 and DH1051 bound to stabilized S ectodomain with affinities of 16 and 19 nM respectively, whereas the infection-enhancing Ab DH1052 bound with 294 nM affinity (Table S3). NSEM reconstructions obtained for nine NTD Abs showed that the Fc γ R-independent, infection-enhancing NTD Abs (DH1053–DH1056) bound to S with their Fab constant domains directed downward toward the virus membrane (Figure 2D), whereas the five neutralizing NTD-directed Abs (DH1048–DH1051) bound to S with the constant domain of the Fab directed upward away from the virus membrane (Figure 2E). The five neutralizing Abs bound the same epitope as Ab 4A8

(Chi et al., 2020), with three of the five having the same angle of approach and heavy-chain gene segment (V_H1-24) as 4A8 (Figures S3D–S3F; Table S2; Chi et al., 2020). These NTD Abs may constitute a neutralizing Ab class that can be elicited in multiple individuals. Thus, S protein Ab epitopes and binding modes were associated with infection-enhancing activity of NTD Abs.

Competition between infection-enhancing and non-infection-enhancing Abs

To determine whether infection-enhancing Abs could compete with non-infection-enhancing Abs for binding to S ectodomain, we performed surface plasmon resonance (SPR) competitive binding assays. RBD Abs segregated into two clusters, where Abs within a cluster blocked each other and Abs in different clusters did not block each other (Figure 3A). One cluster included Abs DH1041, DH1043, and DH1044, and the other cluster included Abs DH1046 and DH1047. NSEM reconstructions showed combinations of DH1041 and DH1047 Fabs or DH1043 and DH1047 Fabs bound simultaneously to different epitopes of the stabilized S trimer (Figure 3B).

NTD Abs also segregated into two clusters where one cluster included neutralizing NTD Abs and a second cluster included non-neutralizing NTD Abs (Figures 3A and 3C). NSEM reconstructions confirmed that the Fabs of neutralizing NTD Ab DH1050.1 and infection-enhancing NTD Ab DH1052 could simultaneously bind to distinct epitopes on a single SARS-CoV-2 S trimer (Figure 3D). DH1054 was unique as it was able to block both infection-enhancing and neutralizing NTD Abs (Figure 3C).

NTD Abs did not compete with RBD Abs for binding to S trimer (Figure 3A), suggesting in a polyclonal mixture of Abs, the SARS-CoV-2 S trimer could bind both RBD and NTD Abs. NSEM showed that 1 or 2 different neutralizing RBD Abs (DH1043 and DH1047) could bind to the same S protomer as neutralizing NTD Abs DH1050.1 or DH1051 (Figures 3E and 3F). Thus, in the presence of a polyclonal Ab response, S trimer could be bound by multiple Fabs of RBD and NTD Abs.

Fc γ R-independent infection enhancement in the presence of neutralizing Abs

Structural determination of Ab binding modes demonstrated that certain infection-enhancing Abs and non-infection-enhancing Abs bound to distinct epitopes on the same S protomer (Figures 3A–3F). Infection-enhancing Ab DH1052 and neutralizing RBD Ab DH1041 were isolated from the same individual. We hypothesized that infection outcome would be dependent on which Ab was present at the highest concentration. When DH1041 neutralization was assessed in the presence of 1,325-fold excess of Ab DH1052, infection enhancement was observed when DH1041 concentration was below 10 ng/mL (Figures 3G and S4A–S4C). A nearly identical result was obtained when we examined neutralization by DH1043 (Figures 3H and S4A–S4C). In 21 SARS-CoV-2-infected humans, RBD and NTD serum IgG titers were comparable (Figures S4D and S4E). Moreover, the prevalence of DH1052 versus DH1041 Abs was assessed using blocking assays and found to be only modestly higher for DH1052 (Figure S4F). Thus, an ~1,000-fold excess of infection-enhancing NTD Ab was required to outcompete the effect of a potent RBD-neutralizing Ab *in vitro*, but such excess amounts

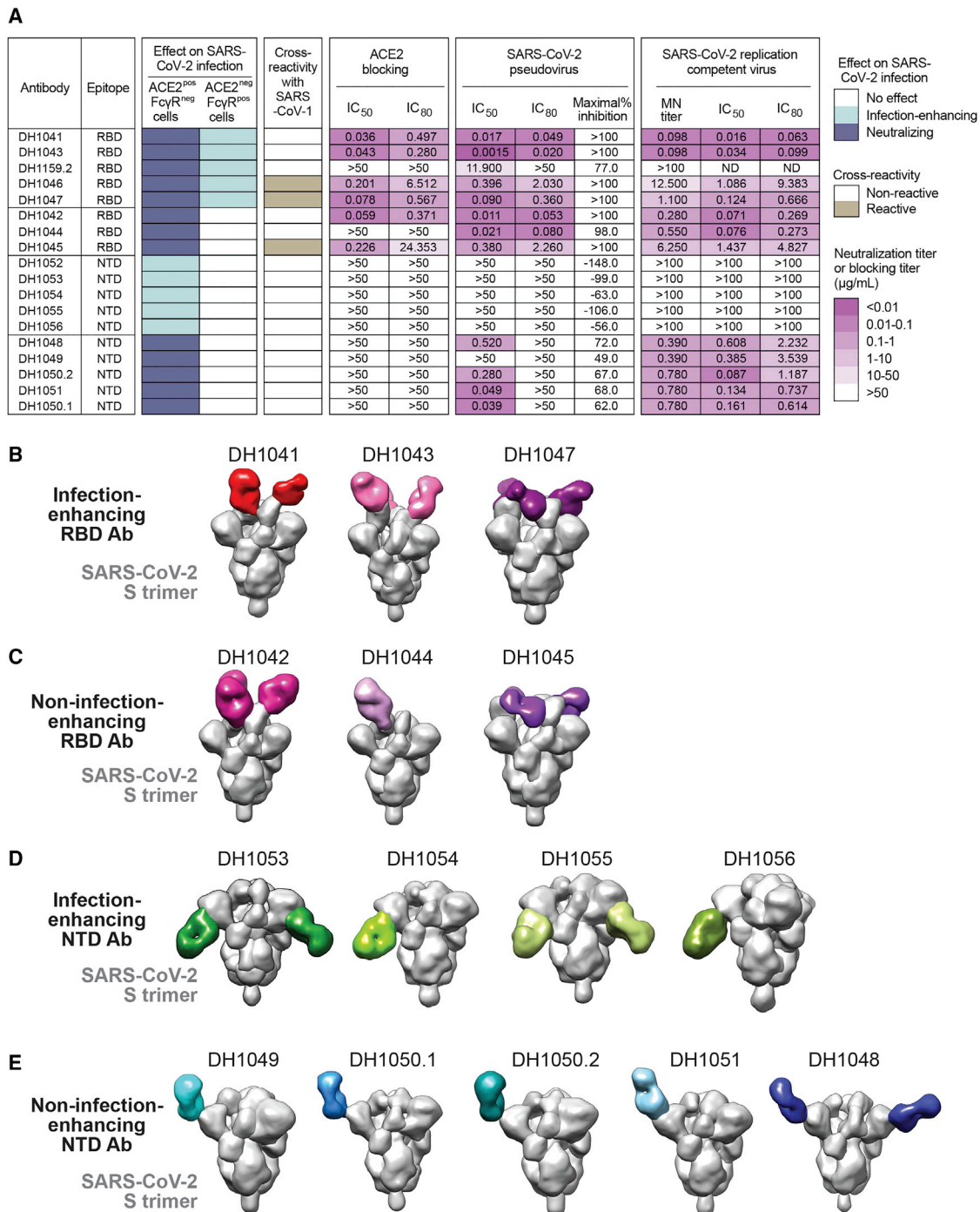
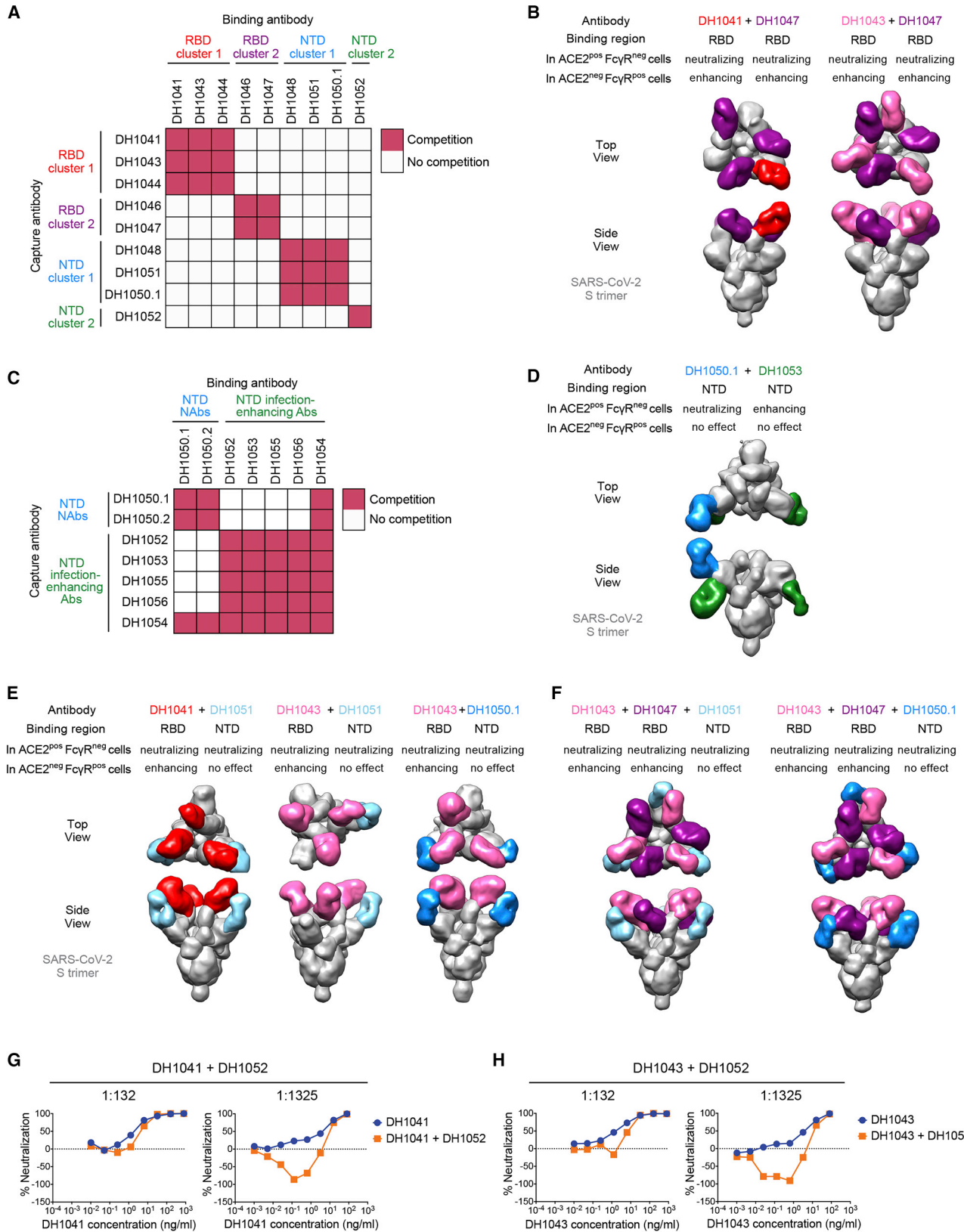


Figure 2. Structural and phenotypic characterization of infection-enhancing and non-infection-enhancing RBD and NTD Abs.

(A) Summary of Ab epitope, binding, and neutralizing or infection-enhancing activity in ACE2-positive/FcγR-negative cells or ACE2-negative/FcγR-positive cells. Ab functions are color-coded based on the key shown at the right. MN titer, micro-neutralization titer; ND, not determined.

(B–E) 3D reconstruction of negative stain electron microscopy images of stabilized SARS-CoV-2 S ectodomain trimers (S-2P; gray) bound to the Fabs (various colors) of (B and D) infection-enhancing or (C and E) non-infection-enhancing RBD or NTD antibodies.

See also [Figure S2](#) and [S3](#).



(legend on next page)

of DH1052 was not observed during natural infection (Figures 3G, 3H, and S4D–S4F).

Cryo-EM structural determination of RBD and NTD-directed Ab epitopes

To visualize atomic level details of their interactions with the S protein, cryo-EM was used for structural determination of selected representative Abs from the panels of RBD and NTD-directed Abs. For all three RBD-directed Abs, the cryo-EM datasets revealed heterogeneous populations of S ectodomain “2P” (S-2P) (Wrapp et al., 2020b) with at least one RBD in the “up” position (Figure 4; Data S1). We did not find any unliganded S or any 3-RBD-down S population, although unliganded S-2P consistently shows a 1:1 ratio of 1-RBD-up and 3-RBD-down populations (Henderson et al., 2020; Walls et al., 2020). All S-2P trimers were stoichiometrically bound to three Fabs, with Abs bound to both up and down RBDs in an S-2P trimer.

We observed that the primary epitopes of DH1041 and DH1043 were centered on the receptor binding motif (RBM; residues 483–506) of the RBD (Figures 4A and 4B; Data S1), providing structural basis for the ACE-2 blocking phenotype of these Abs. While DH1041 utilized its heavy-chain complementarity-determining regions (CDRs) to contact the RBM, the DH1043 paratope included both its heavy and light chains. In contrast, the epitope of Ab DH1047 was focused around the $\alpha 2$ and $\alpha 3$ helices and $\beta 2$ strand that are located outside the N terminus of the RBM (Figure 4C; Data S1). DH1047 also contacted RBD residues 500–506 outside the RBM and stacked against the N-terminal end of the $\alpha 3$ helix. The DH1047 paratope included heavy-chain HCDR2, HCDR3 and light-chain LCDR1 and LCDR3. The HCDR3 stacks against and interacts with the residues in the $\beta 2$ strand. Interactions with the $\beta 2$ strand are also mediated by HCDR2. Similar to DH1041 and DH1043, the DH1047 interacted with an “up” RBD conformation from an adjacent protomer although these interactions were not well characterized due to disorder in that region.

We next determined cryo-EM structures of the NTD-directed neutralizing Abs DH1050.1 (Figure 4D) and NTD-directed infection-enhancing Ab DH1052 (Figure 4E), at 3.4 and 3.0 Å resolutions, respectively. The cryo-EM datasets of DH1050.1- and DH1052-bound complexes showed Fab bound to both 3-RBD-down and 1-RBD-up S-2P spikes (Data S1). Consistent with the NSEM reconstructions, the neutralizing Ab DH1050.1 and the non-neutralizing, infection-enhancing Ab DH1052 bound opposite faces of the NTD, with the epitope for the neutralizing Ab DH1050.1 facing the host cell membrane and the epitope for the non-neutralizing, infection-enhancing Ab DH1052 facing

the viral membrane. The dominant contribution to the DH1050.1 epitope came from NTD loop region 140–158 that stacks against the Ab HCDR3 and extends farther into a cleft formed at the interface of the DH1050.1 HCDR1, HCDR2, and HCDR3 loops. The previously described NTD Ab 4A8 interacts with the same epitope in a similar manner as DH1050.1, with its elongated HCDR3 dominating interactions. Although, DH1050.1 and 4A8 (Chi et al., 2020) show a rotation relative to each other about the stacked HCDR3 and NTD 140–158 loops. The light chains of DH1050.1 and 4A8 do not contact the S protein, which is consistent with their diverse light-chain gene origins (Figure 4E; Data S1). The infection-enhancing NTD-directed Ab DH1052 bound the NTD at an epitope facing the viral membrane and composed of residues spanning 27–32, 59–62, and 211–218, with all the CDR loops of both heavy and light chains involved in contacts with the NTD. We also observed contact of the Ab with the glycan at position 603, as well as the conformationally invariant SD2 region. Thus, we found that the RBD-directed antibodies isolated in this study influenced RBD dynamics and bound only to spike with at least one RBD in the up conformations, and in some cases, also induced the 2-RBD-up and 3-RBD-up spike conformations. In contrast, the NTD-directed antibodies bound to both the 3-RBD-down and 1-RBD-up spikes that are present in the unliganded S-2P.

Effect of *in vitro* infection-enhancing and neutralizing NTD Abs in mouse and macaque models

Next, we assessed the effect of NTD infection-enhancing Ab DH1052 in a COVID-19 disease mouse model where aged BALB/c mice were challenged with the mouse-adapted SARS-CoV-2 MA10 strain (Leist et al., 2020a). DH1052 lacked neutralization of SARS-CoV-2 MA10 (Figures S4G and S4H). DH1052 or a control influenza Ab CH65 was given 12 h prior to SARS-CoV-2 MA10 infection (Figure 5A). Throughout the 4 days of infection, DH1052-infused mice exhibited similar levels of body weight loss and higher survival than mice given CH65 (Figures 5B and 5C). In addition, DH1052-treated mice exhibited lower lung hemorrhagic scores, lower lung viral plaque-forming unit (PFU) titers and lower lung tissue subgenomic RNA (sgRNA) levels compared to control mice (Figures 5D–5F). Therefore, DH1052 treatment resulted in less severe disease and reduced viral replication. FcR-mediated effector functions may have been the mechanism of suppression since DH1052 bound to mouse Fc γ RI and Fc γ RIV (Table S4).

We next examined the effect of infusion of NTD infection-enhancing Ab DH1052, NTD-neutralizing Ab DH1050.1, or control Ab CH65 on SARS-CoV-2 infection in monkeys (Leist et al.,

Figure 3. Simultaneous binding of infection-enhancing and non-infection-enhancing Abs to individual S trimers

(A) Cross-blocking activity of RBD and NTD-neutralizing Abs tested by surface plasmon resonance (SPR). S-2P was captured by one Ab (y axis) followed by binding by the second Ab (x axis).

(B) 3D reconstruction of simultaneous recognition of SARS-CoV-2 S-2P by two RBD Abs DH1041+DH1047 or DH1043+DH1047.

(C) Cross-blocking activity of neutralizing or infection-enhancing NTD Abs tested by SPR and shown as in (A).

(D–F) 3D reconstruction of SARS-CoV-2 S-2P simultaneously bound (D) NTD Abs DH1053 and DH1050.1, (E) RBD infection-enhancing Ab and a NTD non-infection-enhancing Ab, or (F) triple-Ab combinations of RBD Ab DH1043, RBD Ab DH1047, and either NTD Ab DH1051 (left) or DH1050.1 (right).

(G and H) RBD Ab neutralization of SARS-CoV-2 D614G pseudovirus infection of 293T/ACE2 cells in the presence of 132 or 1,325 fold excess of infection-enhancing NTD Ab DH1052.

See also Figure S4.

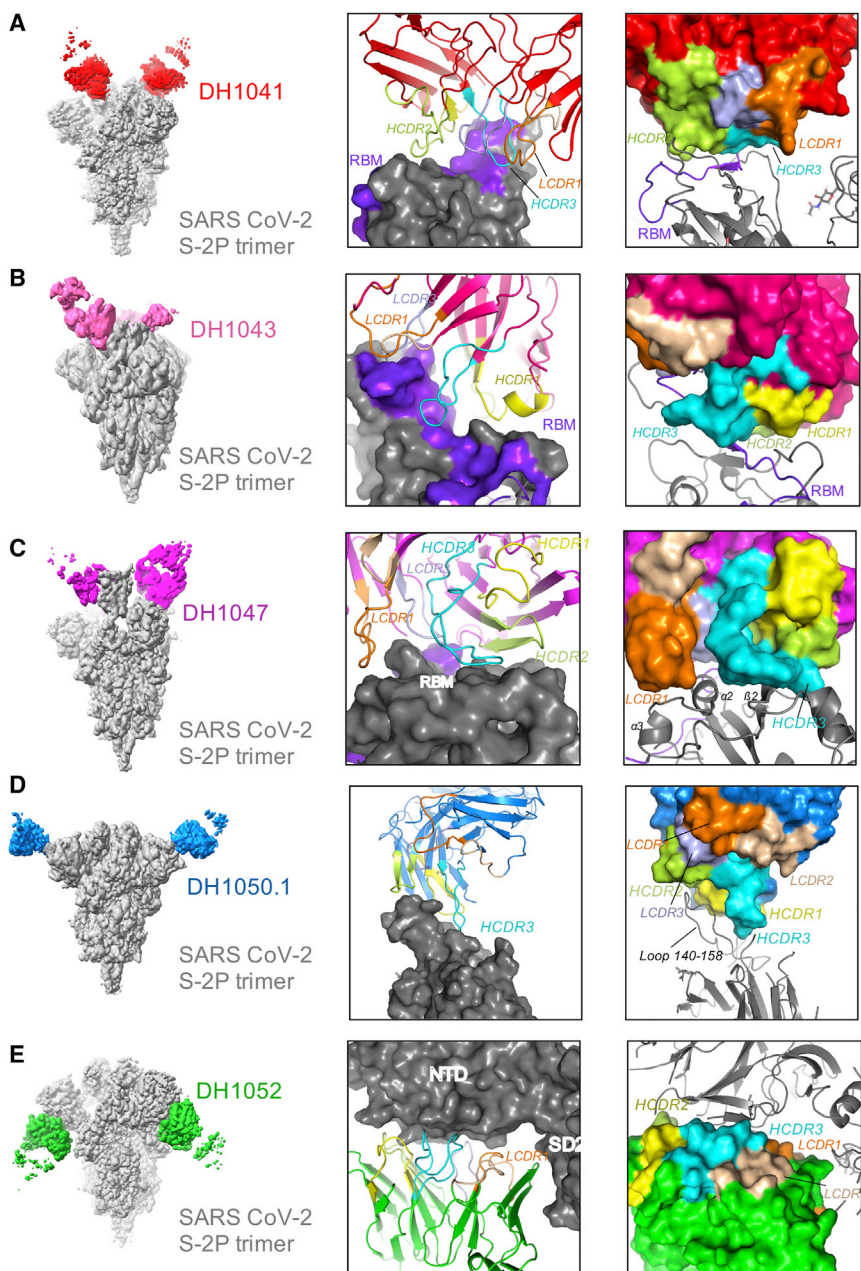


Figure 4. Cryo-electron microscopy of neutralizing and non-neutralizing Abs in complex with SARS-CoV-2 Spike ectodomain

Structures of SARS-CoV-2 S protein in complex with RBD Abs (A) DH1041 (red), (B) DH1043 (pink), (C) DH1047 (magenta), (D) neutralizing NTD Ab DH1050.1 (blue), and (E) infection-enhancing NTD Ab DH1052 (green). Each Ab is bound to S-2P shown in gray with its RBM colored purple blue. (Right) Zoomed-in views of the Ab interactions with S-2P trimers. The Ab complementarity determining (CDR) loops are colored: HCDR1 yellow, HCDR2 lilmon, HCDR3 cyan, LCDR1 orange, LCDR2 wheat and LCDR3 light blue. See also [Data S1](#).

mononuclear inflammation, perivascular and alveolar edema ([Figure S5B](#)), and multiple upregulated BAL cytokines ([Table S5](#)). Immunohistologic analysis demonstrated alveolar and perivascular infiltration of M2-type macrophages in both monkey BB536A and a control monkey BB785E ([Figures S5C–S5E](#)). In contrast, macaques administered DH1050.1, a neutralizing NTD Ab, had lower lung inflammation ([Figures 5L and S5A](#)) and fewer infiltrating macrophages ([Figures S5C–S5E](#)). Infusion of either DH1050.1 or DH1052 reduced viral nucleocapsid antigen ([Figures 5M and S5A](#)), Envelope (E) gene sgRNA, and nucleocapsid (N) gene sgRNA in the BAL ([Figures 5N and 5O](#)). In nasal swab fluid, DH1050.1 and DH1052 reduced E and N gene sgRNA in macaques with the reduction being significant when neutralizing Ab DH1050.1 was infused ([Figures 5P–5Q](#)).

Since DH1052-mediated *in vitro* infection enhancement increased as the Ab concentration increased ([Figures 1D and 1E](#)), we infused an additional 6 cynomolgus macaques with either 30 mg/kg of DH1052 or CH65 control Ab ([Figure S6A](#)). DH1052 infusion suppressed BAL viral

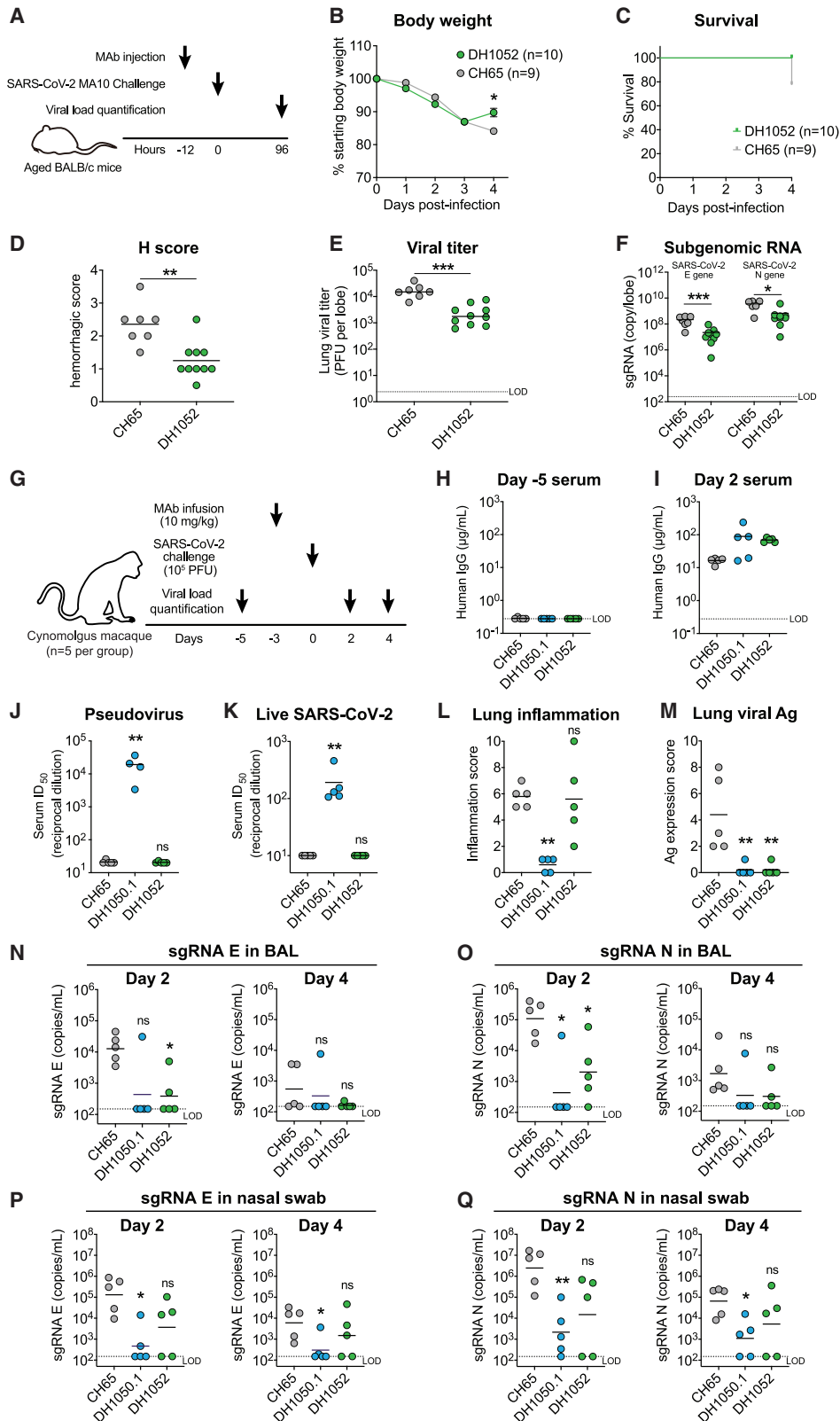
load ([Figures S6B–S6D](#)), significantly reduced virus replication in nasal swab samples ([Figures S6E–S6G](#)), and showed no enhanced immunopathology or cytokine secretion ([Figures S6H–S6K; Table S5](#)). Thus, with high dose (30 mg/kg) of DH1052 Ab, there was no infection enhancement. These results suggested that the lung pathology seen in monkey BB536A was rare and may not have been caused by Ab infusion.

2020b; [Rockx et al., 2020](#)). Cynomolgus macaques were infused with 10 mg of Ab per kg body weight and 3 days later challenged intranasally and intratracheally with 10^5 PFU of SARS-CoV-2 ([Figure 5G](#)). Human Ab infusion resulted in circulating concentrations ranging from 11 to 238 $\mu\text{g}/\text{mL}$ in serum at day 2 post-challenge ([Figures 5H and 5I](#)). Sera with DH1050.1 neutralized SARS-CoV-2 pseudovirus and replication-competent virus, while serum containing DH1052 or CH65 did not neutralize ([Figures 5J and 5K](#)). Four of 5 macaques that received DH1052 had comparable lung inflammation to control CH65-infused macaques 4 days after infection ([Figures 5L and S5A](#)). However, one macaque (BB536A) administered DH1052 showed increased perivascular

load ([Figures S6B–S6D](#)), significantly reduced virus replication in nasal swab samples ([Figures S6E–S6G](#)), and showed no enhanced immunopathology or cytokine secretion ([Figures S6H–S6K; Table S5](#)). Thus, with high dose (30 mg/kg) of DH1052 Ab, there was no infection enhancement. These results suggested that the lung pathology seen in monkey BB536A was rare and may not have been caused by Ab infusion.

Fc γ R-dependent, *in vitro* infection-enhancing RBD Abs do not enhance SARS-CoV-2 infection in mice

Next, we used a SARS-CoV-2 acquisition mouse model to investigate the *in vivo* relevance of RBD-neutralizing Abs that also



(legend on next page)

mediated *in vitro* infection enhancement (Figures 6A and 6B). Aged BALB/c mice were injected intraperitoneally with 300 μ g of Ab and challenged with a SARS-CoV-2 mouse-adapted 2AA MA isolate 12 h later (Dinnon et al., 2020). Mice received either *in vitro* infection-enhancing Ab DH1041, non-infection-enhancing Ab DH1050.1, or a combination of both Abs. Administration of DH1041 alone or in combination with DH1050.1 protected all mice from detectable infectious virus in the lungs 48 h after challenge (Figure 6A). In the setting of therapeutic treatment, administration of DH1041 alone or in combination with DH1050.1 12 h after SARS-CoV-2 challenge significantly reduced lung infectious virus titers (Figure 6B). Thus, while RBD Ab DH1041 could mediate Fc γ R-dependent, *in vitro* infection enhancement, it protected mice from SARS-CoV-2 infection when administered prophylactically or therapeutically.

DH1046 and DH1047 are RBD Abs that cross-neutralize SARS-CoV, SARS-CoV-2, and bat WIV1-CoV (Figures 2A, S2A, S2B, S2I–S2L, and 6C–6E). Both RBD Abs mediated Fc γ R-dependent, *in vitro* SARS-CoV-2 infection enhancement (Figures 1F–1L). We assessed the ability of either DH1046 or DH1047 to enhance or protect against bat WIV1-CoV infection in HFH4-ACE2-transgenic mice (Figures 6F and 6G). Mice administered DH1046 or DH1047 before challenge had no detectable infectious virus in the lung, whereas control IgG administered mice had a mean titer of 84,896 PFU per lung lobe (Figure 6F). Administration of DH1047 after challenge eliminated detectable infectious virus in the lung in 3 of 5 mice (Figure 6G). Therapeutic administration of DH1046 reduced infectious virus titers 10-fold compared to negative control IgG (Figure 6G). Thus, DH1046 and DH1047 did not enhance infection *in vivo* but rather protected mice from SARS-related bat coronavirus infection.

In vitro infection-enhancing RBD Abs in SARS-CoV-2-challenged nonhuman primates

Finally, we assessed RBD Ab infection enhancement in cynomolgus macaques (Figures 7A). After Ab infusion at 10 mg/kg of body weight, serum human IgG concentrations reached 11–228 μ g/mL at day 2 post-challenge (Figures 7B and 7C) and exhibited a wide range of neutralization potencies against SARS-CoV-2 (Figures 7D and 7E). Infusion of RBD Ab DH1041, DH1043, or DH1047 resulted in reduced lung inflammation, undetectable lung viral antigen (Figures 7F, 7G, and S5A), and reduced sgRNA in the upper

and lower respiratory tracts (Figures 7H–7K). RBD Ab DH1046, a weaker neutralizing Ab compared to DH1041, DH1043, or DH1047 (Figure 2A), did not enhance sgRNA E or N in BAL or nasal swab samples (Figures 7H–7K) but protected only a subset of infused monkeys. Two DH1046-infused monkeys had increased lung inflammation scores due to increased total areas of inflammation compared to control Ab monkeys (Figures 7F and S5A) but had no evidence of perivascular or alveolar edema nor evidence of abnormal BAL cytokines (Table S5). Thus, these two animals had more lung involved with inflammatory macrophage infiltration but did not have pathological evidence of vascular leakage. Comparing the DH1046 group to the control IgG group, viral nucleocapsid antigen in the lung was reduced (Figures 7G and S5A). Thus, the weakly neutralizing Ab only partially limited virus replication and lung inflammation.

In vitro infection enhancement by RBD Abs was dependent on Ab concentration, with lower levels of Ab showing the highest magnitude of infection enhancement (Figure 1G). Therefore, we performed an additional passive infusion study with a series of different concentrations of DH1047 (Figure S7A). Cynomolgus macaques were infused with 5, 1, or 0.1 mg of DH1047 per kg of body weight resulting in a wide range of DH1047 concentrations in serum (Figures S7B and S7C). However, none of the groups of macaques had enhanced virus replication (although one monkey in the 0.1 mg/kg group had higher BAL sgRNA E and N than controls) (Figures S7D–S7G), lung inflammation (Figures S7H and S7I), lung viral antigen (Figures S7J–S7K), or higher BAL inflammatory cytokines (Table S5) compared to the control IgG group.

Overall, 45 of 46 spike enhancing Ab-infused monkeys did not show enhanced virus replication *in vivo*, while 3 of 46 Ab-treated monkeys exhibited enhancement of lung pathology, and 1 of 46 Ab-treated monkeys had alveolar and perivascular edema with elevated BAL inflammatory cytokines. In the case of the latter monkey, a follow-up study with 3 times the initial DH1052 Ab dose did not confirm DH1052 infusion resulted in enhanced lung pathology after SARS-CoV-2 challenge.

DISCUSSION

Here, we assessed infection enhancement by SARS-CoV-2 Abs and observed two different types of *in vitro* infection enhancement. First, RBD Abs mediated classic ADE that required Fc γ Rs

Figure 5. NTD Ab DH1052 does not always enhance SARS-CoV-2 replication or disease *in vivo*

(A–F) DH1052 passive immunization and murine SARS-CoV-2 challenge (A) study design, (B) body weight, (C) survival, (D) hemorrhagic scores, (E) lung viral titers, and (F) SARS-CoV-2 envelope (E) and nucleocapsid (N) gene subgenomic RNA (sgRNA).

(G–Q) Reduction of SARS-CoV-2 replication and disease in cynomolgus macaques by prophylactic administration of an NTD-neutralizing Ab DH1050.1 or an NTD *in vitro* infection-enhancing Ab DH1052.

(G) DH1050.1 and DH1052 prophylaxis cynomolgus macaque (n = 5 per group) study design. CH65 was used as a negative control Ab.

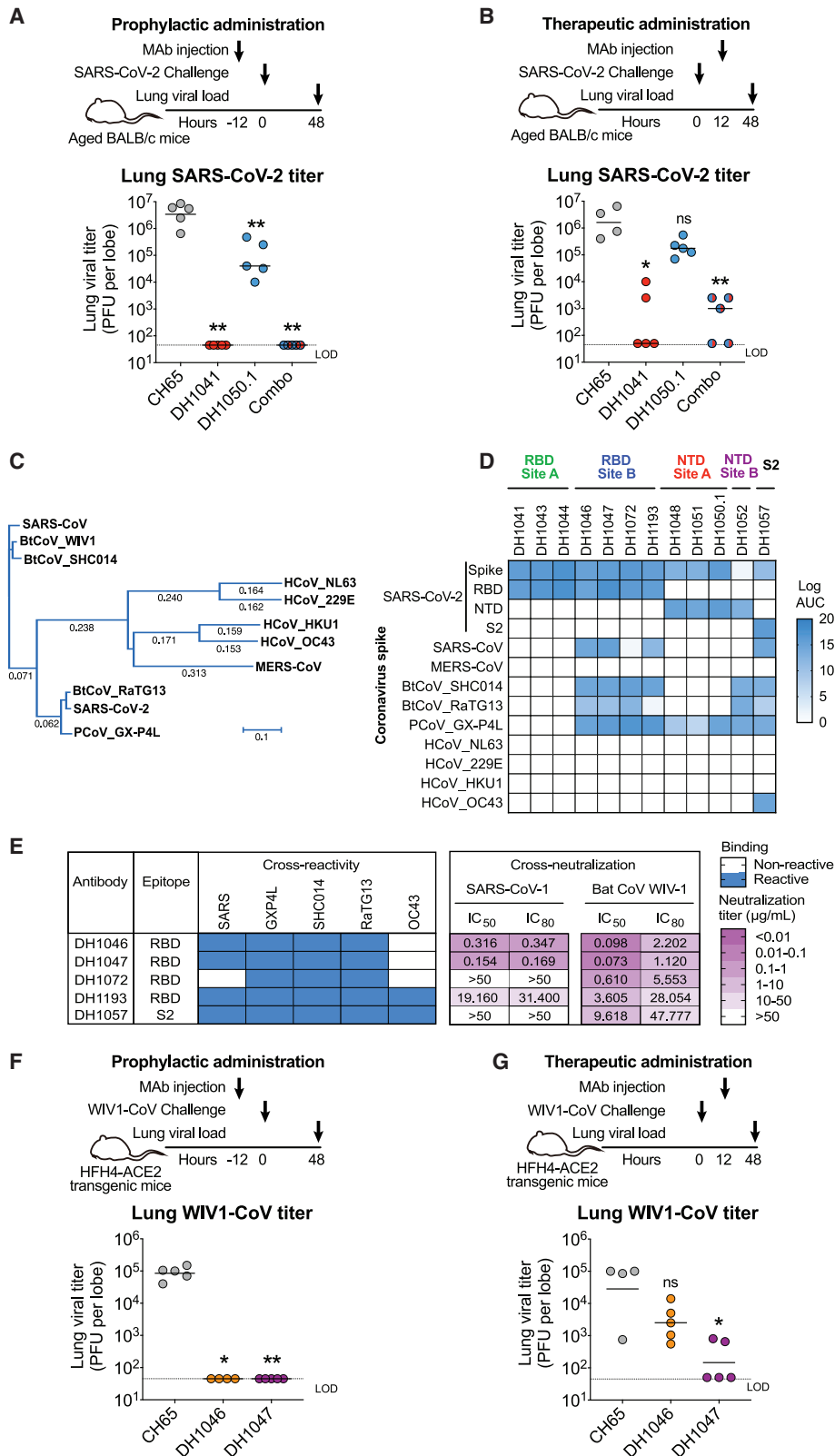
(H and I) Serum human IgG concentrations at (H) day –5 and (I) day 2.

(J and K) Day 2 serum neutralization titers shown as the reciprocal serum dilution that inhibits 50% (ID₅₀) of (J) pseudotyped SARS-CoV-2 replication in 293T/ACE2 cells or (K) SARS-CoV-2 replication in Vero cells.

(L and M) Lung histopathology 4 days post-infection. Lung sections were scored for (L) inflammation by hematoxylin and eosin (H&E) staining, and for (M) the presence of SARS-CoV-2 nucleocapsid by immunohistochemistry (IHC) staining.

(N–Q) Viral load quantified as SARS-CoV-2 E gene sgRNA and N gene sgRNA in (N and O) bronchoalveolar lavage (BAL) or (P and Q) nasal swab fluid on day 2 and day 4 post challenge. LOD, limit of detection. Statistical significance in all the panels were determined using Wilcoxon rank-sum exact test. Horizontal bars are the group mean except in (J and K) where geometric mean is shown. Error bars indicate standard error of the mean. Asterisks show the statistical significance between the indicated group and CH65 control group: ns, not significant, *p < 0.05, **p < 0.01, ***p < 0.001.

See also Figure S4, S5, and S6.



(legend on next page)

and Ab Fc for virus uptake (Lee et al., 2020). Previous studies have demonstrated that uptake of MERS-CoV or SARS-CoV has mostly been mediated by Fc γ R1a on the surface of macrophages (Bournazos et al., 2020; Wan et al., 2020; Yip et al., 2016). In contrast, we identified SARS-CoV-2 RBD Abs utilized Fc γ R1b or Fc γ R1. Second, non-neutralizing NTD Abs mediated Fc γ R-independent infection enhancement in two different Fc γ R-negative, ACE2-expressing cell types. The mechanism of Fc γ R-negative *in vitro* enhancement remains unclear, but one previous study has reported that select NTD Abs can enhance S binding to ACE2 (Liu et al., 2020b).

Macrophages and other phagocytes are the target cells that take up MERS-CoV leading to infection enhancement (Hui et al., 2020; Wan et al., 2020; Zhou et al., 2014). In contrast, neither SARS-CoV nor SARS-CoV-2 productively infect macrophages (Bournazos et al., 2020; Hui et al., 2020; Yip et al., 2016). However, a recent study demonstrated that alveolar macrophages harboring SARS-CoV-2 RNA produce T cell chemoattractants leading to T cell interferon (IFN)- γ production that, in turn, stimulates inflammatory cytokine release from alveolar macrophages (Grant et al., 2021). Why severe lung pathology and inflammatory cytokine production occurred in only 1 of 46 monkeys is unknown but may relate to host-specific differences regulating inflammatory cytokine production (Bastard et al., 2020; Zhang et al., 2020). It is important to note that the one monkey that developed alveolar and perivascular edema and elevated BAL inflammatory cytokines could have been caused by Ab enhancement of disease or could have been due to unknown factors that caused more severe disease in animal BB536A that were unrelated to DH1052 administration. That none of 6 animals infused with a higher dose (30 mg/kg) of DH1052 had enhanced pulmonary disease supports the hypothesis that the lung pathology may have been a severe case of COVID-19 lung disease unrelated to Ab infusion.

Previous studies with vaccine-induced Abs against SARS-CoV have also shown *in vitro* infection enhancement but no *in vivo* infection enhancement in hamsters (Kam et al., 2007). One explanation for this results may be that *in vitro* enhancing Abs may have the ability to suppress SARS-CoV-2 replication *in vivo* through non-neutralizing FcR-mediated Ab effector functions (Bournazos et al., 2020; Schäfer et al., 2021). A recent study in a SARS-CoV-2 mouse model of acquisition suggested that Fc effector functions contribute to the protective activity of SARS-CoV-2-neutralizing Abs C104, C002, and C110 (Schäfer et al., 2021). Thus, Ab effector functions may contribute to the outcome *in vivo* but not be ac-

counted for in SARS-CoV-2 enhancement or neutralization assays *in vitro*. Consistent with previous findings for human IgG (Dekkers et al., 2017), we observed that DH1052 Ab can bind to select murine Fc γ Rs.

In vivo, SARS-CoV-2 S trimers circulate in the presence of a polyclonal Ab response. We observed bivalent and trivalent combinations of Fabs from RBD and NTD-neutralizing Abs can recognize the same protomer of the S trimer. We speculate given the direction of the C-termini of the Fabs and molecular modeling that three IgGs targeting distinct epitopes may be able to interact with the same protomer, if the IgG hinge region is sufficiently flexible and the RBD is in an optimal up conformation for simultaneous engagement. Simultaneous engagement by RBD and NTD Abs could improve synergism of neutralization (Zost et al., 2020a) and avidity of the immune complexes for Fc γ Rs on effector cells (Nagashima et al., 2011; Nagashima et al., 2008; Wang et al., 2017). Additionally, these results indicate three epitopes that Ab prophylactics could target on RBD and NTD in order to occupy S trimers with multiple IgGs.

Limitations of the study

Although rare enhanced immunopathology was observed in monkeys, it is difficult to predict whether this phenomenon will occur in the setting of human infection or vaccination. Furthermore, RBD and NTD antibodies were the focus of this study; therefore, whether antibodies of other specificities mediate ADE warrants further study. Additionally, the macaque model has a rather short course of infection; thus, effects of the SARS-CoV-2 antibody on persistent SARS-CoV-2 infection were not examined here.

Finally, administration of COVID-19 convalescent sera to over 35,000 COVID-19 patients has demonstrated the treatment to be safe and is not associated with enhanced disease (Joyner et al., 2020). Of greater importance is that both the Pfizer/BioNTech and Moderna mRNA-lipid nanoparticle (LNP) vaccine efficacy trials have completed and showed ~95% vaccine efficacy (Jackson et al., 2020; Polack et al., 2020). That the Moderna mRNA-LNP COVID-19 vaccine efficacy trial had 30 severe cases of COVID-19 occur—all in the placebo group (Baden et al., 2021), demonstrated that, if ADE of infection or lung pathology will occur in humans with vaccination, it will be rare. A recent study demonstrated that suboptimal neutralizing Ab level is a significant predictor of severity for SARS-CoV-2 (Garcia-Beltran et al., 2020). Thus, even with the rarity of severe lung pathology associated with presence of anti-spike Ab in animal model studies reported here, it will be important to continue to monitor on-going COVID-19 vaccination for the possibility of vaccine

Figure 6. RBD Abs that mediate Fc γ R-dependent infection enhancement *in vitro* protect mice from SARS-CoV-2 or bat WIV1-CoV challenge

(A and B) Protection of BALB/c mice (n = 5 per group) from mouse-adapted SARS-CoV-2 (SARS-CoV-2 2AA MA) by (A) prophylactic or (B) therapeutic RBD and/or NTD Ab administration. Ab CH65 served as a negative control. Titers of infectious virus in the lung were examined 48 h post-infection.

(C) Maximum likelihood tree of Spike amino acid sequences for human, bat, and pangolin coronaviruses.

(D) Monoclonal RBD, NTD and S2 Ab ELISA binding titer for soluble S protein ectodomains from human and animal coronaviruses. Titers are log area-under-the-curve (AUC).

(E) SARS-CoV and bat WIV1-CoV cross-neutralization titers for cross-reactive RBD and S2 Abs.

(F and G) Protection of HFH4-hACE2-transgenic mice (n = 5 per group) from SARS-related bat WIV1-CoV challenge by (A) prophylactic or (B) therapeutic RBD Ab administration. Lung viral titers were examined at 48 h post-infection. Statistical significance in all the panels were determined using Wilcoxon rank-sum exact test. Horizontal bars are the group mean. Asterisks show the statistical significance between the indicated group and CH65 control group: ns, not significant, *p < 0.05, **p < 0.01.

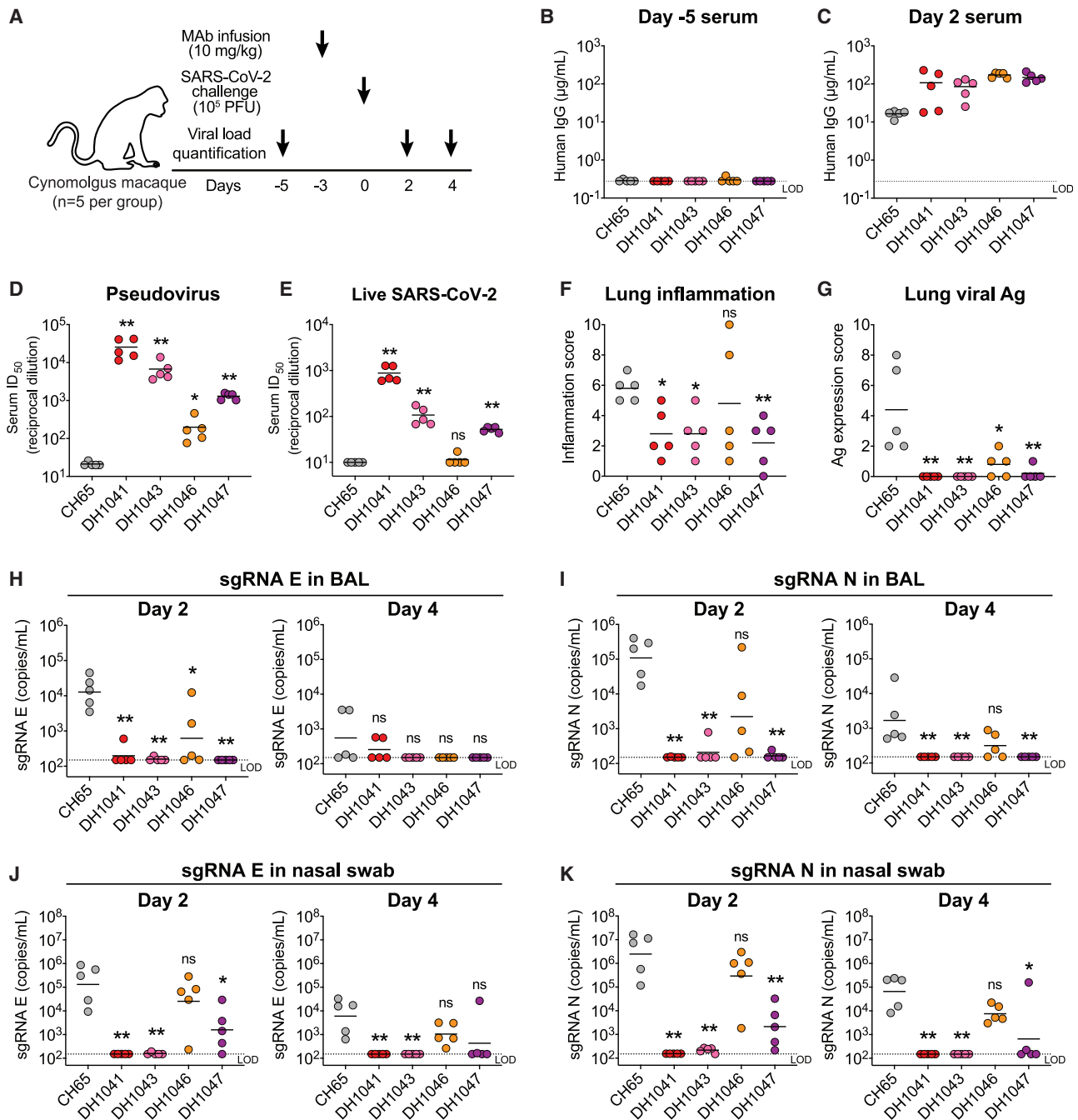


Figure 7. RBD Abs that mediate $Fc\gamma R$ -dependent infection enhancement *in vitro* protect non-human primates from SARS-CoV-2 challenge

(A) Cynomolgus macaques (n = 5 per group) RBD Ab SARS-CoV-2 challenge study design. DH1041, DH1043, DH1046, DH1047, or an irrelevant CH65 were infused into macaques.

(B and C) Serum human IgG concentrations at day -5 (B) and day 2 (C).

(D and E) Day 2 serum neutralization titers shown as the reciprocal serum dilution that inhibits 50% (ID_{50}) of (D) pseudotyped SARS-CoV-2 replication in 293T/ACE2 cells or (E) SARS-CoV-2 replication in Vero cells.

(F and G) Lung histopathology for (F) inflammation by H&E staining and (G) the presence of SARS-CoV-2 nucleocapsid by IHC staining 4 days post-challenge.

(H–K) Viral load quantified as SARS-CoV-2 E gene sgRNA and N gene sgRNA in (H and I) bronchoalveolar lavage (BAL) or (J and K) nasal swab fluid on day 2 and day 4 post-challenge.

Statistical significance in all the panels were determined using Wilcoxon rank-sum exact test. Horizontal bars are the group mean except in (D and E) where group geometric mean is shown. Asterisks show the statistical significance between indicated group and CH65 control group: ns, not significant, *p < 0.05, **p < 0.01.

See also Figure S4, S5, and S7.

associated enhanced disease when suboptimal neutralizing Ab titers are induced (Haynes et al., 2020).

STAR★METHODS

Detailed methods are provided in the online version of this paper and include the following:

- **KEY RESOURCES TABLE**
- **RESOURCE AVAILABILITY**
 - Lead contact
 - Materials availability
 - Data and code availability
- **EXPERIMENTAL MODEL AND SUBJECT DETAILS**
 - Human subjects
 - Symptom data collections
 - Non-human primate model
 - Mouse models
- **METHOD DETAILS**
 - Expression of recombinant viral proteins
 - Antigen-specific single B cell sorting
 - PCR Amplification of human Ab genes
 - Expression of Ab viable region genes as full-length IgG recombinant mAbs
 - Ab binding ELISA
 - Affinity measurements
 - Surface plasmon resonance Ab blocking assay
 - ACE2-blocking assay
 - Negative-stain electron microscopy
 - Image processing of negative stain images
 - Cryo-EM sample preparation, data collection and processing
 - Cryo-EM structure fitting and analysis
 - Live SARS-CoV-2 neutralization assays
 - Pseudo-typed SARS-CoV-2 neutralization assay and infection-enhancing assays
 - Non-human primate protection study
 - Histopathology and Immunohistochemistry (IHC)
 - Luminex assay
 - Mouse protection study
 - Viral RNA extraction and quantification
 - Subgenomic mRNA assay
- **QUANTIFICATION AND STATISTICAL ANALYSIS**

SUPPLEMENTAL INFORMATION

Supplemental information can be found online at <https://doi.org/10.1016/j.cell.2021.06.021>.

ACKNOWLEDGMENTS

We thank the COVID-19 donors enrolled in the Molecular and Epidemiological Study of Suspected Infection protocol (MESSI), the MESSI clinical support team, the Duke Human Vaccine Institute (DHVI) Clinical Accessioning Unit Core, and the DHVI Immunology and Virology Quality Assessment Core for sample procurement, processing, and biobanking. We thank J. Gilmore, S. Slater, K. Hwang, A.Y. Abuahmad, T. Evangelous, C. Jones, K. Anasti, M. Berry, S. Venkatayogi, P. Rawls, L. Smith, J. Hwang, B. Bryan, J. Li, H. Chen, N. De Naeyer, the DHVI Flow Cytometry Facility, and the Duke BMI CORE facility for technical assistance. We thank Drs. M. Gagne and D.C.

Douek at the National Institutes of Health (NIH) for assistant with subgenomic RNA assays. We thank K. Soderberg, E. Donahue, A. Karlsson, A. Newman, and W. Edwards for program management. COVID-19 donor sample processing, flow cytometric sorting, and replication-competent virus neutralization assays were performed in the Duke Regional Biocontainment Laboratory, which received partial support for construction from the NIH, NIAID (UC6-AI058607). This work was supported by NIH, NIAID, DAIDS grant AI142596 (B.F.H.), the State of NC funded by the Coronavirus Aid, Relief, and Economic Security Act (CARES Act) (B.F.H.), the Ting Tsung & Wei Fong Chao Foundation (B.F.H.), NIH supplement to R01 AI145687 (P.A.), NIH grants R01AI157155 and U54CA260543 (R.S.B.), NIH F32 AI152296 (D.R.M.), previous grant NIH NIAID T32 AI007151 (D.R.M.), Burroughs Wellcome Fund Postdoctoral Enrichment Program (D.R.M.), NIH NIAID U19AI142596 grant (B.F.H.), NIH R01 AI146779 and a MassCPR grant (A.G.S.), training grants: NIGMS T32 GM007753 (B.M.H. and T.M.C.), T32 AI007245 (J.F.), and a cooperative agreement with DOD/DARPA (HR0011-17-2-0069; G.D.S). Cryo-EM data were collected at the National Center for Cryo-EM Access and Training and the Simons Electron Microscopy Center located at the New York Structural Biology Center, supported by the NIH Common Fund Transformative High Resolution Cryo-EM program (U24 GM129539) and by grants from the Simons Foundation (SF349247) and NY State. We thank E. Eng, C. Hernandez, and D. Bobe for assistance with cryo-EM experiments. We thank M. DeLong, C. Kneifel, M. Newton, V. Orlikowski, T. Milledge, and D. Lane from the Duke Office of Information Technology and Research Computing, and Duke Research Computing (<https://rc.duke.edu/>; NIH 1S10OD018164-01). We thank L. Pessaint, A. Cook, A. Dodson, K. Steingrebe, and B. Bart at BIOQUAL for assistance with macaque studies. Macaques were obtained by BIOQUAL from the Caribbean Primate Research Center (Grants P40 OD012217 and 2U42OD021458 from ORIP/OD/NIH).

AUTHOR CONTRIBUTIONS

D.L., D.R.M., A.S., X.L., S.M.A., K.C., L.V.T., T.D.S., R.P., V.G., M.D., M.B., T.V.H., T.H.O., E.L., A.F., F.C., G.E.H., A.S., K.T., C.J., L.G.P., C.M., A.M., E.S., D.W.C., K.W.B., M.M., B.M.N., and L.L.S. performed experiments and analyzed data. R.J.E., K. Mansouri, K. Manne, S.G., K.J., M.K., V.S., and P.A. performed structure experiments and analysis. W.R. and Y.W. provided statistical analyses. K.W., C.T.D., T.N.D., G.D.S., D.C.M., C.W.W., E.P., M.A.M., I.N.M., R.S., H.A., M.G.L., and R.S.B. oversaw studies. A.G.S., J.F., B.M.H., T.M.C., I-T.T., T.Z., P.D.K., J.M., and B.G. provided key reagents. K.O.S. and B.F.H. conceived, designed, and supervised the study and evaluated all data. D.L., R.J.E., P.A., K.O.S., and B.F.H. wrote the paper. All authors reviewed and approved the manuscript.

DECLARATION OF INTERESTS

B.F.H., G.D.S., K.O.S., R.P., D.L., P.A., and X.L. have applied for patents concerning SARS-CoV-2 Abs that are related to this work. All other authors declare no conflict of interest.

Received: February 10, 2021

Revised: April 6, 2021

Accepted: June 11, 2021

Published: June 18, 2021

REFERENCES

- Afonine, P.V., Poon, B.K., Read, R.J., Sobolev, O.V., Terwilliger, T.C., Urzhumtsev, A., and Adams, P.D. (2018). Real-space refinement in PHENIX for cryo-EM and crystallography. *Acta Crystallogr. D Struct. Biol.* **74**, 531–544.
- Arvin, A.M., Fink, K., Schmid, M.A., Cathcart, A., Spreafico, R., Havenar-Daughton, C., Lanzavecchia, A., Corti, D., and Virgin, H.W. (2020). A perspective on potential antibody-dependent enhancement of SARS-CoV-2. *Nature* **584**, 353–363.
- Baden, L.R., El Sahly, H.M., Essink, B., Kotloff, K., Frey, S., Novak, R., Diemert, D., Spector, S.A., Rouphael, N., Creech, C.B., et al.; COVE Study Group

- (2021). Efficacy and Safety of the mRNA-1273 SARS-CoV-2 Vaccine. *N. Engl. J. Med.* 384, 403–416.
- Bastard, P., Rosen, L.B., Zhang, Q., Michailidis, E., Hoffmann, H.H., Zhang, Y., Dorgham, K., Philippot, Q., Rosain, J., Béziat, V., et al.; HGID Lab; NIAID-USUHS Immune Response to COVID Group; COVID Clinicians; COVID-STORM Clinicians; Imagine COVID Group; French COVID Cohort Study Group; Milieu Intérieur Consortium; CoV-Contact Cohort; Amsterdam UMC Covid-19 Biobank; COVID Human Genetic Effort (2020). Autoantibodies against type I IFNs in patients with life-threatening COVID-19. *Science* 370, eabd4585.
- Baum, A., Ajithdoss, D., Copin, R., Zhou, A., Lanza, K., Negron, N., Ni, M., Wei, Y., Mohammadi, K., Musser, B., et al. (2020a). REGN-COV2 antibodies prevent and treat SARS-CoV-2 infection in rhesus macaques and hamsters. *Science* 370, 1110–1115.
- Baum, A., Fulton, B.O., Wloga, E., Copin, R., Pascal, K.E., Russo, V., Giordano, S., Lanza, K., Negron, N., Ni, M., et al. (2020b). Antibody cocktail to SARS-CoV-2 spike protein prevents rapid mutational escape seen with individual antibodies. *Science* 369, 1014–1018.
- Berry, J.D., Jones, S., Drebot, M.A., Andonov, A., Sabara, M., Yuan, X.Y., Weingartl, H., Fernando, L., Marszal, P., Gren, J., et al. (2004). Development and characterisation of neutralising monoclonal antibody to the SARS-coronavirus. *J. Virol. Methods* 120, 87–96.
- Bournazos, S., Gupta, A., and Ravetch, J.V. (2020). The role of IgG Fc receptors in antibody-dependent enhancement. *Nat. Rev. Immunol.* 20, 633–643.
- Brouwer, P.J.M., Caniels, T.G., van der Straten, K., Snitselaar, J.L., Aldon, Y., Bangaru, S., Torres, J.L., Okba, N.M.A., Claireaux, M., Kerster, G., et al. (2020). Potent neutralizing antibodies from COVID-19 patients define multiple targets of vulnerability. *Science* 369, 643–650.
- Cao, Y., Su, B., Guo, X., Sun, W., Deng, Y., Bao, L., Zhu, Q., Zhang, X., Zheng, Y., Geng, C., et al. (2020). Potent Neutralizing Antibodies against SARS-CoV-2 Identified by High-Throughput Single-Cell Sequencing of Convalescent Patients' B Cells. *Cell* 182, 73–84.
- Chi, X., Yan, R., Zhang, J., Zhang, G., Zhang, Y., Hao, M., Zhang, Z., Fan, P., Dong, Y., Yang, Y., et al. (2020). A potent neutralizing human antibody reveals the N-terminal domain of the Spike protein of SARS-CoV-2 as a site of vulnerability. *Science* 369, 650–655.
- Coleman, C.M., and Frieman, M.B. (2015). Growth and Quantification of MERS-CoV Infection. *Curr. Protoc. Microbiol.* 37, 15E.2.1–15E.2.19.
- Croll, T.I. (2018). ISOLDE: a physically realistic environment for model building into low-resolution electron-density maps. *Acta Crystallogr. D Struct. Biol.* 74, 519–530.
- Dekkers, G., Bentlage, A.E.H., Stegmann, T.C., Howie, H.L., Lissenberg-Thunnissen, S., Zimring, J., Rispen, T., and Vidarsson, G. (2017). Affinity of human IgG subclasses to mouse Fc gamma receptors. *MAbs* 9, 767–773.
- Dinnon, K.H., 3rd, Leist, S.R., Schäfer, A., Edwards, C.E., Martinez, D.R., Montgomery, S.A., West, A., Yount, B.L., Jr., Hou, Y.J., Adams, L.E., et al. (2020). A mouse-adapted model of SARS-CoV-2 to test COVID-19 countermeasures. *Nature* 586, 560–566.
- Edwards, R.J., Mansouri, K., Stalls, V., Manne, K., Watts, B., Parks, R., Janowska, K., Gobeil, S.M.C., Kopp, M., Li, D., et al. (2021). Cold sensitivity of the SARS-CoV-2 spike ectodomain. *Nat. Struct. Mol. Biol.* 28, 128–131.
- Emsley, P., and Cowtan, K. (2004). Coot: model-building tools for molecular graphics. *Acta Crystallogr. D Biol. Crystallogr.* 60, 2126–2132.
- Emsley, P., Lohkamp, B., Scott, W.G., and Cowtan, K. (2010). Features and development of Coot. *Acta Crystallogr. D Biol. Crystallogr.* 66, 486–501.
- García-Beltrán, W.F., Lam, E.C., Astudillo, M.G., Yang, D., Miller, T.E., Feldman, J., Hauser, B.M., Caradonna, T.M., Clayton, K.L., Nitido, A.D., et al. (2020). COVID-19 neutralizing antibodies predict disease severity and survival. *medRxiv*. Published October 20, 2020. <https://doi.org/10.1101/2020.10.15.20213512>.
- Goddard, T.D., Huang, C.C., Meng, E.C., Pettersen, E.F., Couch, G.S., Morris, J.H., and Ferrin, T.E. (2018). UCSF ChimeraX: Meeting modern challenges in visualization and analysis. *Protein Sci.* 27, 14–25.
- Graham, B.S. (2020). Rapid COVID-19 vaccine development. *Science* 368, 945–946.
- Grant, R.A., Morales-Nebreda, L., Markov, N.S., Swaminathan, S., Querrey, M., Guzman, E.R., Abbott, D.A., Donnelly, H.K., Donayre, A., Goldberg, I.A., et al.; NU SCRIPT Study Investigators (2021). Circuits between infected macrophages and T cells in SARS-CoV-2 pneumonia. *Nature* 590, 635–641.
- Hansen, J., Baum, A., Pascal, K.E., Russo, V., Giordano, S., Wloga, E., Fulton, B.O., Yan, Y., Koon, K., Patel, K., et al. (2020). Studies in humanized mice and convalescent humans yield a SARS-CoV-2 antibody cocktail. *Science* 369, 1010–1014.
- Hassan, A.O., Case, J.B., Winkler, E.S., Thackray, L.B., Kafai, N.M., Bailey, A.L., McCune, B.T., Fox, J.M., Chen, R.E., Alsoussi, W.B., et al. (2020). A SARS-CoV-2 Infection Model in Mice Demonstrates Protection by Neutralizing Antibodies. *Cell* 182, 744–753.
- Hauser, B.M., Sangesland, M., Lam, E.C., Feldman, J., Yousif, A.S., Caradonna, T.M., Balazs, A.B., Lingwood, D., and Schmidt, A.G. (2020). Engineered receptor binding domain immunogens elicit pan-coronavirus neutralizing antibodies. *bioRxiv*, 2020.2012.2007.415216.
- Haynes, B.F., Corey, L., Fernandes, P., Gilbert, P.B., Hotez, P.J., Rao, S., Santos, M.R., Schuitemaker, H., Watson, M., and Arvin, A. (2020). Prospects for a safe COVID-19 vaccine. *Sci. Transl. Med.* 12, eabe0948.
- Henderson, R., Edwards, R.J., Mansouri, K., Janowska, K., Stalls, V., Gobeil, S.M.C., Kopp, M., Li, D., Parks, R., Hsu, A.L., et al. (2020). Controlling the SARS-CoV-2 spike glycoprotein conformation. *Nat. Struct. Mol. Biol.* 27, 925–933.
- Hou, Y.J., Okuda, K., Edwards, C.E., Martinez, D.R., Asakura, T., Dinnon, K.H., 3rd, Kato, T., Lee, R.E., Yount, B.L., Mascenik, T.M., et al. (2020). SARS-CoV-2 Reverse Genetics Reveals a Variable Infection Gradient in the Respiratory Tract. *Cell* 182, 429–446.
- Hsieh, C.L., Goldsmith, J.A., Schaub, J.M., DiVenere, A.M., Kuo, H.C., Javanmardi, K., Le, K.C., Wrapp, D., Lee, A.G., Liu, Y., et al. (2020). Structure-based design of prefusion-stabilized SARS-CoV-2 spikes. *Science* 369, 1501–1505.
- Hui, K.P.Y., Cheung, M.C., Perera, R.A.P.M., Ng, K.C., Bui, C.H.T., Ho, J.C.W., Ng, M.M.T., Kuok, D.I.T., Shih, K.C., Tsao, S.W., et al. (2020). Tropism, replication competence, and innate immune responses of the coronavirus SARS-CoV-2 in human respiratory tract and conjunctiva: an analysis in ex vivo and in-vitro cultures. *Lancet Respir. Med.* 8, 687–695.
- Huo, J., Le Bas, A., Ruza, R.R., Duyvesteyn, H.M.E., Mikolajek, H., Malinauskas, T., Tan, T.K., Rijal, P., Dumoux, M., Ward, P.N., et al. (2020). Neutralizing nanobodies bind SARS-CoV-2 spike RBD and block interaction with ACE2. *Nat. Struct. Mol. Biol.* 27, 846–854.
- Iwasaki, A., and Yang, Y. (2020). The potential danger of suboptimal antibody responses in COVID-19. *Nat. Rev. Immunol.* 20, 339–341.
- Jackson, L.A., Anderson, E.J., Roupael, N.G., Roberts, P.C., Makhene, M., Coler, R.N., McCullough, M.P., Chappell, J.D., Denison, M.R., Stevens, L.J., et al.; mRNA-1273 Study Group (2020). An mRNA Vaccine against SARS-CoV-2 - Preliminary Report. *N. Engl. J. Med.* 383, 1920–1931.
- Jaume, M., Yip, M.S., Cheung, C.Y., Leung, H.L., Li, P.H., Kien, F., Dutry, I., Callendret, B., Escriou, N., Altmeyer, R., et al. (2011). Anti-severe acute respiratory syndrome coronavirus spike antibodies trigger infection of human immune cells via a pH- and cysteine protease-independent FcγR pathway. *J. Virol.* 85, 10582–10597.
- Jones, B.E., Brown-Augsburger, P.L., Corbett, K.S., Westendorf, K., Davies, J., Cujec, T.P., Wiethoff, C.M., Blackbourne, J.L., Heinz, B.A., Foster, D., et al. (2020). LY-CoV555, a rapidly isolated potent neutralizing antibody, provides protection in a non-human primate model of SARS-CoV-2 infection. *bioRxiv*. Published online October 1, 2020. <https://doi.org/10.1101/2020.09.30.318972>.
- Joyner, M.J., Senefeld, J.W., Klassen, S.A., Mills, J.R., Johnson, P.W., Theel, E.S., Wiggins, C.C., Bruno, K.A., Klompas, A.M., Lesser, E.R., et al. (2020). Effect of Convalescent Plasma on Mortality among Hospitalized Patients with COVID-19: Initial Three-Month Experience. *medRxiv*, 2020.2008.2012.20169359.

- Ju, B., Zhang, Q., Ge, J., Wang, R., Sun, J., Ge, X., Yu, J., Shan, S., Zhou, B., Song, S., et al. (2020). Human neutralizing antibodies elicited by SARS-CoV-2 infection. *Nature* **584**, 115–119.
- Kam, Y.W., Kien, F., Roberts, A., Cheung, Y.C., Lamirande, E.W., Vogel, L., Chu, S.L., Tse, J., Guamer, J., Zaki, S.R., et al. (2007). Antibodies against trimeric S glycoprotein protect hamsters against SARS-CoV challenge despite their capacity to mediate FcγRIII-dependent entry into B cells in vitro. *Vaccine* **25**, 729–740.
- Kepler, T.B., Munshaw, S., Wiehe, K., Zhang, R., Yu, J.S., Woods, C.W., Denny, T.N., Tomaras, G.D., Alam, S.M., Moody, M.A., et al. (2014). Reconstructing a B-Cell Clonal Lineage. II. Mutation, Selection, and Affinity Maturation. *Front. Immunol.* **5**, 170.
- Kint, J., Maier, H.J., and Jagt, E. (2015). Quantification of infectious bronchitis coronavirus by titration in vitro and in ovo. *Methods Mol. Biol.* **1282**, 89–98.
- Korber, B., Fischer, W.M., Gnanakaran, S., Yoon, H., Theiler, J., Abfalterer, W., Hengartner, N., Giorgi, E.E., Bhattacharya, T., Foley, B., et al.; Sheffield COVID-19 Genomics Group (2020). Tracking Changes in SARS-CoV-2 Spike: Evidence that D614G Increases Infectivity of the COVID-19 Virus. *Cell* **182**, 812–827.
- Lee, W.S., Wheatley, A.K., Kent, S.J., and DeKosky, B.J. (2020). Antibody-dependent enhancement and SARS-CoV-2 vaccines and therapies. *Nat. Microbiol.* **5**, 1185–1191.
- Leist, S.R., Dinno, K.H., 3rd, Schäfer, A., Tse, L.V., Okuda, K., Hou, Y.J., West, A., Edwards, C.E., Sanders, W., Fritch, E.J., et al. (2020a). A Mouse-Adapted SARS-CoV-2 Induces Acute Lung Injury and Mortality in Standard Laboratory Mice. *Cell* **183**, 1070–1085.
- Leist, S.R., Schäfer, A., and Martinez, D.R. (2020b). Cell and animal models of SARS-CoV-2 pathogenesis and immunity. *Dis. Model. Mech.* **13**, dmm046581.
- Liao, H.X., Levesque, M.C., Nagel, A., Dixon, A., Zhang, R., Walter, E., Parks, R., Whitesides, J., Marshall, D.J., Hwang, K.K., et al. (2009). High-throughput isolation of immunoglobulin genes from single human B cells and expression as monoclonal antibodies. *J. Virol. Methods* **158**, 171–179.
- Liao, H.X., Lynch, R., Zhou, T., Gao, F., Alam, S.M., Boyd, S.D., Fire, A.Z., Roskin, K.M., Schramm, C.A., Zhang, Z., et al.; NISC Comparative Sequencing Program (2013). Co-evolution of a broadly neutralizing HIV-1 antibody and founder virus. *Nature* **496**, 469–476.
- Liebschner, D., Afonine, P.V., Baker, M.L., Bunkóczi, G., Chen, V.B., Croll, T.I., Hintze, B., Hung, L.W., Jain, S., McCoy, A.J., et al. (2019). Macromolecular structure determination using X-rays, neutrons and electrons: recent developments in Phenix. *Acta Crystallogr. D Struct. Biol.* **75**, 861–877.
- Liu, L., Wang, P., Nair, M.S., Yu, J., Rapp, M., Wang, Q., Luo, Y., Chan, J.F., Sahi, V., Figueroa, A., et al. (2020a). Potent neutralizing antibodies against multiple epitopes on SARS-CoV-2 spike. *Nature* **584**, 450–456.
- Liu, Y., Soh, W.T., Tada, A., Arakawa, A., Matsuoka, S., Nakayama, E.E., Li, S., Ono, C., Torii, S., Kishida, K., et al. (2020b). An infectivity-enhancing site on the SARS-CoV-2 spike protein is targeted by COVID-19 patient antibodies. *bioRxiv*, 2020.2012.2018.423358.
- Menachery, V.D., Yount, B.L., Jr., Sims, A.C., Debink, K., Agnihothram, S.S., Gralinski, L.E., Graham, R.L., Scobey, T., Plante, J.A., Royal, S.R., et al. (2016). SARS-like WIV1-CoV poised for human emergence. *Proc. Natl. Acad. Sci. USA* **113**, 3048–3053.
- Nagashima, H., Tezuka, T., Tsuchida, W., Maeda, H., Kohroki, J., and Masuho, Y. (2008). Tandemly repeated Fc domain augments binding avidities of antibodies for FcγRIII, resulting in enhanced antibody-dependent cellular cytotoxicity. *Mol. Immunol.* **45**, 2752–2763.
- Nagashima, H., Ootsubo, M., Fukazawa, M., Motoi, S., Konakahara, S., and Masuho, Y. (2011). Enhanced antibody-dependent cellular phagocytosis by chimeric monoclonal antibodies with tandemly repeated Fc domains. *J. Biosci. Bioeng.* **111**, 391–396.
- Naldini, L., Blömer, U., Gage, F.H., Trono, D., and Verma, I.M. (1996). Efficient transfer, integration, and sustained long-term expression of the transgene in adult rat brains injected with a lentiviral vector. *Proc. Natl. Acad. Sci. USA* **93**, 11382–11388.
- Pak, J.E., Sharon, C., Satkunarajah, M., Auperin, T.C., Cameron, C.M., Kelvin, D.J., Seetharaman, J., Cochrane, A., Plummer, F.A., Berry, J.D., and Rini, J.M. (2009). Structural insights into immune recognition of the severe acute respiratory syndrome coronavirus S protein receptor binding domain. *J. Mol. Biol.* **388**, 815–823.
- Perez, L.G., Costa, M.R., Todd, C.A., Haynes, B.F., and Montefiori, D.C. (2009). Utilization of immunoglobulin G Fc receptors by human immunodeficiency virus type 1: a specific role for antibodies against the membrane-proximal external region of gp41. *J. Virol.* **83**, 7397–7410.
- Pettersen, E.F., Goddard, T.D., Huang, C.C., Couch, G.S., Greenblatt, D.M., Meng, E.C., and Ferrin, T.E. (2004). UCSF Chimera—a visualization system for exploratory research and analysis. *J. Comput. Chem.* **25**, 1605–1612.
- Pinto, D., Park, Y.J., Beltramello, M., Walls, A.C., Tortorici, M.A., Bianchi, S., Jaconi, S., Culap, K., Zatta, F., De Marco, A., et al. (2020). Cross-neutralization of SARS-CoV-2 by a human monoclonal SARS-CoV antibody. *Nature* **583**, 290–295.
- Polack, F.P., Thomas, S.J., Kitchin, N., Absalon, J., Gurtman, A., Lockhart, S., Perez, J.L., Pérez Marc, G., Moreira, E.D., Zerbini, C., et al.; C4591001 Clinical Trial Group (2020). Safety and Efficacy of the BNT162b2 mRNA Covid-19 Vaccine. *N. Engl. J. Med.* **383**, 2603–2615.
- Punjani, A., Rubinstein, J.L., Fleet, D.J., and Brubaker, M.A. (2017). cryo-SPARC: algorithms for rapid unsupervised cryo-EM structure determination. *Nat. Methods* **14**, 290–296.
- Robbiani, D.F., Gaebler, C., Muecksch, F., Lorenzi, J.C.C., Wang, Z., Cho, A., Agudelo, M., Barnes, C.O., Gazumyan, A., Finkin, S., et al. (2020). Convergent antibody responses to SARS-CoV-2 in convalescent individuals. *Nature* **584**, 437–442.
- Rockx, B., Kuiken, T., Herfst, S., Bestebroer, T., Lamers, M.M., Oude Munnink, B.B., de Meulder, D., van Amerongen, G., van den Brand, J., Okba, N.M.A., et al. (2020). Comparative pathogenesis of COVID-19, MERS, and SARS in a nonhuman primate model. *Science* **368**, 1012–1015.
- Rogers, T.F., Zhao, F., Huang, D., Beutler, N., Burns, A., He, W.T., Limbo, O., Smith, C., Song, G., Woehl, J., et al. (2020). Isolation of potent SARS-CoV-2 neutralizing antibodies and protection from disease in a small animal model. *Science* **369**, 956–963.
- Saunders, K.O. (2019). Conceptual Approaches to Modulating Antibody Effector Functions and Circulation Half-Life. *Front. Immunol.* **10**, 1296.
- Schäfer, A., Muecksch, F., Lorenzi, J.C.C., Leist, S.R., Cipolla, M., Bournazos, S., Schmidt, F., Maison, R.M., Gazumyan, A., Martinez, D.R., et al. (2021). Antibody potency, effector function, and combinations in protection and therapy for SARS-CoV-2 infection in vivo. *J. Exp. Med.* **218**, e20201993.
- Scheres, S.H. (2012). A Bayesian view on cryo-EM structure determination. *J. Mol. Biol.* **415**, 406–418.
- Scheres, S.H.W. (2016). Processing of Structurally Heterogeneous Cryo-EM Data in RELION. *Methods Enzymol.* **579**, 125–157.
- Schrödinger, L. (2015). The PyMOL Molecular Graphics System.
- Sempowski, G.D., Saunders, K.O., Acharya, P., Wiehe, K.J., and Haynes, B.F. (2020). Pandemic Preparedness: Developing Vaccines and Therapeutic Antibodies For COVID-19. *Cell* **181**, 1458–1463.
- Sheahan, T.P., Sims, A.C., Graham, R.L., Menachery, V.D., Gralinski, L.E., Case, J.B., Leist, S.R., Pyrc, K., Feng, J.Y., Trantcheva, I., et al. (2017). Broad-spectrum antiviral GS-5734 inhibits both epidemic and zoonotic coronaviruses. *Sci. Transl. Med.* **9**, eaal3653.
- Shi, R., Shan, C., Duan, X., Chen, Z., Liu, P., Song, J., Song, T., Bi, X., Han, C., Wu, L., et al. (2020). A human neutralizing antibody targets the receptor-binding site of SARS-CoV-2. *Nature* **584**, 120–124.
- Suloway, C., Pulokas, J., Fellmann, D., Cheng, A., Guerra, F., Quispe, J., Stagg, S., Potter, C.S., and Carragher, B. (2005). Automated molecular microscopy: the new Legion system. *J. Struct. Biol.* **151**, 41–60.
- Takada, A., Ebihara, H., Feldmann, H., Geisbert, T.W., and Kawaoka, Y. (2007). Epitopes required for antibody-dependent enhancement of Ebola virus infection. *J. Infect. Dis.* **196** (Suppl 2), S347–S356.

- Ubol, S., and Halstead, S.B. (2010). How innate immune mechanisms contribute to antibody-enhanced viral infections. *Clin. Vaccine Immunol.* **17**, 1829–1835.
- Walls, A.C., Park, Y.J., Tortorici, M.A., Wall, A., McGuire, A.T., and Veesler, D. (2020). Structure, Function, and Antigenicity of the SARS-CoV-2 Spike Glycoprotein. *Cell* **181**, 281–292.
- Wan, Y., Shang, J., Sun, S., Tai, W., Chen, J., Geng, Q., He, L., Chen, Y., Wu, J., Shi, Z., et al. (2020). Molecular Mechanism for Antibody-Dependent Enhancement of Coronavirus Entry. *J. Virol.* **94**, e02015, 19.
- Wang, S.F., Tseng, S.P., Yen, C.H., Yang, J.Y., Tsao, C.H., Shen, C.W., Chen, K.H., Liu, F.T., Liu, W.T., Chen, Y.M., and Huang, J.C. (2014). Antibody-dependent SARS coronavirus infection is mediated by antibodies against spike proteins. *Biochem. Biophys. Res. Commun.* **451**, 208–214.
- Wang, Q., Zhang, L., Kuwahara, K., Li, L., Liu, Z., Li, T., Zhu, H., Liu, J., Xu, Y., Xie, J., et al. (2016). Immunodominant SARS Coronavirus Epitopes in Humans Elicited both Enhancing and Neutralizing Effects on Infection in Non-human Primates. *ACS Infect. Dis.* **2**, 361–376.
- Wang, Q., Chen, Y., Pelletier, M., Cvitkovic, R., Bonnell, J., Chang, C.Y., Koksai, A.C., O'Connor, E., Gao, X., Yu, X.Q., et al. (2017). Enhancement of antibody functions through Fc multiplications. *MAbs* **9**, 393–403.
- Wec, A.Z., Wrapp, D., Herbert, A.S., Maurer, D.P., Haslwanter, D., Sakharkar, M., Jangra, R.K., Dieterle, M.E., Lilov, A., Huang, D., et al. (2020). Broad neutralization of SARS-related viruses by human monoclonal antibodies. *Science* **369**, 731–736.
- Whittle, J.R., Zhang, R., Khurana, S., King, L.R., Manischewitz, J., Golding, H., Dormitzer, P.R., Haynes, B.F., Walter, E.B., Moody, M.A., et al. (2011). Broadly neutralizing human antibody that recognizes the receptor-binding pocket of influenza virus hemagglutinin. *Proc. Natl. Acad. Sci. USA* **108**, 14216–14221.
- Wölfel, R., Corman, V.M., Guggemos, W., Seilmaier, M., Zange, S., Müller, M.A., Niemeyer, D., Jones, T.C., Vollmar, P., Rothe, C., et al. (2020). Virological assessment of hospitalized patients with COVID-2019. *Nature* **581**, 465–469.
- Wrammert, J., Smith, K., Miller, J., Langley, W.A., Kokko, K., Larsen, C., Zheng, N.Y., Mays, I., Garman, L., Helms, C., et al. (2008). Rapid cloning of high-affinity human monoclonal antibodies against influenza virus. *Nature* **453**, 667–671.
- Wrapp, D., De Vlieger, D., Corbett, K.S., Torres, G.M., Wang, N., Van Breedam, W., Roose, K., van Schie, L., Hoffmann, M., Pöhlmann, S., et al.; VIB-CMB COVID-19 Response Team (2020a). Structural Basis for Potent Neutralization of Betacoronaviruses by Single-Domain Camelid Antibodies. *Cell* **181**, 1004–1015.
- Wrapp, D., Wang, N., Corbett, K.S., Goldsmith, J.A., Hsieh, C.L., Abiona, O., Graham, B.S., and McLellan, J.S. (2020b). Cryo-EM structure of the 2019-nCoV spike in the prefusion conformation. *Science* **367**, 1260–1263.
- Wu, Y., Wang, F., Shen, C., Peng, W., Li, D., Zhao, C., Li, Z., Li, S., Bi, Y., Yang, Y., et al. (2020). A noncompeting pair of human neutralizing antibodies block COVID-19 virus binding to its receptor ACE2. *Science* **368**, 1274–1278.
- Yilla, M., Harcourt, B.H., Hickman, C.J., McGrew, M., Tamin, A., Goldsmith, C.S., Bellini, W.J., and Anderson, L.J. (2005). SARS-coronavirus replication in human peripheral monocytes/macrophages. *Virus Res.* **107**, 93–101.
- Yip, M.S., Leung, N.H., Cheung, C.Y., Li, P.H., Lee, H.H., Daëron, M., Peiris, J.S., Bruzzone, R., and Jaume, M. (2014). Antibody-dependent infection of human macrophages by severe acute respiratory syndrome coronavirus. *Virology* **471**, 82.
- Yip, M.S., Leung, H.L., Li, P.H., Cheung, C.Y., Dutry, I., Li, D., Daëron, M., Bruzzone, R., Peiris, J.S., and Jaume, M. (2016). Antibody-dependent enhancement of SARS coronavirus infection and its role in the pathogenesis of SARS. *Hong Kong Med. J.* **22** (3, Suppl 4), 25–31.
- Yu, J., Tostanoski, L.H., Peter, L., Mercado, N.B., McMahan, K., Mahrokhian, S.H., Nkolola, J.P., Liu, J., Li, Z., Chandrashekar, A., et al. (2020). DNA vaccine protection against SARS-CoV-2 in rhesus macaques. *Science* **369**, 806–811.
- Zhang, Q., Bastard, P., Liu, Z., Le Pen, J., Moncada-Velez, M., Chen, J., Ogishi, M., Sabli, I.K.D., Hodeib, S., Korol, C., et al.; COVID-STORM Clinicians; COVID Clinicians; Imagine COVID Group; French COVID Cohort Study Group; CoV-Contact Cohort; Amsterdam UMC Covid-19 Biobank; COVID Human Genetic Effort; NIAID-USUHS/TAGC COVID Immunity Group (2020). Inborn errors of type I IFN immunity in patients with life-threatening COVID-19. *Science* **370**, eabd4570.
- Zheng, S.Q., Palovcak, E., Armache, J.P., Verba, K.A., Cheng, Y., and Agard, D.A. (2017). MotionCorr2: anisotropic correction of beam-induced motion for improved cryo-electron microscopy. *Nat. Methods* **14**, 331–332.
- Zhou, J., Chu, H., Li, C., Wong, B.H., Cheng, Z.S., Poon, V.K., Sun, T., Lau, C.C., Wong, K.K., Chan, J.Y., et al. (2014). Active replication of Middle East respiratory syndrome coronavirus and aberrant induction of inflammatory cytokines and chemokines in human macrophages: implications for pathogenesis. *J. Infect. Dis.* **209**, 1331–1342.
- Zhou, D., Duyvesteyn, H.M.E., Chen, C.P., Huang, C.G., Chen, T.H., Shih, S.R., Lin, Y.C., Cheng, C.Y., Cheng, S.H., Huang, Y.C., et al. (2020a). Structural basis for the neutralization of SARS-CoV-2 by an antibody from a convalescent patient. *Nat. Struct. Mol. Biol.* **27**, 950–958.
- Zhou, T., Teng, I.T., Olia, A.S., Cerutti, G., Gorman, J., Nazzari, A., Shi, W., Tsybovsky, Y., Wang, L., Wang, S., et al. (2020b). Structure-Based Design with Tag-Based Purification and In-Process Biotinylation Enable Streamlined Development of SARS-CoV-2 Spike Molecular Probes. *Cell Rep.* **33**, 108322.
- Zost, S.J., Gilchuk, P., Case, J.B., Binshtein, E., Chen, R.E., Nkolola, J.P., Schäfer, A., Reidy, J.X., Trivette, A., Nargi, R.S., et al. (2020a). Potently neutralizing and protective human antibodies against SARS-CoV-2. *Nature* **584**, 443–449.
- Zost, S.J., Gilchuk, P., Chen, R.E., Case, J.B., Reidy, J.X., Trivette, A., Nargi, R.S., Sutton, R.E., Suryadevara, N., Chen, E.C., et al. (2020b). Rapid isolation and profiling of a diverse panel of human monoclonal antibodies targeting the SARS-CoV-2 spike protein. *Nat. Med.* **26**, 1422–1427.
- Zhou, T., Lynch, R.M., Chen, L., Acharya, P., Wu, X., Doria-Rose, N.A., Joyce, M.G., Lingwood, D., Soto, C., Bailer, R.T., et al. (2015). Structural Repertoire of HIV-1-Neutralizing Antibodies Targeting the CD4 Supersite in 14 Donors. *Cell* **161**, 1280–1292. <https://doi.org/10.1016/j.cell.2015.05.007>.

STAR★METHODS

KEY RESOURCES TABLE

Reagent or resource	Source	Identifier
Antibodies		
PE-Cy5 Mouse Anti-Human CD3, Clone# HIT3a	BD Biosciences	Cat#555341; RRID: AB_10698936
BV605 Mouse Anti-Human CD14, Clone# M5E2	Biolegend	Cat#301834, RRID: AB_2563798
BV570 Mouse Anti-Human CD16, Clone# 3G8	Biolegend	Cat# 302035, RRID: AB_2632790
APC-Cy7 Mouse Anti-Human CD19, Clone# SJ25C1	BD Biosciences	Cat# 557791, RRID: AB_396873
FITC Mouse Anti-Human IgD, Clone# IA6-2	BD Biosciences	Cat# 555778, RRID: AB_396113
PerCp-Cy5.5 Mouse Anti-Human IgM, Clone# G20-127	BD Biosciences	Cat# 561285, RRID:AB_10611998
PE-CF594, Mouse Anti-Human CD10, Clone# HI10A	BD Biosciences	Cat# 562396, RRID: AB_11154416
PE-Cy5 Mouse Anti-Human CD235a, Clone# GA-R2	BD Biosciences	Cat# 559944, RRID: AB_397387
PE-Cy7 Mouse Anti-Human CD27, Clone# O323	eBioscience	Cat# 25-0279, RRID: AB_1724039
APC-AF700 Mouse Anti-Human CD38, Clone# LS198-4-2	Beckman Coulter	Cat# B23489, RRID: NA
SARS-CoV/SARS-CoV-2 Spike Ab, Clone# D001	Sino Biological	Cat #40150-D001
Anti-influenza virus hemagglutinin human IgG CH65	(Whittle et al., 2011)	NA
Rabbit polyclonal SARS-CoV-2 nucleocapsid Ab	GeneTex	Cat #GTX135357, RRID:AB_2868464
Rat anti-human CD3, Clone# CD3-12	Bio-Rad	Cat #MCA1477, RRID:AB_321245
Rabbit anti-human Iba1 polyclonal Ab	Wako	Cat# 019-19741, RRID: AB_839504
Rabbit anti-human CD68 polyclonal Ab	Sigma-Millipore	Cat# HPA048982, RRID: AB_2680587
Rabbit anti-human CD163, Clone# EPR19518	Abcam	Cat# ab182422, RRID: AB_2753196
Mouse anti-human HLA-DP/DQ/DR, Clone# CR3/43	Dako	Cat# M0775, RRID: AB_2313661
Rabbit anti-human CD11b, Clone# EP1345Y	Abcam	Cat# ab52478, RRID: AB_868788
HRP goat anti-human IgG	SouthernBiotech	Cat #2040-05, RRID:AB_2795644
HRP goat anti-rabbit IgG	Abcam	Cat #ab97080, RRID:AB_10679808
Biotin mouse anti-human IgG Fc, Clone# H2	Southern Biotech	Cat# 9042-08, RRID:AB_2796608
Bacterial and virus strains		
SARS-CoV-2 D614G pseudotyped virus	(Korber et al., 2020)	NA
SARS-CoV-2 virus, Isolate USA-WA1/2020	BEI Resources	Cat #NR-52281
SARS-CoV-2 nanoLuc virus	(Hou et al., 2020)	NA
SARS-CoV nanoLuc virus	(Sheahan et al., 2017)	NA
WIV1-CoV nanoLuc virus	(Menachery et al., 2016)	NA
SARS-CoV-2 moles-adapted virus 2AA MA	(Dinnon et al., 2020)	NA
SARS-CoV-2 moles-adapted virus MA10	(Leist et al., 2020a)	NA
Biological samples		
Plasma, PBMCs, nasal swabs and bronchoalveolar lavage (BAL) from macaques	This paper	NA
Chemicals, peptides, and recombinant proteins		
LIVE/DEAD Fixable Red Dead Cell Stain Kit	Thermo Fisher Scientific	Cat#L34972
SuperScript III Reverse Transcriptase	Invitrogen	Cat #18080085
dNTP Set, PCR Grade	New England Biolabs	Cat # N0447L
UltraPure DNase/RNase-Free Distilled Water	Invitrogen	Cat #10977
GeneLink Random Hexamer Primers	GeneLink	Cat #26-4000-03
AmpliTaq Gold 360 Mastermix	Thermo Fisher Scientific	Cat #4398881
Expi293 media	Invitrogen	Cat #A1435102

(Continued on next page)

Continued

Reagent or resource	Source	Identifier
Expifectamine	Life Technologies	Cat #A14524
Protein A beads	Pierce	Cat #PI-20334
MfeI-HF	New England Biolabs	R3589L
MluI-HF	New England Biolabs	R3198L
SureBlue Reserve tetramethylbenzidine substrate	KPL	Cat #5120-0081
TaqMan Fast Virus 1-Step Master Mix	ThermoFisher	4444434
QIAAsymphony DSP Virus/Pathogen Midi Kit	QIAGEN	937055
NucleoSpin Gel and PCR Clean-Up	Takara	740609.5
MEGAscript T7 Transcription Kit	ThermoFisher	AM1334
MEGAClear Transcription Clean-Up Kit	ThermoFisher	AM1908
Luciferase Cell Culture Lysis 5x Reagent	Promega	Cat# E1531
Background Reducing Ab Diluent	Agilent	Cat# S3022
PowerVision Poly-HRP anti-Rabbit IgG IHC Detection Systems	Leica	Cat# PV6121
Human ACE2 soluble protein	(Edwards et al., 2021)	NA
SARS-CoV-2 Spike S1+S2 ectodomain (ECD)	Sino Biological	Cat #40589-V08B1
SARS-CoV-2 Spike S2 ECD	Sino Biological	Cat #40590-V08B
SARS-CoV-2 Spike RBD from insect cell sf9	Sino Biological	Cat #40592-V08B
SARS-CoV-2 Spike RBD from mammalian cell 293	Sino Biological	Cat #40592-V08H
SARS-CoV Spike Protein DeltaTM	BEI Resources	Cat #NR-722
SARS-CoV WH20 Spike RBD	Sino Biological	Cat #40150-V08B2
SARS-CoV WH20 Spike S1	Sino Biological	Cat #40150-V08B1
MERS-CoV Spike S1+S2	Sino Biological	Cat #40069-V08B
MERS-CoV Spike S1	Sino Biological	Cat #40069-V08B1
MERS-CoV Spike S2	Sino Biological	Cat #40070-V08B
MERS-CoV Spike RBD	Sino Biological	Cat #40071-V08B1
SARS-CoV CL Protease protein	BEI Resources	Cat #30105
SARS-CoV Membrane (M) protein	BEI Resources	Cat #110705
SARS-CoV-2 Spike NTD	(Zhou et al., 2020b)	NA
SARS-CoV Spike RBD	(Hauser et al., 2020)	NA
MERS-CoV Spike RBD	(Hauser et al., 2020)	NA
SARS-CoV-2 Spike-2P	(Edwards et al., 2021)	NA
SARS-CoV-2 Spike-HexaPro	(Edwards et al., 2021)	NA

Critical commercial assays

MILLIPLEX MAP Non-Human Primate Cytokine/Chemokine Panel, 25-analyte multiplex bead array	Millipore	Cat #PRCYT2MAG40K
Bright-Glo Luciferase Assay System	Promega	Cat #2650
Britelite Luminescence Reporter Gene Assay System	PerkinElmer Life Sciences	Cat #6066761
Nano-Glo Luciferase Assay System	Promega	Cat #N1150

Deposited data

Structure of SARS-CoV-2 S protein in complex with Receptor Binding Domain Ab DH1041	This paper	PDB: 7LAA, EMD- 23246
Structure of SARS-CoV-2 S protein in complex with Receptor Binding Domain Ab DH1047	This paper	PDB: 7LD1, EMD- 23279
Structure of SARS-CoV-2 S protein in complex with N-terminal domain Ab DH1050.1	This paper	PDB: 7LCN, EMD- 23277
Structure of SARS-CoV-2 S protein in complex with N-terminal domain Ab DH1052	This paper	PDB: 7LAB, EMD- 23248

(Continued on next page)

Continued

Reagent or resource	Source	Identifier
SARS-CoV-2 Spike Protein Trimer bound to DH1043 fab	This paper	PDB: 7LJR, EMD- 23400
Negative stain EM structure of Ab DH1041 Fab in complex with SARS-CoV-2 Hexapro spike	This paper	EMD-22920
Negative stain EM structure of Ab DH1042 Fab in complex with SARS-CoV-2 2P spike	This paper	EMD-22921
Negative stain EM structure of Ab DH1043 Fab in complex with SARS-CoV-2 Hexapro spike	This paper	EMD-22923
Negative stain EM structure of Ab DH1044 Fab in complex with SARS-CoV-2 2P spike	This paper	EMD-22929
Negative stain EM structure of Ab DH1045 Fab in complex with SARS-CoV-2 Hexapro spike	This paper	EMD-22930
Negative stain EM structure of Ab DH1047 Fab in complex with SARS-CoV-2 Hexapro spike	This paper	EMD-22933
Negative stain EM structure of Ab DH1048 Fab in complex with SARS-CoV-2 Hexapro spike	This paper	EMD-22936
Negative stain EM structure of Ab DH1049 Fab in complex with SARS-CoV-2 2P spike	This paper	EMD-22942
Negative stain EM structure of Ab DH1050.1 Fab in complex with SARS-CoV-2 Hexapro spike	This paper	EMD-22944
Negative stain EM structure of Ab DH1050.2 Fab in complex with SARS-CoV-2 2P spike	This paper	EMD-22945
Negative stain EM structure of Ab DH1051 Fab in complex with SARS-CoV-2 Hexapro spike	This paper	EMD-22946
Negative stain EM structure of Ab DH1053 Fab in complex with SARS-CoV-2 2P spike in the 1-RBD-up state	This paper	EMD-22947
Negative stain EM structure of Ab DH1053 Fab in complex with SARS-CoV-2 2P spike in the 3-RBD-down state	This paper	EMD-22948
Negative stain EM structure of Ab DH1054 Fab in complex with SARS-CoV-2 2P spike	This paper	EMD-22951
Negative stain EM structure of Ab DH1055 Fab in complex with SARS-CoV-2 2P spike	This paper	EMD-22952
Negative stain EM structure of Ab DH1056 Fab in complex with SARS-CoV-2 2P spike	This paper	EMD-22953
Negative stain EM structure of Ab Fabs DH1043 and DH1051 in complex with SARS-CoV-2 2P spike	This paper	EMD-22955
Negative stain EM structure of Ab Fabs DH1041 and DH1051 in complex with SARS-CoV-2 2P spike	This paper	EMD-22956
Negative stain EM structure of Ab Fabs DH1043 and DH1047 in complex with SARS-CoV-2 2P spike	This paper	EMD-22957
Negative stain EM structure of Ab Fabs DH1047 and DH1051 in complex with SARS-CoV-2 2P spike	This paper	EMD-22958
Negative stain EM structure of Ab Fabs DH1045 and DH1050.1 in complex with SARS-CoV-2 2P spike	This paper	EMD-22969
Negative stain EM structure of Ab Fabs DH1043 and DH1050.1 in complex with SARS-CoV-2 2P spike	This paper	EMD-22970
Negative stain EM structure of Ab Fabs DH1041 and DH1047 in complex with SARS-CoV-2 2P spike	This paper	EMD-22971
Negative stain EM structure of Ab Fabs DH1050.1 and DH1053 in complex with SARS-CoV-2 2P spike	This paper	EMD-22984

(Continued on next page)

Continued

Reagent or resource	Source	Identifier
Negative stain EM structure of Ab Fabs DH1043, DH1047 and DH1050.1 in complex with SARS-CoV-2 2P spike	This paper	EMD-22985
Negative stain EM structure of Ab Fabs DH1043, DH1047 and DH1051 in complex with SARS-CoV-2 2P spike	This paper	EMD-22986

Experimental models: Cell lines

TZM-bl	NIH, ARRRP	Cat #8129
TZM-bl expressing Fc γ RI	(Perez et al., 2009)	NA
TZM-bl expressing Fc γ RIIIa	(Perez et al., 2009)	NA
TZM-bl expressing Fc γ RIIIb	(Perez et al., 2009)	NA
TZM-bl expressing Fc γ RIII	(Perez et al., 2009)	NA
Expi 293i	Invitrogen	Cat #14527
293T/ACE2	(Korber et al., 2020)	NA
Vero E6	ATCC	Cat# CRL-1586

Experimental models: Organisms/strains

BALB/c mouse	Envigo	NA
HFH4-hACE2 transgenic mice	(Menachery et al., 2016)	NA
Cynomolgus macaques	BioQUAL	NA

Oligonucleotides

VH1 Leader-A 5'- ATGGACTGGACCTGGAGGAT -3' (PCRa primer)	Thermo Fisher Scientific	NA
VH1 Leader-A 5'- ATGGACTGGACCTGGAGCAT -3' (PCRa primer)	Thermo Fisher Scientific	NA
VH1 Leader-A 5'- ATGGACTGGACCTGGAGAAT -3' (PCRa primer)	Thermo Fisher Scientific	NA
VH1 Leader-A 5'- GGTCCTCTTTGTGGTGGC -3' (PCRa primer)	Thermo Fisher Scientific	NA
VH1 Leader-A 5'- ATGGACTGGACCTGGAGGGT -3' (PCRa primer)	Thermo Fisher Scientific	NA
VH1 Leader-A 5'- ATGGACTGGATTTGGAGGAT -3' (PCRa primer)	Thermo Fisher Scientific	NA
VH1 Leader-A 5'- AGGTCCTCTTTGTGGTGGCAG -3' (PCRa primer)	Thermo Fisher Scientific	NA
VH1 Leader-A 5'- ATGGACATACTTTGTTCCACGCTC -3' (PCRa primer)	Thermo Fisher Scientific	NA
VH1 Leader-A 5'- ATGGACACACTTTGCTCCACGCT -3' (PCRa primer)	Thermo Fisher Scientific	NA
VH1 Leader-A 5'- ATGGACACACTTTGCTACACACTC -3' (PCRa primer)	Thermo Fisher Scientific	NA
VH1 Leader-A 5'- CCGACGGGAATTCTCACAG -3' (PCRa primer)	Thermo Fisher Scientific	NA
VH1 Leader-A 5'- CTGTTATCCTTTGGGTGTCTGCAC -3' (PCRa primer)	Thermo Fisher Scientific	NA
VH1 Leader-A 5'- GGTGGCATTGGAGGGAATGTT -3' (PCRa primer)	Thermo Fisher Scientific	NA
VH1 Leader-A 5'- CGAYGACCACGTTCCCATCT -3' (PCRa primer)	Thermo Fisher Scientific	NA
VH1 Leader-A 5'- TAGTCCTTGACCAGGCAGC -3' (PCRa primer)	Thermo Fisher Scientific	NA
VH1 Leader-A 5'- TAAAAGGTGTCAGTGT -3' (PCRa primer)	Thermo Fisher Scientific	NA

(Continued on next page)

Continued

Reagent or resource	Source	Identifier
VH1 Leader-A 5'- TAAGAGGTGCCAGTGT –3' (PCRa primer)	Thermo Fisher Scientific	NA
VH1 Leader-A 5'- TAGAAGGTGCCAGTGT –3' (PCRa primer)	Thermo Fisher Scientific	NA
VH1 Leader-A 5'- TACAAGGTGCCAGTGT –3' (PCRa primer)	Thermo Fisher Scientific	NA
VH1 Leader-A 5'- TTAAGCTGCCAGTGT –3' (PCRa primer)	Thermo Fisher Scientific	NA
VH1 Leader-A 5'- ATGAAACACTGTGGTTCTT –3' (PCRa primer)	Thermo Fisher Scientific	NA
VH1 Leader-A 5'- TTCTCCAAGGAGTCTGT –3' (PCRa primer)	Thermo Fisher Scientific	NA
VH1 Leader-A 5'- GCTATTTTTAAGGTGCCAGTGT –3' (PCRa primer)	Thermo Fisher Scientific	NA
VH1 Leader-A 5'- ATGAAACACCTGTGGTTCTTCC –3' (PCRa primer)	Thermo Fisher Scientific	NA
VH1 Leader-A 5'- ATGAAACACCTGTGGTTCTT –3' (PCRa primer)	Thermo Fisher Scientific	NA
VH1 Leader-A 5'- ATGAAGCACCTGTGGTTCTT –3' (PCRa primer)	Thermo Fisher Scientific	NA
VH1 Leader-A 5'- CCTCCACAGTGAGAGTCTG –3' (PCRa primer)	Thermo Fisher Scientific	NA
VH1 Leader-A 5'- ATGTCTGTCTCCTTCCTCATC –3' (PCRa primer)	Thermo Fisher Scientific	NA
VH1 Leader-A 5'- GGCAGCAGCAACAGGTGCCCA –3' (PCRa primer)	Thermo Fisher Scientific	NA
VH1 Leader-A 5'- GCTCAGCTCCTGGGGCT –3' (PCRa primer)	Thermo Fisher Scientific	NA
VH1 Leader-A 5'- GGAARCCCCAGCDCAGC –3' (PCRa primer)	Thermo Fisher Scientific	NA
VH1 Leader-A 5'- CTSTTSCTYTGGATCTCTG –3' (PCRa primer)	Thermo Fisher Scientific	NA
VH1 Leader-A 5'- CTSTCTGCTCTGGGYTCC –3' (PCRa primer)	Thermo Fisher Scientific	NA
VH1 Leader-A 5'- GAGGCAGTCCAGATTTCAA –3' (PCRa primer)	Thermo Fisher Scientific	NA
VH1 Leader-A 5'- CCTGGGCCAGTCTGTG –3' (PCRa primer)	Thermo Fisher Scientific	NA
VH1 Leader-A 5'- CTCCTCASCTCCTCACT –3' (PCRa primer)	Thermo Fisher Scientific	NA
VH1 Leader-A 5'- GGCCTCTATGWGCTGAC –3' (PCRa primer)	Thermo Fisher Scientific	NA
VH1 Leader-A 5'- GTTCTGTGGTTTCTTCTGAGCTG –3' (PCRa primer)	Thermo Fisher Scientific	NA
VH1 Leader-A 5'- ACAGGGTCTCTCTCCAG –3' (PCRa primer)	Thermo Fisher Scientific	NA
VH1 Leader-A 5'- ACAGGTCTCTGTGCTCTGC –3' (PCRa primer)	Thermo Fisher Scientific	NA
VH1 Leader-A 5'- CCCTCTCSCAGSCTGTG –3' (PCRa primer)	Thermo Fisher Scientific	NA
VH1 Leader-A 5'- TCTTGGGCCAATTTTATGC –3' (PCRa primer)	Thermo Fisher Scientific	NA
VH1 Leader-A 5'- ATTCYAGRGTGTGGTGAC –3' (PCRa primer)	Thermo Fisher Scientific	NA

(Continued on next page)

Continued

Reagent or resource	Source	Identifier
VH1 Leader-A 5'- CAGTGGTCCAGGCAGGG -3' (PCRa primer)	Thermo Fisher Scientific	NA
VH1 Leader-A 5'- AGGCCACTGTCACAGCT -3' (PCRa primer)	Thermo Fisher Scientific	NA
VH1-Int tag 5'- CTGGGTTCCAGGTTCCACTGGTGACCAGGTG CAGCTGGTRCAGTCTGGG -3' (PCRb primer)	Thermo Fisher Scientific	NA
VH2-Int tag 5'- CTGGGTTCCAGGTTCCACTGGTGACCA GRGCACCTTGARGGAGTCTGGTCC -3' (PCRb primer)	Thermo Fisher Scientific	NA
VH3-Int tag 5'- CTGGGTTCCAGGTTCCACTGGTG ACGAGGTCAGCTGGTGGAGTCTGGG -3' (PCRb primer)	Thermo Fisher Scientific	NA
VH4-Int tag 5'- CTGGGTTCCAGGTTCCACTGGT GACCAGGTGCAGCTGCAGGAGTCGG -3' (PCRb primer)	Thermo Fisher Scientific	NA
VH5-Int tag 5'- CTGGGTTCCAGGTTCCACTGGTGACG ARGTGCAGCTGGTGCAGTCTGGAG -3' (PCRb primer)	Thermo Fisher Scientific	NA
VH6-Int tag 5'- CTGGGTTCCAGGTTCCACTGGTGACC AGGTACAGCTGCAGCAGTCAGGTCC -3' (PCRb primer)	Thermo Fisher Scientific	NA
IgG-int 5'- GGGCCGCTGTGCCCCAGAGGTGCTCYTGGA -3' (PCRb primer)	Thermo Fisher Scientific	NA
IgM-int 5'- GGGCCGCTGTGCCCCAGAGGTGGAATTCTC ACAGGAGACGAGG -3' (PCRb primer)	Thermo Fisher Scientific	NA
IgD-int 5'- GGGCCGCTGTGCCCCAGAGGTGTGTCTGC ACCCTGATATGATGG -3' (PCRb primer)	Thermo Fisher Scientific	NA
IgA1-int 5'- GGGCCGCTGTGCCCCAGAGGTGCTGGTGC TGCAGAGGCTCAG -3' (PCRb primer)	Thermo Fisher Scientific	NA
IgA2-int 5'- GGGCCGCTGTGCCCCAGAGGTGCTGGTG CTGTGAGGCTCAG -3' (PCRb primer)	Thermo Fisher Scientific	NA
VK1-Int tag 5'- CTGGGTTCCAGGTTCCACTGGTGACGA CATCCAGWTGACCCAGTCTC -3' (PCRb primer)	Thermo Fisher Scientific	NA
VK2-Int tag 5'- CTGGGTTCCAGGTTCCACTGGTGACGAT ATTGTGATGACCCAGWCTCCAC -3' (PCRb primer)	Thermo Fisher Scientific	NA
VK3-Int tag 5'- CTGGGTTCCAGGTTCCACTGGTGACG AAATTGTGTTGACRCAGTCTCCA -3' (PCRb primer)	Thermo Fisher Scientific	NA
VK4-Int tag 5'- CTGGGTTCCAGGTTCCACTGGTGACG ACATCGTATGACCCAGTCTC -3' (PCRb primer)	Thermo Fisher Scientific	NA
VK5-Int tag 5'- CTGGGTTCCAGGTTCCACTGGTGAC GAAACGACACTCACGAGTCTC -3' (PCRb primer)	Thermo Fisher Scientific	NA

(Continued on next page)

Continued

Reagent or resource	Source	Identifier
VK6-Int tag 5'- CTGGGTCCAGGTCCACTGGTGA CGAAATTGTGCTGACWCAGTCTCCA -3' (PCRb primer)	Thermo Fisher Scientific	NA
VK7-Int tag 5'- CTGGGTCCAGGTCCACTGGTGA CGACATTGTGCTGACCCAGTCT -3' (PCRb primer)	Thermo Fisher Scientific	NA
CK-int 5'- GGGAAAGATGAAGACAGATGGT -3' (PCRb primer)	Thermo Fisher Scientific	NA
VL1-Int tag 5'- CTGGGTCCAGGTCCACTGGTG ACCAGTCTGTGYTGACKCAGCC -3' (PCRb primer)	Thermo Fisher Scientific	NA
VL2-Int tag 5'- CTGGGTCCAGGTCCACTGGTGA CCAGTCTGCCCTGACTCAGCC -3' (PCRb primer)	Thermo Fisher Scientific	NA
VL3-Int tag 5'- CTGGGTCCAGGTCCACTGGTGA CTCYTATGAGCTGACWCAGCCAC -3' (PCRb primer)	Thermo Fisher Scientific	NA
VL3I-Int tag 5'- CTGGGTCCAGGTCCACTGGTGA CTCTTCTGAGCTGACTCAGGACCC -3' (PCRb primer)	Thermo Fisher Scientific	NA
VL4ab-Int tag 5'- CTGGGTCCAGGTCCACTGGT GACCAGCYTGTGCTGACTCAATC -3' (PCRb primer)	Thermo Fisher Scientific	NA
VL4c-Int tag 5'- CTGGGTCCAGGTCCACTGGTG ACCTGCCTGTGCTGACTCAGC -3' (PCRb primer)	Thermo Fisher Scientific	NA
VL5,9-Int tag 5'- CTGGGTCCAGGTCCACTGGT GACCAGSCTGTGCTGACTCAGCC -3' (PCRb primer)	Thermo Fisher Scientific	NA
VL6-Int tag 5'- CTGGGTCCAGGTCCACTGGT GACAATTTTATGCTGACTCAGCCCCACT -3' (PCRb primer)	Thermo Fisher Scientific	NA
VL7,8-Int tag 5'- CTGGGTCCAGGTCCACTGGTGA CCAGRCTGTGGTGACYCAGGAG -3' (PCRb primer)	Thermo Fisher Scientific	NA
VL10-Int tag 5'- CTGGGTCCAGGTCCACTGGTGA CCAGGCAGGGCWGACTCAG -3' (PCRb primer)	Thermo Fisher Scientific	NA
CL-int 5'- GGGYGGGAACAGAGTGACC -3' (PCRb primer)	Thermo Fisher Scientific	NA
VH_Tag fwd seq 5'- CTGGGTCCAGGTCCACTGGTGAC -3' (Sequencing primer)	Thermo Fisher Scientific	NA
CK_int 5'- GGGAAAGATGAAGACAGATGGT -3' (Sequencing primer)	Thermo Fisher Scientific	NA
CL_int 5'- GGGYGGGAACAGAGTGACC -3' (Sequencing primer)	Thermo Fisher Scientific	NA
HV13221H_R474 5'- GCTGTGCCCCAGAGGTG -3' (Sequencing primer)	Thermo Fisher Scientific	NA
VH1 Leader-A 5'- ATGGACTGGACCTGGAGGAT -3' (PCRa primer)	Thermo Fisher Scientific	NA
VH1 Leader-A 5'- ATGGACTGGACCTGGAGCAT -3' (PCRa primer)	Thermo Fisher Scientific	NA
VH1 Leader-A 5'- ATGGACTGGACCTGGAGAAT -3' (PCRa primer)	Thermo Fisher Scientific	NA
VH1 Leader-A 5'- GGTTCTCTTTGTGGTGGC -3' (PCRa primer)	Thermo Fisher Scientific	NA
VH1 Leader-A 5'- ATGGACTGGACCTGGAGGGT -3' (PCRa primer)	Thermo Fisher Scientific	NA
VH1 Leader-A 5'- ATGGACTGGATTTGGAGGAT -3' (PCRa primer)	Thermo Fisher Scientific	NA

(Continued on next page)

Continued

Reagent or resource	Source	Identifier
VH1 Leader-A 5'- AGGTTCCCTCTTTGTGGTGGCAG -3' (PCRa primer)	Thermo Fisher Scientific	NA
VH1 Leader-A 5'- ATGGACATACTTTGTTCCACGCTC -3' (PCRa primer)	Thermo Fisher Scientific	NA
VH1 Leader-A 5'- ATGGACACACTTTGCTCCACGCT -3' (PCRa primer)	Thermo Fisher Scientific	NA
VH1 Leader-A 5'- ATGGACACACTTTGCTACACACTC -3' (PCRa primer)	Thermo Fisher Scientific	NA
VH1 Leader-A 5'- CCGACGGGGAATTCTCACAG -3' (PCRa primer)	Thermo Fisher Scientific	NA
VH1 Leader-A 5'- CTGTTATCCTTTGGGTGTCTGCAC -3' (PCRa primer)	Thermo Fisher Scientific	NA
VH1 Leader-A 5'- GGTGGCATTGGAGGGAATGTT -3' (PCRa primer)	Thermo Fisher Scientific	NA
VH1 Leader-A 5'- CGAYGACCACGTTCCCATCT -3' (PCRa primer)	Thermo Fisher Scientific	NA
VH1 Leader-A 5'- TAGTCCTTGACCAGGCAGC -3' (PCRa primer)	Thermo Fisher Scientific	NA
VH1 Leader-A 5'- TAAAAGGTGTCCAGTGT -3' (PCRa primer)	Thermo Fisher Scientific	NA
VH1 Leader-A 5'- TAAGAGGTGTCCAGTGT -3' (PCRa primer)	Thermo Fisher Scientific	NA
VH1 Leader-A 5'- TAGAAGGTGTCCAGTGT -3' (PCRa primer)	Thermo Fisher Scientific	NA
VH1 Leader-A 5'- TACAAGGTGTCCAGTGT -3' (PCRa primer)	Thermo Fisher Scientific	NA
VH1 Leader-A 5'- TTAAAGCTGTCCAGTGT -3' (PCRa primer)	Thermo Fisher Scientific	NA
VH1 Leader-A 5'- ATGAAACATCTGTGGTTCTT -3' (PCRa primer)	Thermo Fisher Scientific	NA
VH1 Leader-A 5'- TTCTCCAAGGAGTCTGT -3' (PCRa primer)	Thermo Fisher Scientific	NA
VH1 Leader-A 5'- GCTATTTTTAAAGGTGTCCAGTGT -3' (PCRa primer)	Thermo Fisher Scientific	NA
VH1 Leader-A 5'- ATGAAACACCTGTGGTTCTTCC -3' (PCRa primer)	Thermo Fisher Scientific	NA
VH1 Leader-A 5'- ATGAAACACCTGTGGTTCTT -3' (PCRa primer)	Thermo Fisher Scientific	NA
VH1 Leader-A 5'- ATGAAGCACCTGTGGTTCTT -3' (PCRa primer)	Thermo Fisher Scientific	NA
VH1 Leader-A 5'- CCTCCACAGTGAGAGTCTG -3' (PCRa primer)	Thermo Fisher Scientific	NA
VH1 Leader-A 5'- ATGTCTGTCTCCTTCTCATC -3' (PCRa primer)	Thermo Fisher Scientific	NA
VH1 Leader-A 5'- GGCAGCAGCAACAGGTGCCCA -3' (PCRa primer)	Thermo Fisher Scientific	NA
VH1 Leader-A 5'- GCTCAGCTCCTGGGGCT -3' (PCRa primer)	Thermo Fisher Scientific	NA
VH1 Leader-A 5'- GGAARCCCCAGCDCAGC -3' (PCRa primer)	Thermo Fisher Scientific	NA
VH1 Leader-A 5'- CTSTTSCTYTGGATCTCTG -3' (PCRa primer)	Thermo Fisher Scientific	NA
VH1 Leader-A 5'- CTSTGCTCTGGGYTCC -3' (PCRa primer)	Thermo Fisher Scientific	NA

(Continued on next page)

Continued

Reagent or resource	Source	Identifier
VH1 Leader-A 5'- GAGGCAGTTCCAGATTCAA –3' (PCRa primer)	Thermo Fisher Scientific	NA
VH1 Leader-A 5'- CCTGGGCCAGTCTGTG –3' (PCRa primer)	Thermo Fisher Scientific	NA
VH1 Leader-A 5'- CTCCTCASYCTCCTCACT –3' (PCRa primer)	Thermo Fisher Scientific	NA
VH1 Leader-A 5'- GGCCTCCTATGWGCTGAC –3' (PCRa primer)	Thermo Fisher Scientific	NA
VH1 Leader-A 5'- GTTCTGTGGTTTCTTCTGAGCTG –3' (PCRa primer)	Thermo Fisher Scientific	NA
VH1 Leader-A 5'- ACAGGGTCTCTCTCCCAG –3' (PCRa primer)	Thermo Fisher Scientific	NA
VH1 Leader-A 5'- ACAGGTCTCTGTGCTCTGC –3' (PCRa primer)	Thermo Fisher Scientific	NA
VH1 Leader-A 5'- CCCTCTCSCAGSCTGTG –3' (PCRa primer)	Thermo Fisher Scientific	NA
VH1 Leader-A 5'- TCTTGGGCCAATTTTATGC –3' (PCRa primer)	Thermo Fisher Scientific	NA
VH1 Leader-A 5'- ATTCYCAGRCTGTGGTGAC –3' (PCRa primer)	Thermo Fisher Scientific	NA
VH1 Leader-A 5'- CAGTGGTCCAGGCAGGG –3' (PCRa primer)	Thermo Fisher Scientific	NA
VH1 Leader-A 5'- AGGCCACTGTACAGCT –3' (PCRa primer)	Thermo Fisher Scientific	NA
VH1-Int tag 5'- CTGGGTTCCAGGTTCCACTGGTGACCAGGTG CAGCTGGTRCAGTCTGGG –3' (PCRb primer)	Thermo Fisher Scientific	NA
VH2-Int tag 5'- CTGGGTTCCAGGTTCCACTGGTGACCAGR GCACCTTGARGGAGTCTGGTCC –3' (PCRb primer)	Thermo Fisher Scientific	NA
VH3-Int tag 5'- CTGGGTTCCAGGTTCCACTGGTGACGAGG TKCAGCTGGTGGAGTCTGGG –3' (PCRb primer)	Thermo Fisher Scientific	NA
VH4-Int tag 5'- CTGGGTTCCAGGTTCCACTGGTGACCAG GTGCAGCTGCAGGAGTCCG –3' (PCRb primer)	Thermo Fisher Scientific	NA
VH5-Int tag 5'- CTGGGTTCCAGGTTCCACTGGTGAC GARGTGCAGCTGGTGCAGTCTGGAG –3' (PCRb primer)	Thermo Fisher Scientific	NA
VH6-Int tag 5'- CTGGGTTCCAGGTTCCACTGGTGACC AGGTACAGCTGCAGCAGTCAGGTCC –3' (PCRb primer)	Thermo Fisher Scientific	NA
IgG-int 5'- GGGCCGCTGTGCCCCAGAGGTGCT CYTGGA –3' (PCRb primer)	Thermo Fisher Scientific	NA
IgM-int 5'- GGGCCGCTGTGCCCCAGAGGTGGAA TTCTCACAGGAGACGAGG –3' (PCRb primer)	Thermo Fisher Scientific	NA
IgD-int 5'- GGGCCGCTGTGCCCCAGAGGTGTGT CTGCACCCTGATATGATGG –3' (PCRb primer)	Thermo Fisher Scientific	NA
IgA1-int 5'- GGGCCGCTGTGCCCCAGAGGTGCT GGTGTGCAGAGGCTCAG –3' (PCRb primer)	Thermo Fisher Scientific	NA
IgA2-int 5'- GGGCCGCTGTGCCCCAGAGGTGCTG GTGCTGTCGAGGCTCAG –3' (PCRb primer)	Thermo Fisher Scientific	NA

(Continued on next page)

Continued

Reagent or resource	Source	Identifier
VK1-Int tag 5'- CTGGGTCCAGGTCCACTGGTGAC GACATCCAGWTGACCCAGTCTC -3' (PCRb primer)	Thermo Fisher Scientific	NA
VK2-Int tag 5'- CTGGGTCCAGGTCCACTGGTGAC GATATTGTGATGACCCAGWCTCCAC -3' (PCRb primer)	Thermo Fisher Scientific	NA
VK3-Int tag 5'- CTGGGTCCAGGTCCACTGGTGAC GAAATTGTGTTGACRCAGTCTCCA -3' (PCRb primer)	Thermo Fisher Scientific	NA
VK4-Int tag 5'- CTGGGTCCAGGTCCACTGGTGA CGACATCGTGATGACCCAGTCTC -3' (PCRb primer)	Thermo Fisher Scientific	NA
VK5-Int tag 5'- CTGGGTCCAGGTCCACTGGTGA CGAAACGACACTCACGCAGTCTC -3' (PCRb primer)	Thermo Fisher Scientific	NA
VK6-Int tag 5'- CTGGGTCCAGGTCCACTGGTGACGAA ATTGTGCTGACWCAGTCTCCA -3' (PCRb primer)	Thermo Fisher Scientific	NA
VK7-Int tag 5'- CTGGGTCCAGGTCCACTGGTG ACGACATTGTGCTGACCCAGTCT -3' (PCRb primer)	Thermo Fisher Scientific	NA
CK-int 5'- GGGAAAGATGAAGACAGATGGT -3' (PCRb primer)	Thermo Fisher Scientific	NA
VL1-Int tag 5'- CTGGGTCCAGGTCCACTGGTG ACCAGTCTGTGYTGACKCAGCC -3' (PCRb primer)	Thermo Fisher Scientific	NA
VL2-Int tag 5'- CTGGGTCCAGGTCCACTGGT GACCAGTCTGCCCTGACTCAGCC -3' (PCRb primer)	Thermo Fisher Scientific	NA
VL3-Int tag 5'- CTGGGTCCAGGTCCACTGG TGACTCYATGAGCTGACWCAGCCAC -3' (PCRb primer)	Thermo Fisher Scientific	NA
VL3l-Int tag 5'- CTGGGTCCAGGTCCACTGG TGACTCTTCTGAGCTGACTCAGGACCC -3' (PCRb primer)	Thermo Fisher Scientific	NA
VL4ab-Int tag 5'- CTGGGTCCAGGTCCACTGGT GACCAGCYGTGCTGACTCAATC -3' (PCRb primer)	Thermo Fisher Scientific	NA
VL4c-Int tag 5'- CTGGGTCCAGGTCCACT GGTGACCTGCCTGTGCTGACTCAGC -3' (PCRb primer)	Thermo Fisher Scientific	NA
VL5,9-Int tag 5'- CTGGGTCCAGGTCCACT GGTGACCAGSCTGTGCTGACTCAGCC -3' (PCRb primer)	Thermo Fisher Scientific	NA
VL6-Int tag 5'- CTGGGTCCAGGTCCACTGGTG ACAATTTTATGCTGACTCAGCCCCACT -3' (PCRb primer)	Thermo Fisher Scientific	NA
VL7,8-Int tag 5'- CTGGGTCCAGGTCCACTGGT GACCAGRCTGTGGTGACYCAGGAG -3' (PCRb primer)	Thermo Fisher Scientific	NA
VL10-Int tag 5'- CTGGGTCCAGGTCCACTGGTG ACCAGGCAGGGCWGACTCAG -3' (PCRb primer)	Thermo Fisher Scientific	NA
CL-int 5'- GGGYGGGAACAGAGTGACC -3' (PCRb primer)	Thermo Fisher Scientific	NA
VH_Tag fwd seq 5'- CTGGGTCCAGGTCC ACTGGTGAC -3' (Sequencing primer)	Thermo Fisher Scientific	NA
CK_int 5'- GGGAAAGATGAAGACAGATGGT -3' (Sequencing primer)	Thermo Fisher Scientific	NA
CL_int 5'- GGGYGGGAACAGAGTGACC -3' (Sequencing primer)	Thermo Fisher Scientific	NA

(Continued on next page)

Continued

Reagent or resource	Source	Identifier
HV13221H_R474 5'- GCTGTGCCCCC AGAGGTG –3' (Sequencing primer)	Thermo Fisher Scientific	NA
SARS-CoV-2 or WIV1-CoV E gene subgenomic RNA primer/probe: forward primer: 5'- CGATCTCTTGATAGATCTGTTCT C-3'; reverse primer: 5'-ATATTGCAGCAGTACGCACACA –3'; Probe: 5'-FAM-ACACTAGCCATCCTTACT GCGCTTCG-BHQ1-3'.	Taqman	NA
SARS-CoV-2 N gene subgenomic RNA primer/ probe: forward primer: 5'-CGATCTCTTGATAG TCTGTTCT C-3'; reverse primer: 5'-GGTGAACC AAGACGCAGTAT-3'; Probe: 5'-FAM-TAACCAG AATGGAGAACGCAGTG GG-BHQ1-3'.	Taqman	NA
WIV1-CoV N gene subgenomic RNA primer/probe: forward primer: 5'-CGATCTCTTGATAGTCTGTTCT C-3'; reverse primer: 5'-TGTGAACCAAGACGCAGT ATTA T-3'; Probe: 5'-FAM-TAACCAGAATGGAGG ACGCAATG GG-BHQ1-3';	Taqman	NA
SARS-CoV-2 total viral RNA E gene primer/probe: forward primer: 5'-ACAGGTACGTTAATAGTTAATA GCGT-3', reverse primer: 5'-ATATTGCAGCAGTAC GCACACA –3'; probe: 5'-6FAM/ACACTAGCCATCC TACTGCGCT TCG/IABkFQ-3'.	Taqman	NA
Recombinant DNA		
HV1301409_4A (human IgG1_4A heavy chain backbone)	Genscript	NA
pH510049_VRC_LS.v2 (human IgG1_ LS heavy chain backbone)	Genscript	NA
HV1301410 (human kappa chain backbone)	Genscript	NA
HV1301414.v2 (human lambda chain backbone)	Genscript	NA
pcDNA3.1-SARS-CoV-2_SgE (for making subgenomic RNA standard RNA)	Genscript	NA
pcDNA3.1-SARS-CoV-2_SgN (for making subgenomic RNA standard RNA)	Genscript	NA
pcDNA3.1-WIV1-CoV_SgN (for making subgenomic RNA standard RNA)	Genscript	NA
Software and algorithms		
Diva	BD Biosciences	https://www.bdbiosciences.com/en-us
FlowJo v9.9.4	FlowJo	https://www.flowjo.com
GraphPad Prism v8.3.1	GraphPad Software Inc	https://www.graphpad.com/scientific-software/prism/
SAS v9.4	SAS Institute	NA
Cloanalyst Program	(Kepler et al., 2014)	NA
Biacore S200 Evaluation software	Cytiva	NA
Coot	(Emsley et al., 2010)	Version 0.8.9.2
Relion	(Scheres, 2012; Scheres, 2016)	Version 3.1
Phenix	(Afonine et al., 2018; Liebschner et al., 2019)	Version 1.17
UCSF Chimera	(Pettersen et al., 2004)	http://www.cgl.ucsf.edu/chimera/
ISOLDE	(Croll, 2018)	Version 1.1

(Continued on next page)

Continued

Reagent or resource	Source	Identifier
Chimera X	(Goddard et al., 2018)	https://www.rbvi.ucsf.edu/chimerax/
PyMol	The PyMOL Molecular Graphics System (Schrö and dinger, 2015).	https://www.pymol.org/2/
Leginon system	(Suloway et al., 2005).	NA
cryoSPARC	(Punjani et al., 2017)	https://cryosparc.com
Bio-Plex Manager Software	Bio-Rad	NA
Adobe Illustrator 2020	Adobe	NA
Adobe Photoshop CC 2019	Adobe	NA

RESOURCE AVAILABILITY

Lead contact

Further information and requests for reagents should be directed and will be fulfilled by the lead contact Kevin O. Saunders (kevin.saunders@duke.edu).

Materials availability

Abs and other reagents generated in this study are available from the lead contact with a completed Materials Transfer Agreement.

Data and code availability

The data that support the findings of this study are available from the corresponding authors on request.

EXPERIMENTAL MODEL AND SUBJECT DETAILS

Human subjects

Nasopharyngeal swabs and peripheral blood samples were collected from a convalescent COVID-19 donor (MESSI ID #450905) on designated days after reported onset of COVID symptoms. The SARS-CoV donor PBMC were provided by the NIH/VRC. Human specimens were collected and used with the informed consent of study participants and in compliance with the Duke University Medical Center Institutional Review Board (DUHS IRB Pro00100241).

Symptom data collections

Participant self-reported symptoms were recorded at each time-point for 39 symptom categories (nasal discharge, nasal congestion, sneezing, coughing, shortness of breath, malaise, throat discomfort, fever, headache, shaking chills, loss of smell, loss of taste, excessive sweating, dizziness, pain behind the eyes, itchy/watery eyes, visual blurring, hearing problems, ear pain, confusion, stiff neck, swollen glands, palpitations, chest pain, pain in joints, muscle soreness, fatigue, loss of appetite, abdominal pain, nausea/vomiting, diarrhea, swelling, itchy skin, rash, skin lesions, unusual bleeding, red fingers or toes, red eyes, other: specify). Each symptom was scored on a scale of 0–4, with 0 indicating not present, 1 mild, 2 moderate, 3 severe, and 4 very severe symptoms. Daily symptom count (number of non-zero symptom categories) and symptom severity (sum of all symptom scores) were determined for each survey time point. At enrollment, date of symptom onset was determined, and an initial “historical” symptom survey recorded maximum score for each symptom category between symptom onset and study enrollment.

Non-human primate model

In total, 62 outbred adult male and female cynomolgus macaques (*Macaca fascicularis*), 2–4 kg body weight, were randomly allocated to groups. The study protocol and all veterinarian procedures were approved by the Bioqual IACUC per a memorandum of understanding with the Duke IACUC, and were performed based on standard operating procedures. Macaques were housed and maintained in an Association for Assessment and Accreditation of Laboratory Animal Care-accredited institution in accordance with the principles of the National Institute of Health. All studies were carried out in strict accordance with the recommendations in the Guide for the Care and Use of Laboratory Animals of the National Institutes of Health in BIOQUAL (Rockville, MD). BIOQUAL is fully accredited by AAALAC and through OLAW, Assurance Number A-3086. All physical procedures associated with this work were done under anesthesia to minimize pain and distress in accordance with the recommendations of the Weatherall report, “The use of non-human primates in research.” Teklad 5038 Primate Diet was provided once daily by animal size and weight. The diet was supplemented with fresh fruit and vegetables. Fresh water was given *ad libitum*. All monkeys were maintained in accordance with the Guide for the Care and Use of Laboratory Animals.

Mouse models

Eleven to twelve-month old female immunocompetent BALB/c mice purchased from Envigo (BALB/c AnNHsd, stock# 047) were used for SARS-CoV-2 *in vivo* protection experiments as described previously (Dinnon et al., 2020; Leist et al., 2020a). Ten-week-old *HFH4-hACE2* transgenic mice were bred and maintained at the University of North Carolina at Chapel Hill and used for WIV-1 *in vivo* protection experiments. Mice were housed in groups of five animals per cage and fed standard chow diet. The study was carried out in accordance with the recommendations for care and use of animals by the Office of Laboratory Animal Welfare (OLAW), National Institutes of Health and the Institutional Animal Care. All mouse studies were performed at the University of North Carolina (Animal Welfare Assurance #A3410-01) using protocols (19-168) approved by the UNC Institutional Animal Care and Use Committee (IACUC) and all mouse studies were performed in a BSL3 facility at UNC.

METHOD DETAILS

Expression of recombinant viral proteins

The SARS-CoV-2 ectodomain constructs were produced and purified as described previously (Wrapp et al., 2020b). Plasmids encoding Spike-2P and HexaPro (Hsieh et al., 2020) were transiently transfected in FreeStyle 293F cells (Thermo Fisher) using Turbo293 (SpeedBiosystems). The cultures were collected on Day 6 post transfection. The cells were separated from the medium by centrifugation. Protein were purified from filtered cell supernatants by StrepTactin resin (IBA) and additionally by size exclusive chromatography using Superose 6 10/300 increase column (GE Healthcare) in 2mM Tris pH 8, 200mM NaCl, 0.02% NaN₃. SARS-CoV-2 NTD was produced as previously described (Zhou et al., 2020b). SARS-CoV RBD and MERS-CoV Spike RBD were cloned into pVRC8400 vector for mammalian expression (FreeStyle 293F or Expi293F suspension cells). The construct contains an HRV 3C-cleavable C-terminal SBP-8xHis tag. Supernatants were harvested 5 days post-transfection and passaged directly over Cobalt-TALON resin (Takara) followed by size exclusion chromatography on Superdex 200 Increase (GE Healthcare) in 1x PBS. Typical yields from FreeStyle 293F cells are approximately 50 mg/liter culture. Affinity tags can be removed using HRV 3C protease (ThermoScientific) and the protein repurified using Cobalt-TALON resin to remove the protease, tag and non-cleaved protein.

Antigen-specific single B cell sorting

Plasmablasts were sorted by flow cytometry from the SARS-CoV-2 donor on Day 11 and Day 15 post symptom onset. PBMCs were stained with optimal concentrations of the following fluorochrome-Ab conjugates: IgD PE (Clone# IA6-2, BD Biosciences, Catalog# 555779), CD3 PE-Cy5 (Clone# HIT3a, BD Biosciences, Catalog# 555341), CD10 PE-CF594 (Clone# HI10A, BD Biosciences, Catalog# 562396), CD27 PE-Cy7 (Clone# O323, eBioscience, Catalog# 25-0279), CD38 APC-Alexa Fluor (AF) 700 (Clone# LS198-4-2, Beckman Coulter, Catalog# B23489), CD19 APC-Cy7 (Clone# LJ25C1, BD Biosciences, Catalog# 561743), CD16 BV570 (Clone# 3G8, Biolegend, Catalog# 302035), CD14 BV605 (Clone# M5E2, Biolegend, Catalog# 301834), and CD20 BV650 (Clone# 2H7, BD, Catalog# 563780). The cells were then labeled with Fixable Aqua Live/Dead Cell Stain Kit (Invitrogen, Catalog# L34957). On a BD FACSAria II flow cytometer (BD Biosciences), plasmablasts were identified as viable CD14⁻/CD16⁻/CD19⁺/CD20^{low}/IgD⁻/CD27^{high}/CD38^{high} cells and sorted as single cells into 96-well plates containing lysis buffer. Sorted plates were frozen at -80°C in the DHVI Flow Facility under BSL3 precautions in the Duke Regional Biocontainment Laboratory (Durham, NC) until processing.

Antigen-specific memory B cells (MBCs) were isolated by flow cytometric sorting from the SARS-CoV-2 donor on Day 36 post symptom onset, and a donor with SARS-CoV history. PBMCs were stained with IgD FITC (Clone# IA6-2, BD Biosciences, Catalog# 555778), IgM PerCp-Cy5.5 (Clone# G20-127, BD Biosciences, Catalog# 561285), CD10 PE-CF594 (Clone# HI10A, BD Biosciences, Catalog# 562396), CD3 PE-Cy5 (Clone# HIT3a, BD Biosciences, Catalog# 555341), CD235a PE-Cy5 (Clone# GA-R2, BD Biosciences, Catalog# 559944), CD27 PE-Cy7 (Clone# O323, eBioscience, Catalog# 25-0279), CD38 APC-AF700 (Clone# LS198-4-2, Beckman Coulter, Catalog# B23489), CD19 APC-Cy7 (Clone# LJ25C1, BD Biosciences, Catalog# 561743), CD14 BV605 (Clone# M5E2, Biolegend, Catalog# 301834), CD16 BV570 (Clone# 3G8, Biolegend, Catalog# 302035), and fluorescent-labeled SARS-CoV-2 Spike probes (AF647-conjugated Spike-2P, PE-conjugated Spike-2P, AF647-conjugated NTD, AF647-conjugated RBD, VioBright 515-conjugated RBD). The cells were then labeled with Fixable Aqua Live/Dead Cell Stain Kit (Invitrogen, Catalog# L34957). On a BD FACSAria II flow cytometer (BD Biosciences), antigen-specific MBCs were identified as viable CD3⁺/CD14⁻/CD16⁻/CD235a⁺/CD19⁺/IgD⁻/probe⁺ cells and were sorted as single cells into 96-well plates containing lysis buffer. Collection plates were immediately frozen in a dry ice/ethanol bath, and stored at -80°C in the DHVI Flow Facility under BSL3 precautions in the Duke Regional Biocontainment Laboratory until processing. Flow cytometric data were analyzed using FlowJo version 10.

PCR Amplification of human Ab genes

Ab genes were amplified by RT-PCR from flow cytometry-sorted single B cells using the methods as described previously (Liao et al., 2009; Wrammert et al., 2008) with modification. The PCR-amplified genes were then purified and sequenced with 10 μM forward and reverse primers. Sequences were analyzed by using the human library in Cloanalyzer for the VDJ arrangements of the immunoglobulin IGHV, IGKV, and IGLV sequences and mutation frequencies (Kepler et al., 2014). Clonal relatedness of V_HD_HJ_H and V_LJ_L sequences was determined as previously described (Liao et al., 2013).

Expression of Ab viable region genes as full-length IgG recombinant mAbs

Transient transfection of recombinant Abs was performed as previously described (Liao et al., 2009). Briefly, purified PCR products were used for overlapping PCR to generate linear human IgG expression cassettes. The expression cassettes were transfected into Expi293F cells using ExpiFectamine (Thermo Fisher Scientific, Catalog# A14525 and A14527). The supernatant samples containing recombinant IgGs were used for IgG quantification and preliminary ELISA binding screening.

The down-selected human Ab genes were then synthesized and cloned (GenScript) into a human IgG1 backbone (HV1301409_4A) with 4A mutations to enhance circulation half-life and Ab-dependent cell-mediated cytotoxicity (ADCC) or a human IgG1 backbone (pH510049_VRC_LS.v2) with a LS mutation to extend Ab half-life (Saunders, 2019). Recombinant IgG Abs were then produced in HEK293i suspension cells by transfection with ExpiFectamine and purified using Protein A resin. The purified IgG Abs were run in SDS-PAGE for Coomassie blue staining and western blot for quality control and then used for the downstream experiments.

Ab binding ELISA

For ELISA binding assays of coronavirus Spike Abs, the antigen panel included SARS-CoV-2 Spike S1+S2 ectodomain (ECD) (SINO, Catalog # 40589-V08B1), SARS-CoV-2 Spike-2P (Wrapp et al., 2020b), SARS-CoV-2 Spike S2 ECD (SINO, Catalog # 40590-V08B), SARS-CoV-2 Spike RBD from insect cell sf9 (SINO, Catalog # 40592-V08B), SARS-CoV-2 Spike RBD from mammalian cell 293 (SINO, Catalog # 40592-V08H), SARS-CoV-2 Spike NTD-Biotin, SARS-CoV Spike Protein DeltaTM (BEI, Catalog # NR-722), SARS-CoV WH20 Spike RBD (SINO, Catalog # 40150-V08B2), SARS-CoV WH20 Spike S1 (SINO, Catalog #40150-V08B1), SARS-CoV RBD, MERS-CoV Spike S1+S2 (SINO, Catalog # 40069-V08B), MERS-CoV Spike S1 (SINO, Catalog #40069-V08B1), MERS-CoV Spike S2 (SINO, Catalog #40070-V08B), MERS-CoV Spike RBD (SINO, Catalog #40071-V08B1), MERS-CoV Spike RBD. In preliminary ELISA screening of the transient transfection supernatants, we also screened the Abs against SARS-CoV CL Protease protein (BEI, Catalog # 30105) and SARS-CoV Membrane (M) protein (BEI, Catalog # 110705).

For binding ELISA, 384-well ELISA plates were coated with 2 $\mu\text{g/mL}$ of antigens in 0.1 M sodium bicarbonate overnight at 4°C. Plates were washed with PBS + 0.05% Tween 20 and blocked with blocked with assay diluent (PBS containing 4% (w/v) whey protein, 15% Normal Goat Serum, 0.5% Tween-20, and 0.05% Sodium Azide) at room temperature for 1 hour. Purified mAb samples in 3-fold serial dilutions in assay diluent starting at 100 $\mu\text{g/mL}$, or un-diluted transfection supernatant were added and incubated for 1 hour, followed by washing with PBS-0.1% Tween 20. HRP-conjugated goat anti-human IgG secondary Ab (SouthernBiotech, catalog# 2040-05) was diluted to 1:10,000 and incubated at room temperature for 1 hour. These plates were washed four times and developed with tetramethylbenzidine substrate (SureBlue Reserve- KPL). The reaction was stopped with 1 M HCl, and optical density at 450 nm (OD_{450}) was determined.

Affinity measurements

SPR measurements of SARS-CoV-2 Ab Fab binding to Spike-2P or Spike-HexaPro proteins were performed using a Biacore S200 instrument (Cytiva, formerly GE Healthcare, DHVI BIA Core Facility, Durham, NC) in HBS-EP+ 1x running buffer. The Spike proteins were first captured onto a Series S Streptavidin chip to a level of 300-400 RU for Spike-2P and 350-450 resonance units (RU) for Spike-HexaPro. The Ab Fabs were injected at 0.5 to 500 nM over the captured S proteins using the single cycle kinetics injection mode at a flow rate of 50 $\mu\text{L/min}$. Association phase was maintained with either 120 or 240 s injections of each Fab at increasing concentrations followed by a dissociation of 600 s after the final injection. After dissociation, the S proteins were regenerated from the streptavidin surface using a 30 s pulse of Glycine pH1.5. Results were analyzed using the Biacore S200 Evaluation software (Cytiva). A blank streptavidin surface along with blank buffer binding were used for double reference subtraction to account for non-specific protein binding and signal drift. Subsequent curve fitting analyses were performed using a 1:1 Langmuir model with a local R_{max} for the Fabs with the exception of DH1050.1 Fab which was fit using the heterogeneous ligand model with local R_{max} . The reported binding curves are representative of two datasets.

Surface plasmon resonance Ab blocking assay

RBD and NTD Abs binding to S protein was measured by surface plasmon resonance (BIAcore 3000; Cytiva, formerly GE Healthcare, DHVI BIA Core Facility, Durham, NC) analysis. Ab binding competition and blocking were measured by SPR following immobilization by amine coupling of monoclonal Abs to CM5 sensor chips (BIAcore/Cytiva). Ab competition experiments were performed by mixing S protein and mAb (30 minutes incubation) followed by injection for 5 minutes at 50 $\mu\text{L/min}$. In separate assays and from analysis of binding to an identical epitope binding ligand, it was determined that S protein at 20 μM and Ab at 200 μM bind to complete saturation. Ab blocking assays were performed by co-injecting S protein (20 μM) over mAb immobilized surfaces for 3 minutes at 30 $\mu\text{L/min}$ and a test Ab (200 μM) for 3 minutes at 30 $\mu\text{L/min}$. The dissociation of the Ab sandwich complex with the spike protein was monitored for 10 minutes with buffer flow and then a 24 s injection of Glycine pH2.0 for regeneration. Blank buffer binding was used for subtraction to account for signal drift. Data analyses were performed with BIA-evaluation 4.1 software (BIAcore/Cytiva).

ACE2-blocking assay

For ACE-2 blocking assays, plates were coated as stated above with 2 $\mu\text{g/mL}$ recombinant ACE-2 protein, then washed and blocked with 3% BSA in 1X PBS. While assay plates blocked, purified Abs were diluted as stated above, only in 1% BSA with 0.05% Tween-20. In a separate dilution plate Spike-2P protein was mixed with the Abs at a final concentration equal to the EC_{50} at which spike binds

to ACE-2 protein. The mixture was allowed to incubate at room temperature for 1 hour. Blocked assay plates were then washed and the Ab-spike mixture was added to the assay plates for a period of 1 hour at room temperature. Plates were washed and a polyclonal rabbit serum against the same Spike-2P protein was added for 1 hour, washed and detected with goat anti rabbit-HRP (Abcam cat# ab97080) followed by TMB substrate. The extent to which Abs were able to block the binding of spike protein to ACE-2 was determined by comparing the optical density (OD) at 450 nm of Ab plus spike to the OD of wells containing spike protein without Ab. The following formula was used to calculate percent blocking: $\text{blocking\%} = (100 - (\text{OD Ab+spike} / \text{OD of spike only}) * 100)$.

Negative-stain electron microscopy

Fab fragments were prepared by digesting the IgG with Lys-C, as described previously (Zhou et al., 2015). For each Fab-spike complex, an aliquot of spike protein at ~1-5 mg/ml concentration that had been flash frozen and stored at -80°C was thawed in an aluminum block at 37°C for 5 minutes; then 1-4 μl of spike was mixed with sufficient Fab to give a 9:1 molar ratio of Fab to spike and incubated for 1 hour at 37°C . The complex was then cross-linked by diluting to a final spike concentration of 0.1 mg/ml into room-temperature buffer containing 150 mM NaCl, 20 mM HEPES pH 7.4, 5% glycerol, and 7.5 mM glutaraldehyde. After 5 minutes cross-linking, excess glutaraldehyde was quenched by adding sufficient 1 M Tris pH 7.4 stock to give a final concentration of 75 mM Tris and incubated for 5 minutes. For negative stain, carbon-coated grids (EMS, CF300-cu-UL) were glow-discharged for 20 s at 15 mA, after which a 5- μl drop of quenched sample was incubated on the grid for 10-15 s, blotted, and then stained with 2% uranyl formate. After air drying, grids were imaged with a Philips EM420 electron microscope operated at 120 kV, at 82,000x magnification and images captured with a 2k x 2k CCD camera at a pixel size of 4.02 Å.

Image processing of negative stain images

The RELION 3.0 program was used for all negative stain image processing. Images were imported, CTF-corrected with CTFFIND, and particles were picked using a spike template from previous 2D class averages of spike alone. Extracted particle stacks were subjected to 2-3 rounds of 2D class averaging and selection to discard junk particles and background picks. Cleaned particle stacks were then subjected to 3D classification using a starting model created from a bare spike model, PDB: 6vsb, low-pass filtered to 30 Å. Classes that showed clearly-defined Fabs were selected for final refinements followed by automatic filtering and B-factor sharpening with the default Relion post-processing parameters.

Cryo-EM sample preparation, data collection and processing

To prepare Ab-bound complexes of the SARS-CoV-2 2P spike, the spike at a final concentration of 1-2 mg/mL, in a buffer containing 2 mM Tris pH 8.0, 200 mM NaCl and 0.02% NaN₃, was incubated with 5-6 fold molar excess of the Ab Fab fragments for 30-60 min. 0.5% final concentration of glycerol was added to the sample right before freezing. 2.5 μL of protein was deposited on a Quantifoil-1.2/1.3 holey carbon grid that had been glow discharged in a PELCO easiGlow Glow Discharge Cleaning System for 15 s at 15 mA. After a 30 s incubation in > 95% humidity and 22°C , excess protein was blotted away for 2.5 s using a Whatman #1 filter paper before being plunge frozen into liquid ethane using a Leica EM GP2 plunge freezer (Leica Microsystems). Cryo-EM data were collected on a Titan Krios (Thermo Fisher) equipped with a K3 detector (Gatan). Data were acquired using the Legion system (Suloway et al., 2005). All the datasets were energy filtered through either a 20eV or 30eV slit. The dose was fractionated over 50 raw frames and collected at 50ms framerate. Individual frames were aligned and dose-weighted (Zheng et al., 2017). CTF estimation, particle picking and all downstream data processing steps were carried out in cryoSPARC (Punjani et al., 2017). After two rounds of 2D classifications during which junk particles were discarded, heterogeneous refinement was performed using low pass filtered maps of unliganded spike as inputs. The output maps showed densities of the bound Fabs, which were further classified by heterogeneous refinement, followed by non-uniform refinement to obtain the final reconstructions that were used for model fitting.

Cryo-EM structure fitting and analysis

Previously published SARS-CoV-2 ectodomain structures of the all 'down' state (PDB: 6VXX) and single RBD 'up' state (PDB: 6VYB), and models of 2-RBD-up and 3-RBD-up states derived from these, were used to fit the cryo-EM maps in Chimera (Pettersen et al., 2004). Models of Fabs were generated in SWIS-MODEL and docked into the cryo-EM reconstructions using Chimera. Mutations were made in Coot (Emsley and Cowtan, 2004). Coordinates were fit to the maps using ISOLDE (Croll, 2018) followed by iterative refinement using Phenix (Afonine et al., 2018) real space refinement and subsequent manual coordinate fitting in Coot as needed. Structure and map analysis were performed using PyMol (Schroder and Dinger, 2015), Chimera (Pettersen et al., 2004) and ChimeraX (Goddard et al., 2018).

Live SARS-CoV-2 neutralization assays

The SARS-CoV-2 virus (Isolate USA-WA1/2020, NR-52281) was deposited by the Centers for Disease Control and Prevention and obtained through BEI Resources, NIAID, NIH. SARS-CoV-2 Micro-neutralization (MN) assays were adapted from a previous study (Berry et al., 2004). In short, sera or purified Abs were diluted two-fold and incubated with 100 TCID₅₀ virus for 1 hour. These dilutions are used as the input material for a TCID₅₀. Each batch of MN includes a known neutralizing control Ab (Clone D001; SINO, CAT# 40150-D001). Data are reported as the last concentration at which a test sample protects Vero E6 cells.

SARS-CoV-2 Plaque Reduction Neutralization Test (PRNT) were performed in the Duke Regional Biocontainment Laboratory BSL3 (Durham, NC) as previously described with virus-specific modifications (Berry et al., 2004). Briefly, two-fold dilutions of a test sample (e.g., serum, plasma, purified Ab) were incubated with 50 PFU SARS-CoV-2 virus (isolate USA-WA1/2020, NR-52281) for 1 hour. The Ab/virus mixture is used to inoculate Vero E6 cells in a standard plaque assay (Coleman and Frieman, 2015; Kint et al., 2015). Briefly, infected cultures are incubated at 37°C, 5% CO₂ for 1 hour. At the end of the incubation, 1 mL of a viscous overlay (1:1 2X DMEM and 1.2% methylcellulose) is added to each well. Plates are incubated for 4 days. After fixation, staining and washing, plates are dried and plaques from each dilution of each sample are counted. Data are reported as the concentration at which 50% of input virus is neutralized. A known neutralizing control Ab is included in each batch run (Clone D001; SINO, CAT# 40150-D001). GraphPad Prism was used to determine IC₅₀ values.

SARS-CoV-2 nano-luciferase (nanoLuc), SARS-CoV nanoLuc and WIV1-CoV nanoLuc replication-competent virus neutralization assay were described previously (Hou et al., 2020; Menachery et al., 2016; Sheahan et al., 2017).

Pseudo-typed SARS-CoV-2 neutralization assay and infection-enhancing assays

Neutralization of SARS-CoV-2 Spike-pseudotyped virus was performed by adopting an infection assay described previously (Korber et al., 2020) with lentiviral vectors and infection in either 293T/ACE2.MF (the cell line was kindly provided by Drs. Mike Farzan and Huihui Mu at Scripps). Cells were maintained in DMEM containing 10% FBS and 50 µg/ml gentamicin. An expression plasmid encoding codon-optimized full-length spike of the Wuhan-1 strain (VRC7480), was provided by Drs. Barney Graham and Kizzmekia Corbett at the Vaccine Research Center, National Institutes of Health (USA). The D614G mutation was introduced into VRC7480 by site-directed mutagenesis using the QuikChange Lightning Site-Directed Mutagenesis Kit from Agilent Technologies (Catalog # 210518). The mutation was confirmed by full-length spike gene sequencing. Pseudovirions were produced in HEK293T/17 cells (ATCC cat. no. CRL-11268) by transfection using Fugene 6 (Promega, Catalog #E2692). Pseudovirions for 293T/ACE2 infection were produced by co-transfection with a lentiviral backbone (pCMV ΔR8.2) and firefly luciferase reporter gene (pHR' CMV Luc) (Naldini et al., 1996). Culture supernatants from transfections were clarified of cells by low-speed centrifugation and filtration (0.45 µm filter) and stored in 1 mL aliquots at -80°C.

For 293T/ACE2 neutralization assays, a pre-titrated dose of virus was incubated with 8 serial 3-fold or 5-fold dilutions of mAbs in duplicate in a total volume of 150 µl for 1 hr at 37°C in 96-well flat-bottom poly-L-lysine-coated culture plates (Corning Biocoat). Cells were suspended using TrypLE express enzyme solution (Thermo Fisher Scientific) and immediately added to all wells (10,000 cells in 100 µL of growth medium per well). One set of 8 control wells received cells + virus (virus control) and another set of 8 wells received cells only (background control). After 66-72 hr of incubation, medium was removed by gentle aspiration and 30 µL of Promega 1x lysis buffer was added to all wells. After a 10-minute incubation at room temperature, 100 µl of Bright-Glo luciferase reagent was added to all wells. After 1-2 minutes, 110 µl of the cell lysate was transferred to a black/white plate (Perkin-Elmer). Luminescence was measured using a PerkinElmer Life Sciences, Model Victor2 luminometer. Neutralization titers are the mAb concentration (IC₅₀/IC₈₀) at which relative luminescence units (RLU) were reduced by 50% and 80% compared to virus control wells after subtraction of background RLUs. Negative neutralization values are indicative of infection-enhancement. Maximum percent inhibition (MPI) is the reduction in RLU at the highest mAb concentration tested.

For the TZM-bl neutralization assays, a pre-titrated dose of virus was incubated with serial 3-fold dilutions of test sample in duplicate in a total volume of 150 µl for 1 hr at 37°C in 96-well flat-bottom culture plates. Freshly trypsinized cells (10,000 cells in 100 µL of growth medium containing 75 µg/ml DEAE dextran) were added to each well. One set of control wells received cells + virus (virus control) and another set received cells only (background control). After 68-72 hours of incubation, 150 µL of cultured medium was removed from each well, and 100ul of Britelite Luminescence Reporter Gene Assay System (PerkinElmer Life Sciences) were added and plates incubated for 2 min at room temperature. After this period 150 µL of the lysate was transferred to black solid plates (Costar) for measurements of luminescence in a Perkin Elmer instrument. Neutralization titers are the serum dilution at which relative luminescence units (RLU) were reduced by 50% and 80% compared to virus control wells after subtraction of background RLUs. MPI is the reduction in RLU at the highest mAb concentration tested. Infection-enhancing assays were performed with the same format but using TZM-bl cell lines stably expressing each of the four human FcγR receptors (Perez et al., 2009). In this assay an increase in RLUs over the virus control signal represents FcR-mediated entry.

Non-human primate protection study

Groups of five cynomolgus macaques (2-4 kg) were given intravenous infusion with Abs at 10 mg/kg body weight on Day -3, relative to infectious virus challenge. For each animal, 10⁵ PFU (~10⁶ TCID₅₀) SARS-CoV-2 virus (isolate USA-WA1/2020) were diluted in 4 mL, and were given by 1 mL intranasally and 3 mL intratracheally on Day 0. Plasma and serum samples were collected on Day -5, 0, 2, and 4. Nasal swabs, nasal washes, and bronchoalveolar lavage (BAL) were collected on Day -5, 2, and 4.

Histopathology and Immunohistochemistry (IHC)

Lung specimen from nonhuman primates were fixed in 10% neutral buffered formalin, processed, and blocked in paraffin for histological analysis. All samples were sectioned at 5 µm and stained with hematoxylin-eosin (H&E) for routine histopathology. Sections were examined under light microscopy using an Olympus BX51 microscope and photographs were taken using an Olympus DP73 camera.

Staining for SARS-CoV-2 antigen was achieved on the Bond RX automated system with the Polymer Define Detection System (Leica) used per manufacturer's protocol. Tissue sections were dewaxed with Bond Dewaxing Solution (Leica) at 72°C for 30 min then subsequently rehydrated with graded alcohol washes and 1x Immuno Wash (StatLab). Heat-induced epitope retrieval (HIER) was performed using Epitope Retrieval Solution 1 (Leica), heated to 100°C for 20 minutes. A peroxide block (Leica) was applied for 5 min to quench endogenous peroxidase activity prior to applying the SARS-CoV-2 Ab (1:2000, GeneTex, GTX135357). Abs were diluted in Background Reducing Ab Diluent (Agilent). The tissue was subsequently incubated with an anti-rabbit HRP polymer (Leica) and colorized with 3,3'-Diaminobenzidine (DAB) chromogen for 10 min. Slides were counterstained with hematoxylin. For macrophage staining, Abs for the following markers were used: CD3 (T cell marker; Bio Rad, Catalog # MCA1477; 1:600 dilution), Iba1 (macrophage marker; Wako, Catalog # 019-19741; 1:800 dilution), CD68 (M1 macrophage marker, Sigma-Millipore, Catalog # HPA048982; 1:1000 dilution), CD163 (M2 macrophage marker; Abcam, Catalog # ab182422; 1:500 dilution), HLA-DP/DQ/DR (Catalog # M1 macrophage marker; Dako, Catalog # M0775; 1:100 dilution), CD11b (monocyte/granulocyte marker; Abcam, Catalog # ab52478; 1:1000 dilution).

Samples were evaluated by a board-certified veterinary pathologist in a blinded manner. Sections of the left caudal (Lc), right mid-dle (Rm), and right caudal (Rc) lung were evaluated and scored for the presence of inflammation by H&E staining, and for the presence of SARS-CoV-2 nucleocapsid by IHC staining. The sums of Lc, Rm, and Rc scores in each animal shown in figures.

Luminex assay

For cytokine profiling, 7-fold concentrated cynomolgus macaques BAL samples were measured using a 25-analyte multiplex bead array (Millipore, catalog # PRCYT2MAG40K) including sCD137, Eotaxin, sFasL, FGF-2, Fractalkine, Granzyme A, Granzyme B, IL-1 α , IL-2, IL-4, IL-6, IL-16, IL-17A, IL-17E/IL-25, IL-21, IL-22, IL-23, IL-28A, IL-31, IL-33, IP-10, MIP-3 α , Perforin, RANTES, TNF β . Samples were prepared according to the manufacturer's recommended protocol and read using a Flexmap 3D suspension array reader (Luminex Corp.). Data were analyzed using Bio-Plex manager software v6.2 (Bio-Rad).

For human Ab quantification, SARS-CoV-2 Spike-2P protein, A/Solomon Islands/3/2006 hemagglutinin (HA) protein or bovine serum albumen (Sigma) was carbodiimide coupled to MagPlex-C beads (Luminex Corp) according to the bead manufacturer's protocol. Briefly, beads were washed in H₂O then activated by incubation with 5 mg/mL sulfo-N-hydroxysulfosuccinimide and 5 mg/mL 1-ethyl-3-(3-dimethylaminopropyl) carbodiimide hydrochloride (ThermoFisher) for 20 minutes. Activated beads were washed twice in PBS (ThermoFisher) and then vortexed at 1,500 RPM for two hours at room temperature with 25 μ g protein per 5.0×10^6 beads. Labeled beads were washed in PBS (ThermoFisher), 1% BSA, 0.02% Tween-20, 0.05% Sodium Azide (all Sigma), counted using a hemacytometer and stored at -80°C. NHP sera were diluted 1:200 in assay buffer (PBS, 1% BSA, pH 7.4, GIBCO), then 50 μ L of diluted sera or monoclonal Ab 3-fold serially diluted in assay buffer (1000-0.45ng/mL) was added to a 96-well plate and mixed with 50 μ L of assay buffer containing 2500 BSA-conjugated beads (negative control) plus 2500 HA or Spike-conjugated beads. The plate was shaken at 800 RPM for 60 minutes at room temperature, washed twice in assay buffer and then 100 μ L 4 μ g/mL biotin-conjugated mouse anti-human IgG Fc clone H2 (Southern Biotech) in assay buffer was added to every well. The plate was shaken at 800 RPM for 30 minutes at room temperature, washed two times in assay buffer and then 50 μ L 4 μ g/mL streptavidin-r-phycoerythrin (Invitrogen) in assay buffer was added to every well. The plate was shaken at 800 RPM for 30 minutes at room temperature and washed twice in assay buffer. Beads were resuspended in 150 μ L/well assay buffer, shaken at 800 RPM for 15 minutes at room temperature and then analyzed on a BioPlex 200 bead reader (Bio-Rad). Sera antigen-specific Ab concentrations were calculated using Bio-Plex Manager software (Bio-Rad) by extrapolating from the results of the serially-diluted monoclonal Ab. Sera with Abs above the upper limit of quantitation were re-assayed at 1:1000 or 1:5000. The limit of detection (LOD) for this assay is 0.278 μ g/mL.

Mouse protection study

Eleven to twelve-month old female immunocompetent BALB/c mice purchased from Envigo (BALB/c AnNHsd, stock# 047) were used for SARS-CoV-2 *in vivo* protection experiments as described previously (Dinnon et al., 2020). Ten-week-old HFH4-hACE2 transgenic mice were bred and maintained at the University of North Carolina at Chapel Hill and used for WIV-1 *in vivo* protection experiments. Mice were housed in groups of five animals per cage and fed standard chow diet. Virus inoculations were performed under anesthesia (Ketamine and Xylazine) and effort was taken to minimize animal suffering. For evaluating the prophylactic efficacy of mAbs, mice were intraperitoneally treated with 300 μ g of each mAb or 150 μ g of each mAb in combination 12 hours prior to infection. Mice were infected intranasally with 10^5 PFU of mouse-adapted SARS-CoV-2 2AA MA (Dinnon et al., 2020) or WIV-1. For evaluating the therapeutic efficacy of mAbs, mice were intraperitoneally treated with 300 μ g of each mAb or 150 μ g of each mAb in combination 12 hours following infection. Forty-eight hours post infection, mice were sacrificed, and lungs were harvested for viral titer as measured by plaque assays and RNA analysis. In another study, fifty-two weeks old female BALB/c mice were i.p. injected with DH1052 (200 μ g/mice, n = 10) or CH65 control Ab (200 μ g/mice, n = 9). After 12 hours, mice were challenged with 10^4 PFU of mouse-adapted SARS-CoV-2 MA10 virus (Leist et al., 2020a). Mice were sacrificed at day 4 post infection, and lungs were harvested for viral titer as measured by plaque assays and RNA analysis. The study was carried out in accordance with the recommendations for care and use of animals by the Office of Laboratory Animal Welfare (OLAW), National Institutes of Health and the Institutional An-

imal Care. All mouse studies were performed at the University of North Carolina (Animal Welfare Assurance #A3410-01) using protocols (19-168) approved by the UNC Institutional Animal Care and Use Committee (IACUC) and all mouse studies were performed in a BSL3 facility at UNC.

Viral RNA extraction and quantification

The assay for SARS-CoV-2 quantitative Polymerase Chain Reaction (qPCR) detects total RNA using the WHO primer/probe set E_Sarbeco (Charité/Berlin). A QIAAsymphony SP (QIAGEN, Hilden, Germany) automated sample preparation platform along with a virus/pathogen DSP midi kit and the *complex800* protocol were used to extract viral RNA from 800 μ L of pooled samples. A reverse primer specific to the envelope gene of SARS-CoV-2 (5'-ATA TTG CAG CAG TAC GCA CAC A-3') was annealed to the extracted RNA and then reverse transcribed into cDNA using SuperScriptTM III Reverse Transcriptase (Thermo Fisher Scientific, Waltham, MA) along with RNase Out (Thermo Fisher Scientific, Waltham, MA). The resulting cDNA was treated with RNase H (Thermo Fisher Scientific, Waltham, MA) and then added to a custom 4x TaqManTM Gene Expression Master Mix (Thermo Fisher Scientific, Waltham, MA) containing primers and a fluorescently labeled hydrolysis probe specific for the envelope gene of SARS-CoV-2 (forward primer 5'-ACA GGT ACG TTA ATA GTT AAT AGC GT-3', reverse primer 5'-ATA TTG CAG CAG TAC GCA CAC A-3', probe 5'-6FAM/AC ACT AGC C/ZENA TCC TTA CTG CGC TTC G/IABkFQ-3'). The qPCR was carried out on a QuantStudio 3 Real-Time PCR System (Thermo Fisher Scientific, Waltham, MA) using the following thermal cycler parameters: heat to 50°C, hold for 2 min, heat to 95°C, hold for 10 min, then the following parameters are repeated for 50 cycles: heat to 95°C, hold for 15 s, cool to 60°C and hold for 1 minute. SARS-CoV-2 RNA copies per reaction were interpolated using quantification cycle data and a serial dilution of a highly characterized custom DNA plasmid containing the SARS-CoV-2 envelope gene sequence. Mean RNA copies per milliliter were then calculated by applying the assay dilution factor (DF = 11.7). The limit of detection (LOD) for this assay is approximately 62 RNA copies per milliliter of sample.

Subgenomic mRNA assay

SARS-CoV-2 E gene and N gene subgenomic mRNA (sgRNA) was measured by a one-step RT-qPCR adapted from previously described methods (Wölfel et al., 2020; Yu et al., 2020). To generate standard curves, a SARS-CoV-2 E gene sgRNA sequence, including the 5'UTR leader sequence, transcriptional regulatory sequence (TRS), and the first 228 bp of E gene, was cloned into a pcDNA3.1 plasmid. For generating SARS-CoV-2 N gene sgRNA, the E gene was replaced with the first 227 bp of N gene. The respective pcDNA3.1 plasmids were linearized, transcribed using MEGAscript T7 Transcription Kit (ThermoFisher, Catalog # AM1334), and purified with MEGAclean Transcription Clean-Up Kit (ThermoFisher, Catalog # AM1908). The purified RNA products were quantified on Nanodrop, serially diluted, and aliquoted as E sgRNA or N sgRNA standards.

RNA extracted from animal samples or standards were then measured in Taqman custom gene expression assays (ThermoFisher Scientific). For these assays we used TaqMan Fast Virus 1-Step Master Mix (ThermoFisher, catalog # 4444432) and custom primers/probes targeting the E gene sgRNA (forward primer: 5' CGATCTCTTGATAGATCTGTTCTCE 3'; reverse primer: 5' ATATTGCAGCAGT ACGCACACA 3'; probe: 5' FAM-ACACTAGCCATCCTTACTGCGCTTCG-BHQ1 3') or the N gene sgRNA (forward primer: 5' CGATCTCTTGATAGATCTGTTCTC 3'; reverse primer: 5' GGTGAA CCAAGACGCAGTAT 3'; probe: 5' FAM-TAACCAGAATGGA-GAACGCAGTG GG-BHQ1 3'). RT-qPCR reactions were carried out on a QuantStudio 3 Real-Time PCR System (Applied Biosystems) or a StepOnePlus Real-Time PCR System (Applied Biosystems) using the program below: reverse transcription at 50°C for 5 minutes, initial denaturation at 95°C for 20 s, then 40 cycles of denaturation-annealing-extension at 95°C for 15 s and 60°C for 30 s. Standard curves were used to calculate E or N sgRNA in copies per ml; the limit of detections (LOD) for both E and N sgRNA assays were 12.5 copies per reaction or 150 copies per mL of BAL/nasal swab fluid.

QUANTIFICATION AND STATISTICAL ANALYSIS

Data were plotted using Prism GraphPad 8.0. Exact Wilcoxon rank sum test with an alpha level of 0.05 was performed to compare differences between groups using SAS 9.4 (SAS Institute, Cary, NC). No adjustments were made to the p values for multiple comparisons.

Supplemental figures

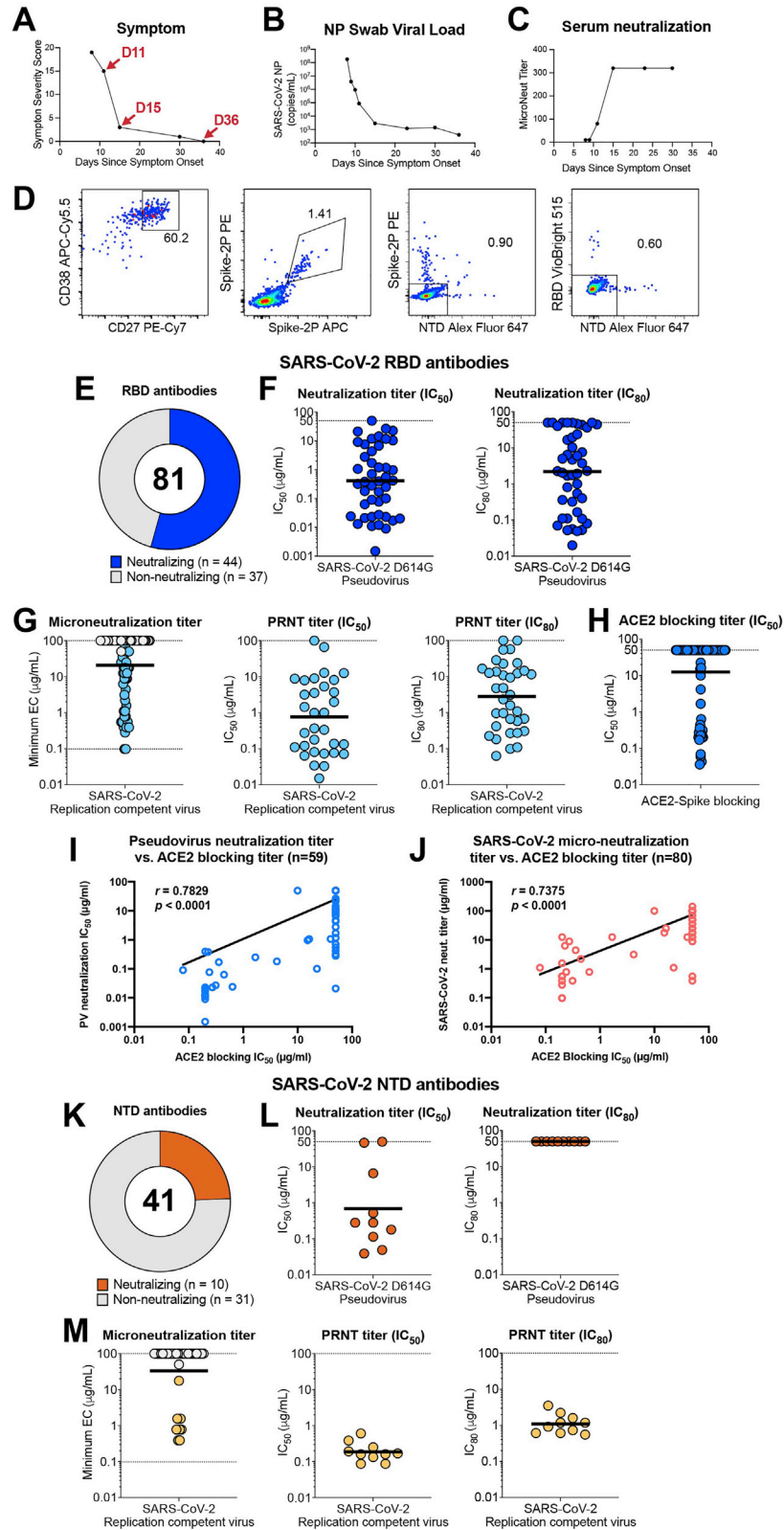


Figure S1. Isolation of SARS-CoV-2-reactive Abs from single cell-sorted plasmablasts and memory B cells of SARS-CoV-2 and SARS-CoV-1 convalescent donors, related to Figure 1

(A) Symptom severity scores of the COVID-19 convalescent donor. The method to determine severity score is in supplementary online material. Red arrows indicate the blood sampling time points that we used to isolate Abs.

(B) Viral load from nasopharyngeal (NP) swabs.

(C) Serum micro-neutralization titer. Micro-Neutralization titers were defined as the highest serum dilution that neutralize all the virus, or 99% inhibitory concentration (IC_{99}).

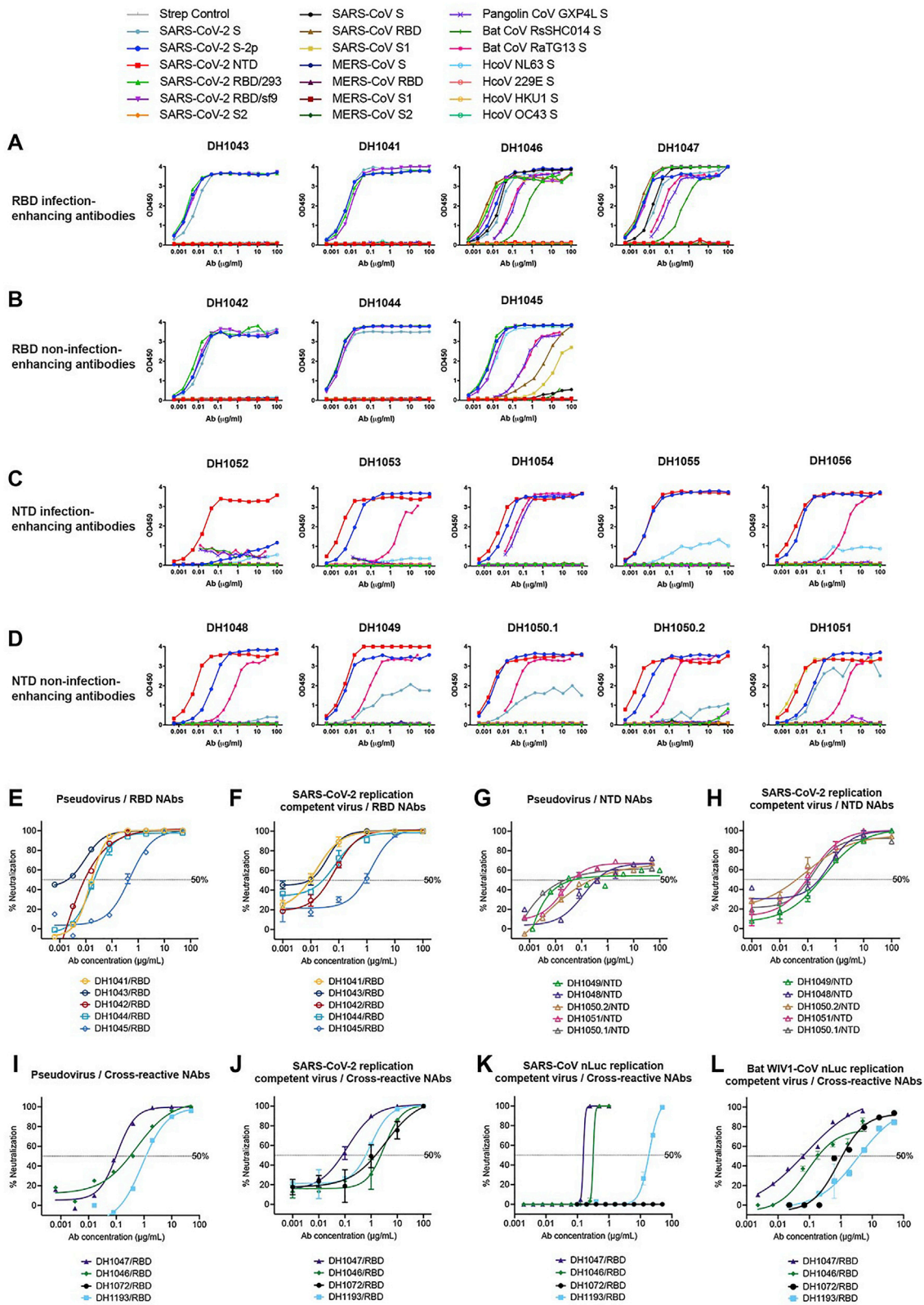
(D) Flow cytometry gating strategy for unbiased plasmablasts sorting or antigen specific-memory B cells sorting. At day 11 and day 15 post onset of COVID-19 symptom, plasmablasts ($CD14^-/CD16^-/CD3^-/CD235a^-/CD19^+/CD20^{low}/IgD^-/CD27^{high}/CD38^{high}$) from a SARS-CoV-2 donor. Antigen specific B cells from SARS-CoV-1 and SARS-CoV-2 donors were sorted with different combinations of the SARS-CoV-2 S-2P, RBD, NTD probes. Representative data for sorting Spike double positive, Spike⁺ or NTD⁺, as well as RBD⁺ or NTD⁺ subsets were shown.

(E-H) RBD Ab neutralization activity. (E) Proportion of SARS-CoV-2 RBD Abs ($n = 81$) that exhibited detectable neutralization in the microneutralization assay. (F) Neutralization IC_{50} and IC_{80} of RBD neutralizing Abs (NAbs) against pseudotyped SARS-CoV-2. (G) Microneutralization titer, plaque reduction neutralization test (PRNT) IC_{50} and IC_{80} of RBD NAbs against replication-competent SARS-CoV-2. Microneutralization titer was defined as the lowest Ab concentration that neutralized all the virus, or 99% inhibitory concentration (IC_{99}). Abs with undetectable microneutralization titers are shown as gray symbols and nAbs are represented by blue symbols. (H) RBD NAbs blocking of ACE2 binding to SARS-CoV-2 Spike (S) protein. Blocking titer is shown as IC_{50} .

(I-J) Correlation analysis of RBD Abs between neutralization and ACE2 blocking activities. Spearman correlation analysis were performed for (I) ACE2 blocking IC_{50} versus PV neutralization IC_{50} , as well as (J) for ACE2 blocking IC_{50} versus SARS-CoV-2 neutralization titers (indicated by the lowest concentration that shows no CPE). Purified RBD Abs in [Tables S1](#) and [S2](#) that have pseudovirus neutralization data ($n = 59$) or SARS-CoV-2 micro-neutralization assay data ($n = 80$) were used in this analysis. P values (p) and correlation coefficients (r) are indicated for each figure.

(K-M) Neutralization activity of NTD Abs. (K) Proportion of SARS-CoV-2 NTD Abs ($n = 41$) that exhibited detectable neutralization in the microneutralization assay.

(L) Neutralization IC_{50} and IC_{80} of NTD neutralizing Abs against pseudotyped SARS-CoV-2. (M) Microneutralization titer, PRNT IC_{50} and IC_{80} of NTD neutralizing Abs against replication-competent SARS-CoV-2. Abs with undetectable microneutralization titers are shown as gray symbols and neutralizing Abs are represented by orange symbols. Horizontal bars represent the geometric means for each group of Abs.



(legend on next page)

Figure S2. Binding and neutralization activities of down-selected SARS-CoV-2 Abs, related to Figure 2

(A-D) ELISA binding curves of down-selected Abs. Different SARS-CoV-2 or other CoV viral antigens were coated on plates and detected with serial diluted (A) RBD infection-enhancing Abs, (B) RBD non-infection-enhancing Abs, (C) NTD infection-enhancing Abs, and (D) NTD non-infection-enhancing Abs.

(E-F) Neutralization curves for RBD Abs against pseudotyped (E) and replication-competent (F) SARS-CoV-2.

(G-H) Neutralization curves for NTD Abs against pseudotyped (G) and replication-competent (H) SARS-CoV-2.

(I-L) Neutralization curves for cross-neutralizing Abs against pseudotyped (I) and replication-competent (J) SARS-CoV-2, SARS-CoV-1 nanoluciferase (nLuc) virus (L), and Bat WIV1-CoV nLuc virus (L).

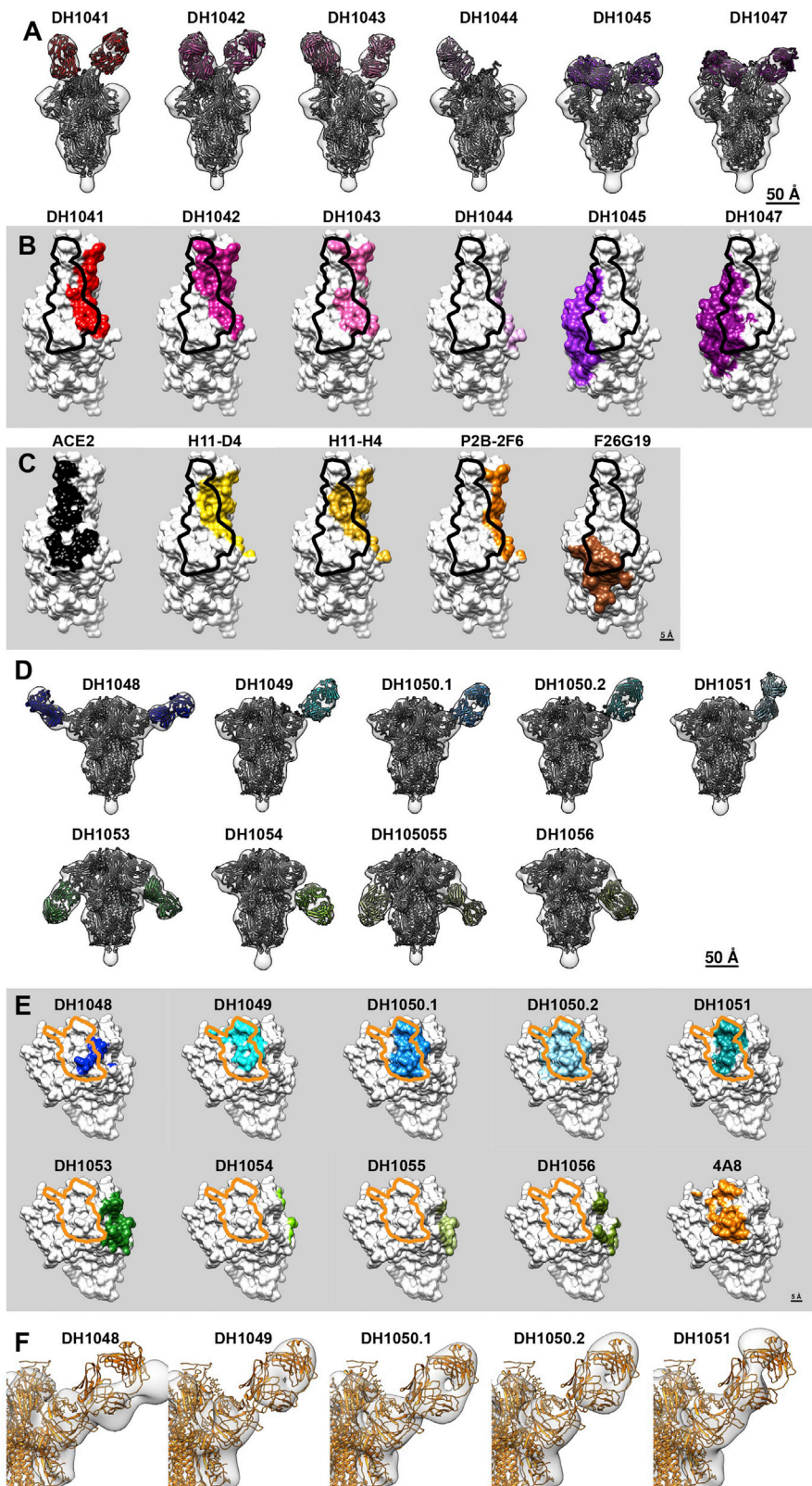


Figure S3. Comparison of RBD and NTD epitopes from NSEM, related to Figure 2

(A) A spike model (PDB: 6ZGE) and corresponding Fab homology models were manually docked and rigidly fit into each negative stain density map.

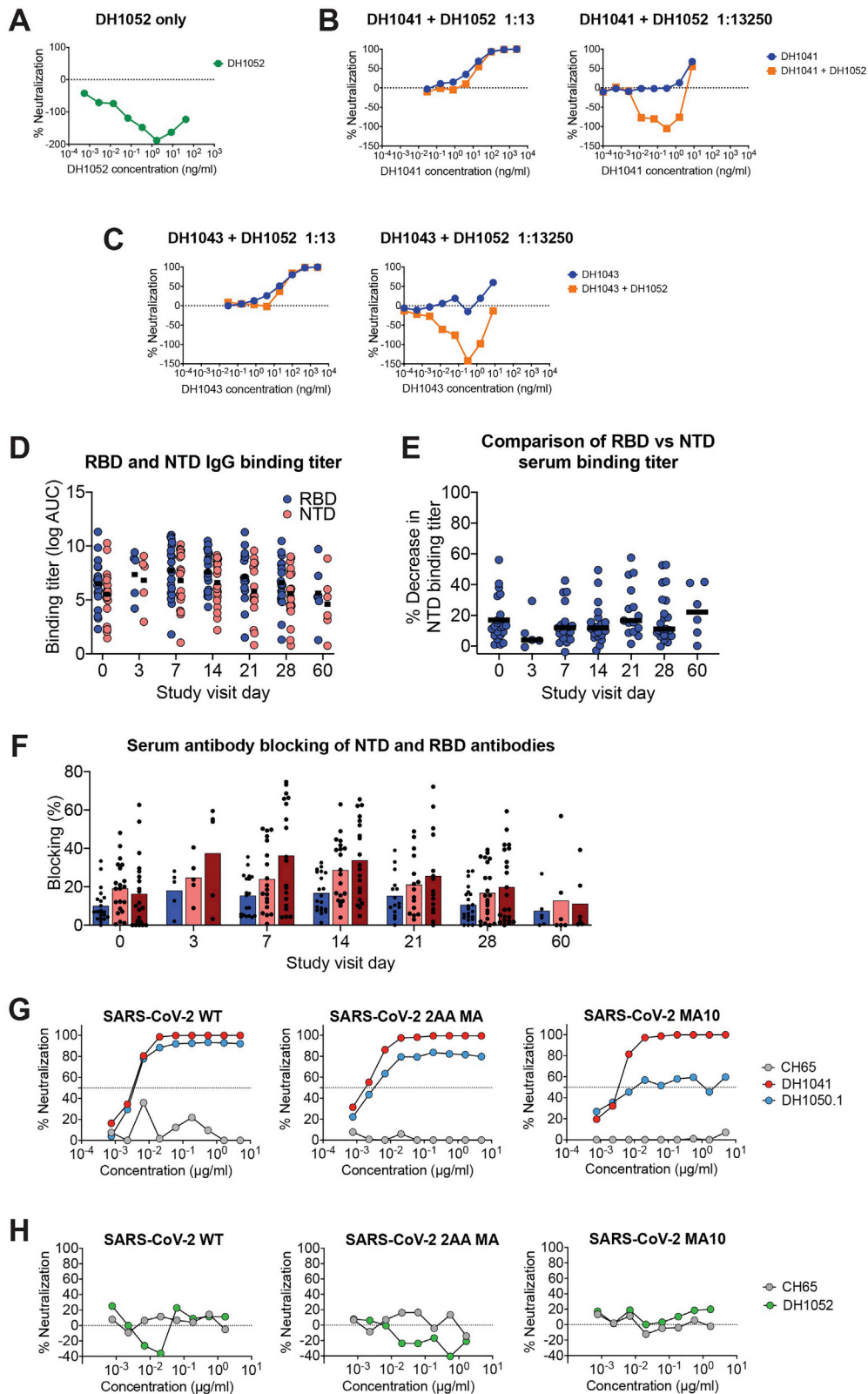
(B) The RBD of each model is enlarged and shown as a white surface, with the putative epitope of each Ab colored. Black outline indicates the ACE2 binding footprint.

(C) Comparison to ACE2 footprint and epitopes of three published Abs with similar epitopes. See main text for references.

(D) A spike model (PDB: 6ZGE) and corresponding Fab homology models were manually docked and rigidly fit into each negative stain density map.

(E) The NTD of each model is enlarged and shown as a white surface, with the epitope of each Ab colored. Orange outline indicates the epitope of Ab 4A8, shown at bottom right. Outlines illustrate that the neutralizing Abs DH1048-51 share the same epitope, whereas the infection-enhancing Abs DH1053-56 bind a distinct epitope.

(F) The model of spike complex with Fab 4A8 (orange ribbons, PDB: 7C2L) is rigidly fit into each of the NSEM maps (transparent surfaces). The close fit of 4A8 into DH1049, DH1050.1 and DH1050.2 indicate these have the same approach angle as 4A8, whereas DH1048 and DH1051 have slightly different approaches.



(legend on next page)

Figure S4. *In vitro* analysis of human Abs and SARS-CoV-2-infected serum samples, related to Figures 3, 5 and 7

(A-C) Effect of combining infection-enhancing RBD and NTD Abs on SARS-CoV-2 pseudovirus infection in ACE2-expressing cells. The infection-enhancing NTD Ab DH1052 was tested alone (A) or mixed with infection-enhancing RBD Abs DH1041 (B) or DH1043 (C) in 1:13 ratio or 1:13250 ratio, respectively. The NTD:RBD Ab mixtures (orange), as well as RBD Ab alone (blue), were five-fold serially diluted and tested for neutralization against SARS-CoV-2 D614G pseudovirus in 293T/ACE2 cells.

(D-F) Comparison of RBD and NTD directed serum Ab responses in SARS-CoV-2 infected humans.

(D) Serum IgG binding titers to RBD (blue) and NTD (salmon) as measured by ELISA as log area-under-curve (AUC). Each symbol represents an individual study participant, with the mean binding titer for the visit day shown as a black horizontal bar.

(E) Percent decrease in binding to NTD relative to RBD binding titer. Each symbol represents the change in binding titer for an individual study subject. Mean decrease is shown as a black horizontal bar.

(F) Serum blocking of RBD neutralizing Ab DH1041 (blue) or NTD neutralizing Ab DH1050.1 (salmon), or non-neutralizing Ab DH1052 (burgundy) binding to SARS-CoV-2 spike. Black symbols show individual study participants. Mean blocking percentage for the visit day is shown as a filled bar.

(G-H) Neutralization activities of neutralizing and enhancing Abs against wild-type (WT) and -mouse-adapted SARS-CoV-2.

(G) NTD neutralizing Abs DH1050.1, RBD neutralizing and enhancing Abs DH1041 were tested for neutralization activities against WT virus, mouse-adapted 2AA MA virus, and mouse-adapted MA10 virus in live virus neutralization assay. CH65 Ab was used as a control. Mean value of neutralization (%) from duplicate wells were shown.

(H) NTD enhancing Ab DH1052 and control Ab CH65 were tested for neutralization activities against WT virus, mouse adapted 2AA MA virus, and mouse-adapted MA10 virus in live virus neutralization assay. Mean values of neutralization (%) from duplicate wells were shown.

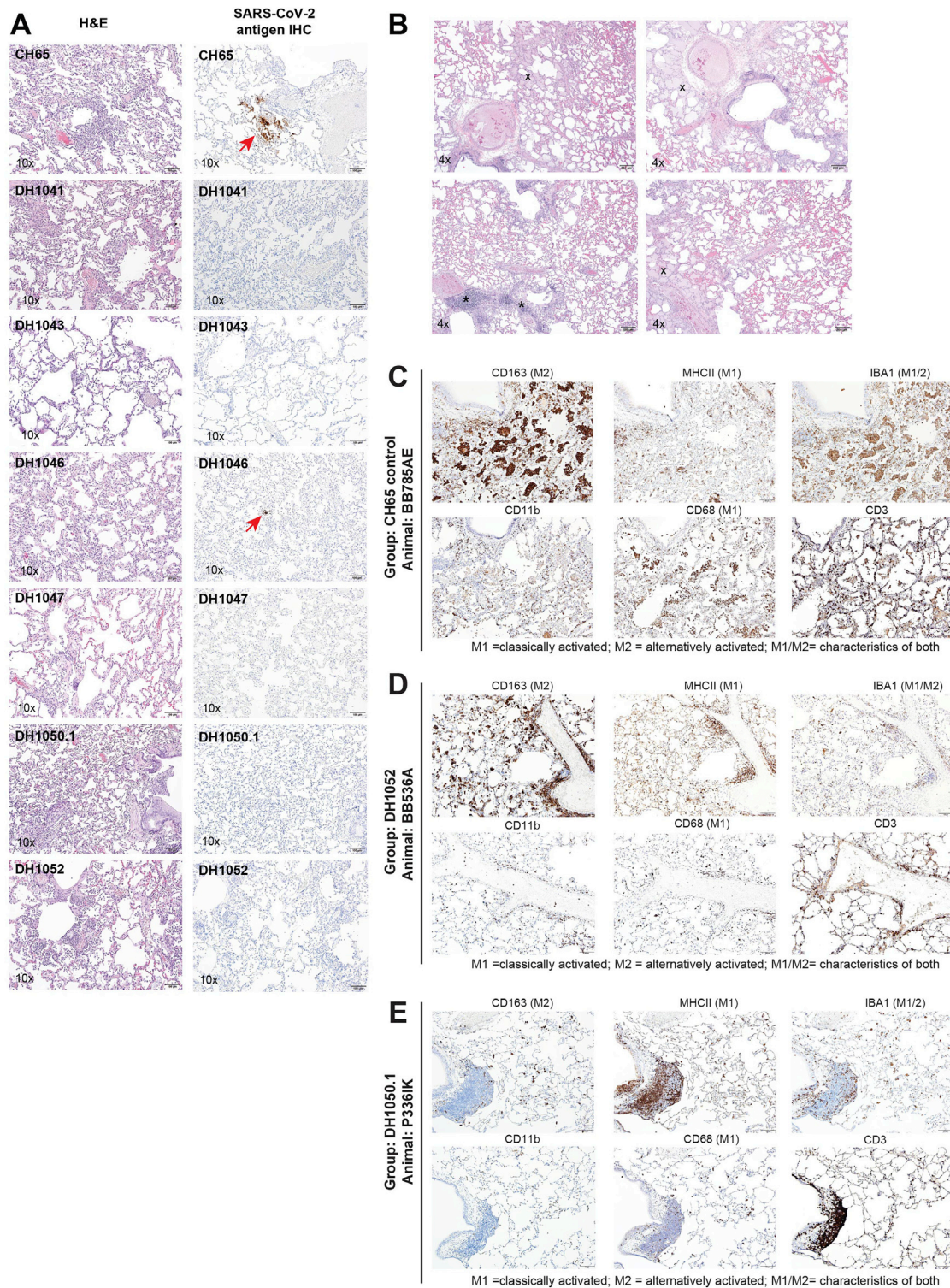


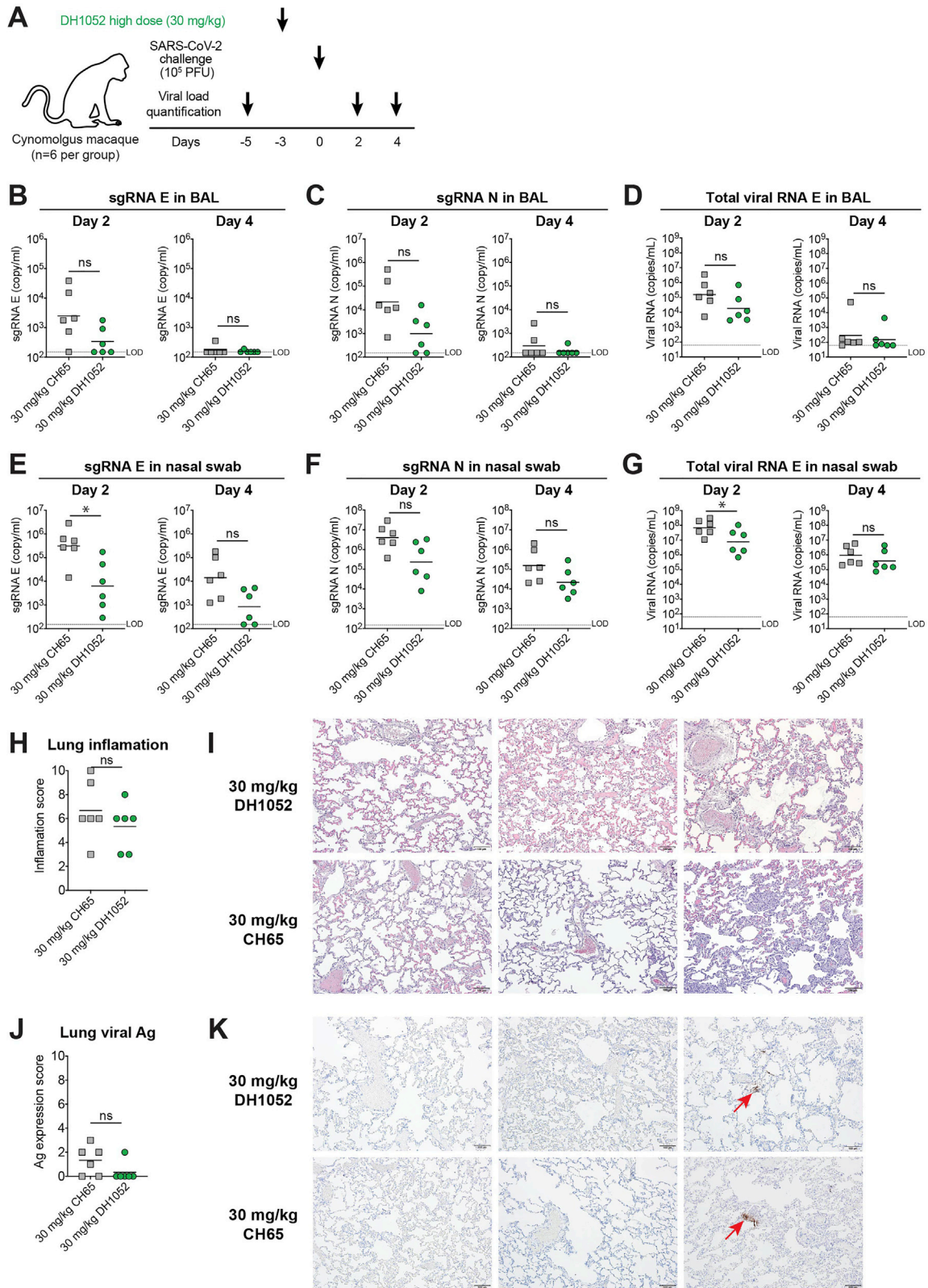
Figure S5. Lung histopathology of Ab-treated and SARS-CoV-2 challenged cynomolgus macaques, related to Figures 5 and 7

(A) Representative images of hematoxylin and eosin (H&E) staining and SARS-CoV-2 antigen immunohistochemistry (IHC) staining from each group. All images were taken at 10x magnification. The images in this figure are representative of the average severity of pathologic processes observed and recorded during microscopic evaluation. Red arrows indicate SARS-CoV-2 infection foci.

(B) Following microscopic evaluation of DH1052, 1 animal (BB536A) out of 5 animals in this group exhibited histologic features that was substantially more severe than the rest of the cohort and may suggest some degree of Ab-mediated disease enhancement. The features were characterized by prominent perivascular (legend continued on next page)

mononuclear inflammation (*) and a substantial amount of perivascular and alveolar edema (fluid; X). These findings suggest a vaso-centric process with some degree of altered vascular permeability. The remaining 4 animals in DH1052 group had inflammatory changes that ranged from minimal to moderate severity and more infiltrates were mixed and predominantly polymorphonuclear with lesser mononuclear cell involvement and present in the alveolar spaces.

(C-E) Expression of macrophage activation markers in macaque lung tissues. An animal from the CH65 control group (C), the DH1052-treated animal (BB536A) that exhibited substantially more severe lung inflammation (D), and an animal from the NTD NAb DH1050.1 group (E) were selected for Immunohistochemistry (IHC) staining. Immunohistochemical staining was performed using MHCII, CD68, IBA1 and CD163 to detect classically activated macrophages (M1) and/or alternatively activated macrophages (M2). CD11b is a macrophage/monocyte marker and CD3 is a T cell marker. All images are 10x magnification; scale bars = 100 μ m.



(legend on next page)

Figure S6. High-dose NTD enhancing Ab DH1052 does not enhance SARS-CoV-2 replication or disease *in vivo*, related to Figure 5

(A) Diagram of the macaque study design showing cynomolgus macaques ($n = 5$ per group) were infused with high dose (30 mg/kg body weight) DH1052 or an irrelevant control CH65 Ab 3 days before 10^5 PFU of SARS-CoV-2 challenge via intranasal and intratracheal routes. Viral load including viral RNA and subgenomic RNA (sgRNA) were measured at the indicated pre-challenge and post-challenge time points. Lungs were harvested on Day 4 post-challenge for histopathology analysis.

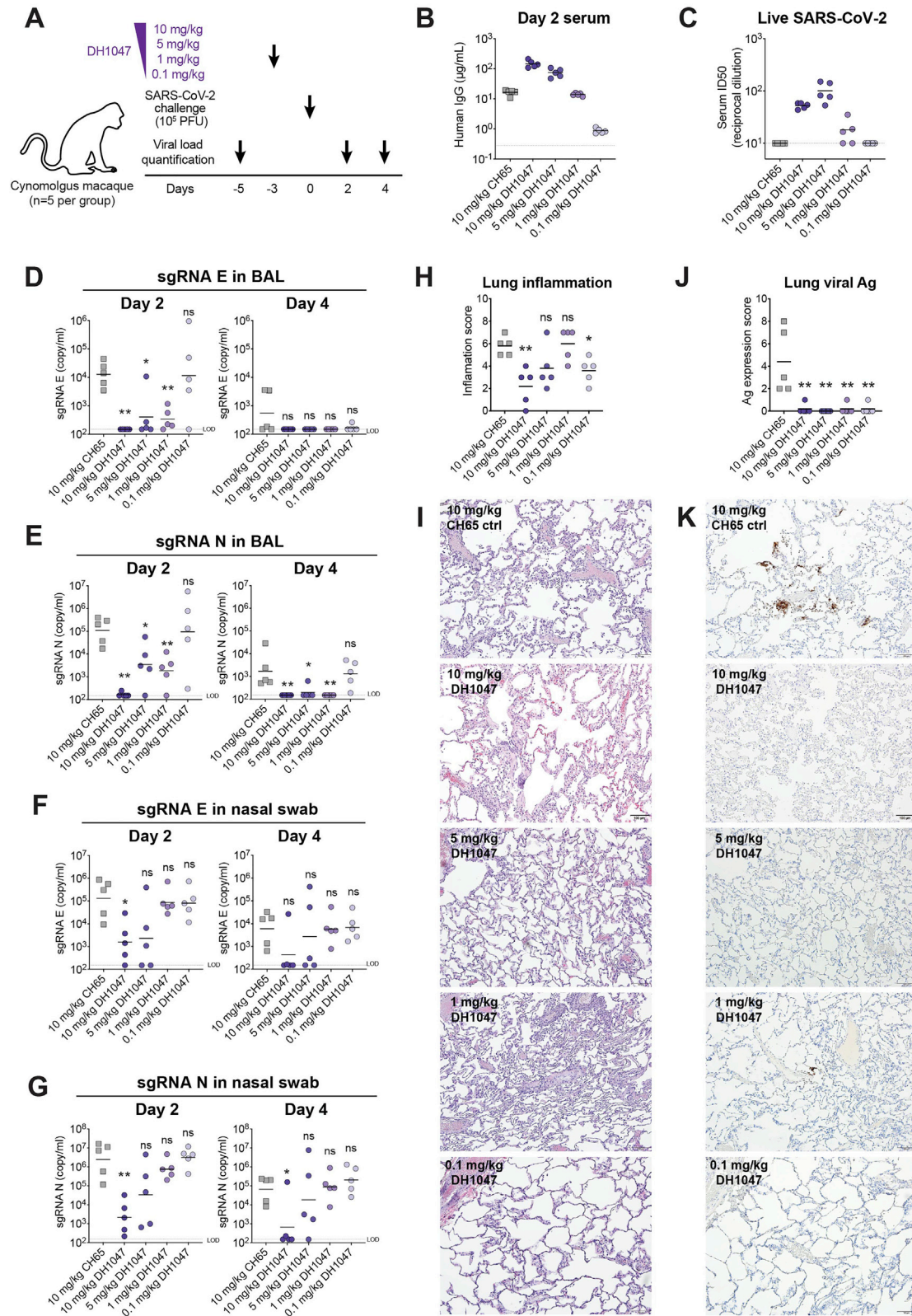
(B-D) SARS-CoV-2 (B) E gene sgRNA, (C) N gene sgRNA and (D) E gene total viral RNA in bronchoalveolar lavage (BAL) on Day 2 and Day 4 post challenge.

(E-G) SARS-CoV-2 (E) E gene sgRNA, (F) N gene sgRNA and (G) E gene total viral RNA in nasal swab on Day 2 and Day 4 post challenge.

(H-I) Lung inflammation. Sections of the left caudal (Lc), right middle (Rm), and right caudal (Rc) lung were evaluated and scored for the presence of inflammation by hematoxylin and eosin (H&E) staining. (H) Summary of inflammation scores. Symbols indicate the sums of Lc, Rm, and Rc scores in each animal. (I) Representative images of lung H&E staining.

(J-K) Immunohistochemistry (IHC) staining for the presence of SARS-CoV-2 nucleocapsid in lungs. (J) Summary of IHC scores. Symbols indicate the sums of Lc, Rm, and Rc scores in each animal. (K) Representative images of lung IHC staining. Red arrows indicate SARS-CoV-2 infection foci.

LOD, limit of detection. Horizontal bars are the group mean except in (C) where group geometric mean is shown. Statistical significance in all the panels were determined using Wilcoxon rank sum exact test. Asterisks show the statistical significance between the indicated group and CH65 control group: ns, not significant, * $p < 0.05$, ** $p < 0.01$, *** $p < 0.001$.



(legend on next page)

Figure S7. Different doses of a cross-neutralizing Ab DH1047 treatments do not enhance SARS-CoV-2 replication *in vivo*, related to Figure 7

(A) Diagram of the macaque study design. Cynomolgus macaques ($n = 5$ per group) were infused with DH1047 at the dose of 10 mg/kg, 5 mg/kg, 1 mg/kg, 0.1 mg/kg weight. Macaques treated with 10 mg/kg weight of DH65 Ab were set as the control group. Three days post-infusion, 10^5 PFU of SARS-CoV-2 challenge via intranasal and intratracheal routes. Viral load including viral RNA and subgenomic RNA (sgRNA) were measured at the indicated pre-challenge and post-challenge time points. Lungs were harvested on Day 4 post-challenge for histopathology analysis.

(B) Serum human IgG concentrations at Day 2.

(C) Day 2 serum neutralization titers shown as the reciprocal serum dilution that inhibits 50% (ID_{50}) of SARS-CoV-2 replication in Vero cells.

(D-E) SARS-CoV-2 (D) E gene sgRNA and (E) N gene sgRNA in bronchoalveolar lavage (BAL) on Day 2 and Day 4 post challenge.

(F-G) SARS-CoV-2 (F) E gene sgRNA and (G) N gene sgRNA in nasal swab on Day 2 and Day 4 post challenge.

(H-I) Lung inflammation. Sections of the left caudal (Lc), right middle (Rm), and right caudal (Rc) lung were evaluated and scored for the presence of inflammation by hematoxylin and eosin (H&E) staining. (H) Summary of inflammation scores. Symbols indicate the sums of Lc, Rm, and Rc scores in each animal. (I) Representative images of lung H&E staining.

(J-K) Immunohistochemistry (IHC) staining for the presence of SARS-CoV-2 nucleocapsid in lungs. (J) Summary of IHC scores. Symbols indicate the sums of Lc, Rm, and Rc scores in each animal. (K) Representative images of lung IHC staining. Red arrows indicate SARS-CoV-2 infection foci.

LOD, limit of detection. Horizontal bars are the group mean except in (C) where group geometric mean is shown. Statistical significance in all the panels were determined using Wilcoxon rank sum exact test. Asterisks show the statistical significance between the indicated group and CH65 control group: ns, not significant, * $p < 0.05$, ** $p < 0.01$, *** $p < 0.001$.